UNCLASSIFIED

A COMPUTER SIMULATION OF DIGITAL RECORDING

Final Development Report

29 December 1966 through 29 December 1967

RR 67-36 29 December 1967

AMPEX CORPORATION

RESEARCH AND ENGINEERING PUBLICATION

UNCLASSIFIED

A COMPUTER SIMULATION OF DIGITAL RECORDING

by

J. Mallinson
C. Steele
L. Lienhard

Final Development Progress Report
29 December 1966 through 29 December 1967
Contract No. 951785 (Subcontract)
Prime Contract No. NAS 7-100
Ampex Report RR 67-36

Jet Propulsion Laboratory
California Institute of Technology
4800 Oak Grove Drive
Pasadena, California 91103

SUBMITTED BY J. C. Mallinson

J. C. Mallinson
Project Engineer

APPROVED BY V. E. Ragosine

V. E. Ragosine
Manager of Physics,
Asst. Director of Research

Ampex Corporation
401 Broadway
Redwood City, California 94063

NOTICE

This report was prepared as an account of Government-sponsored work. Neither the United States, nor the National Aeronautics and Space Administration (NASA), nor any person acting on behalf of NASA:

a. Makes warranty or representation, expressed or implied, with respect to the accuracy, completeness, or usefulness of the information contained in this report, or that the use of any information, apparatus, method, or process disclosed in this report may not infringe privately-owned rights; or

b. Assumes any liabilities with respect to the use of, or for damages resulting from the use of any information, apparatus, method, or process disclosed in this report.

As used above, "person acting on behalf of NASA" includes any employee or contractor of NASA, or employee of such contractor, to the extent that such employees or contractor of NASA, or employee of such contractor prepares, disseminates, or provides access to, any information pursuant to his employment with such contractor.

Requests for copies of this report should be referred to:

National Aeronautics and Space Administration
Office of Scientific and Technical Information
Washington 25, D.C.

Attention: AFSS-A

CONTENTS

CONTENTS (Cont)

1.0 INTRODUCTION

This report contains all the results obtained to date with the use of a computer simulation of the tape recording process, the tape demagnetization-remagnetization cycle, the readout process and several detector processes.

After a description of the programs (JPL-4 and JPL-6), the report is divided into two parts. The first deals with the pure tape recording studies made. These include all phenomena up to and including the reproduce head output.

The second part deals with the problems associated with detection, drop-outs, noise and other signal processing operations.

PRECEDING PAGE BLANK NOT FILMED.

2.0 DESCRIPTION OF THE FOURIER SERIES COMPUTER PROGRAM (JPL-4)

2.1 Program Deck JPL-4

2.1.1 General Description

This deck simulates a tape recorder in the recording and reproduction of digital information, and the detection of the reproduced signal. The program is designed to operate with a periodic input signal in which each period contains a six-bit binary digital information in a self-clocking code. The program computes first the magnetization recorded on tape (neglecting magnetic particle interaction) then the voltage output of the reproduce head, and finally the detector output.

2.1.2 Input-Output

Table 2.1 gives a full description of the data cards needed with this program. A set of these five data cards is needed for each reproduce head output voltage curve that is computed. If only such an output voltage curve is needed, these five cards, with FLAG set to 0.0 is sufficient. If, however, the detector output must be computed, then a zero sample signal and a one sample signal must be computed, as described below. Each of these sample signals requires in turn the computation of its own output voltage curve. When detector output computations are made, the first five data cards, with FLAG set to 1.0, provide the zero sample signal, and the next five data cards, with FLAG set to 2.0 provide the one sample signal. Following the computation and storage of these two sample signals, each additional set of 5 data cards, with FLAG set to zero will result in the computation of a reproduce head output voltage curve, the cross correlation functions of this curve with respect to the zero sample and the one sample, and the detector output.

Table 2.1 Data Card Description for JPL-4B Program

Data Card No.	Format	Variable	Type	Description
1	8F10.0	RLAMBDA	REAL	The length along the magnetic tape, in microinches, of one 6-bit period of the input signal.
		G	REAL	One-half of the record head gap width, in microinches.
		HSAT	REAL	Saturating value of magnetic field, in oersteds.
		HMIN	REAL	Switching value of magnetic field, in oersteds.
		H0	REAL	Deep-in-gap magnetic field in the record head, in oersteds.
		A	REAL	Head-to-tape spacing, in microinches.
		DR		Sum of the head-to-tape spacing and tape thickness in microinches.
		SYM		If the number of ones in the 6-bit code is even, SYM = 1.0; if this number is odd, SYM = -1.0.
2	8F10.0	FLAG	REAL	If the reproduced signal for a 6-bit code is to be computed, FLAG = 0. If a zero sample is to be computed, FLAG = 1.0. If a one sample is to be computed FLAG = 2.0.
3	8I10	NPP	INTEGER	The number of points used to represent the magnetization on each half-bit of tape.
		NH	INTEGER	The number of harmonics used to represent the magnetization on tape.
		NY	INTEGER	The number of values of y (see Fig. 1) at which the magnetization is computed.
4 and 5	8F10.0	PULSE	REAL	PULSE is an array of 12 numbers (either ones or minus ones) that represents the 6-bit code.

The program now provides for printing out the input data and the detector output. The user can easily provide for additional print-outs as needed.

In different applications of this program it is desirable from time to time to plot a wide variety of different computed variables. One might, for example, wish to plot the magnetization on tape, the reproduce head voltage either or both of the cross correlation functions, or the detectability. The detailed operations needed for plotting are most easily provided by a special subroutine. Plots can then be provided at any desired points in the program simply by inserting at these points the appropriate call statements to the plot program.

2.1.3 Computation of Magnetization on Tape and Output Voltage from Reproduce Head

Figure 1 shows the dimensions used in the formula given below. The distance above the record head to the point at which the magnetization is computed is Y and the distance along the tape axis from the record head center line to this point is X. This is the axial distance to that point from the point on tape that is above the record head center line at t = 0. Thus

$$X_r = X + vt \qquad (1)$$

where v is tape velocity and t is time. The component of record head magnetic field in the X direction is H_x.

The magnetization on tape is first computed using a non-interacting model. Demagnetizing effects are considered later, as indicated below. The remanent magnetization on the tape is assumed to be entirely in the longitudinal direction. The magnetization M, written at the point (X, Y) on tape, is given as a function by H_x by

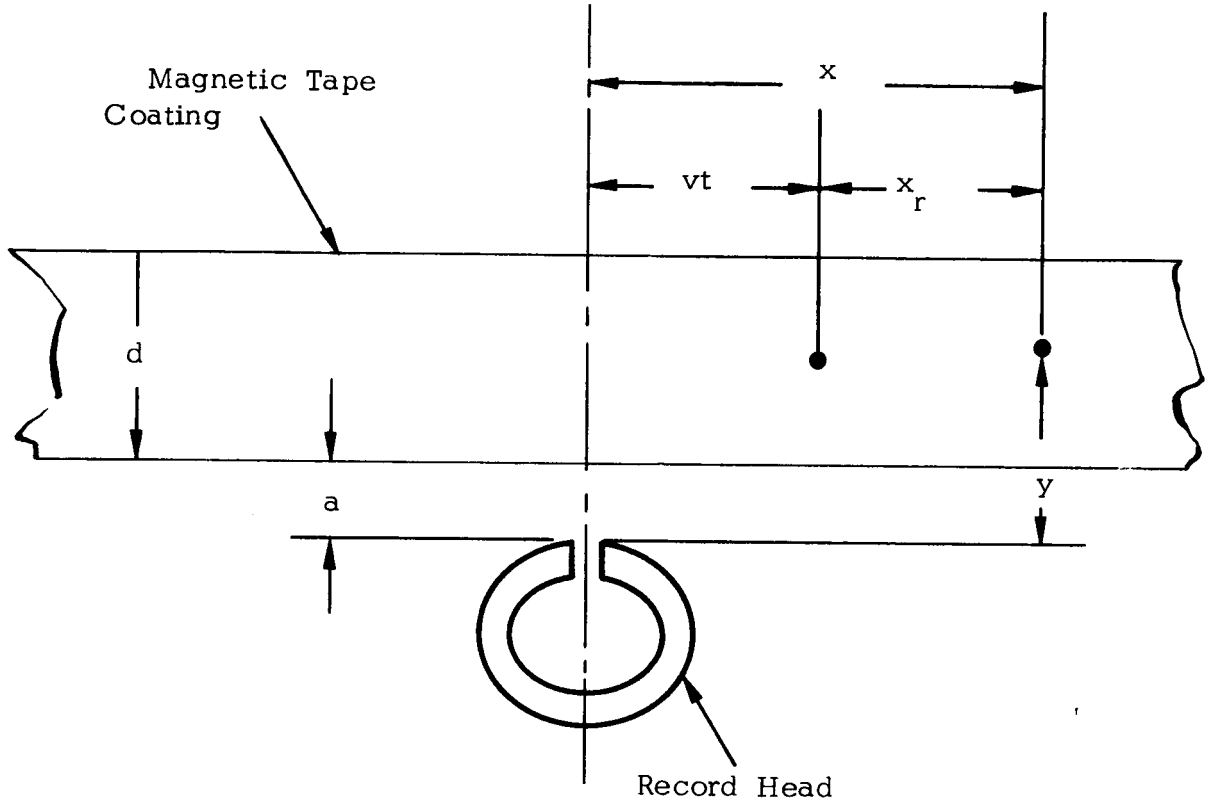

Fig. 1 Tape Recorder Coordinate System

$$M(X_r, Y) = M_o(H_x(X, Y, t_o)) + \sum_{i=1}^{n} \Delta M(H_x(X, Y, t_i)) \tag{2}$$

where t_o is the point in time at which the point (X, Y) passes through the second head center plane and t_i, $1 \leq i \leq n$ are the points in time between successive bits. In the last term on the right of Eq. (2), n is the total number of non-zero values of $M[H_x, (X, Y, t_i)]$ and X is expressed in terms of X_r and t_i by Eq. (1). In turn,

$$M_o = 0$$

if $$|H_x| < H_1 \tag{3}$$

$$M_o = \frac{\chi}{2}\left(H_x - \frac{H_x}{|H_x|} H_1\right) \tag{4}$$

if $$H_1 < |H_x| < H_2 \tag{5}$$

and

$$M_o = \frac{H_x}{|H_x|} \tag{6}$$

if $$|H_x| > H_2$$

where χ is the susceptibility of the magnetic material (see Fig. 2), H_1 is the threshold value of the magnetic field at which switching can take place and H_2 is the saturating value of the magnetic field. In turn,

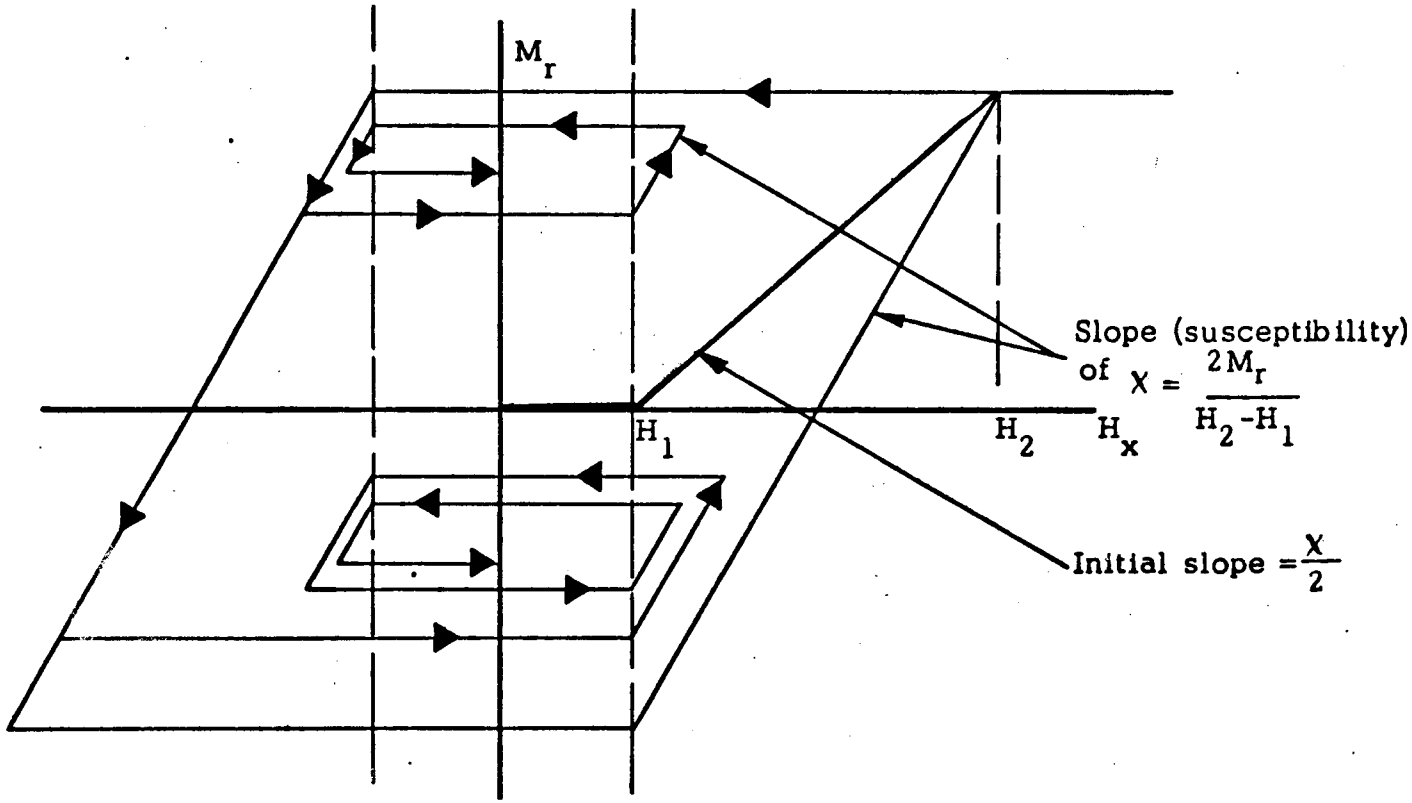

Fig. 2 Non-Interacting Model of Tape Remanence

$$\Delta M = 0 \tag{7}$$

if $|H_x| < H_1$,

$$\Delta M = \chi \left(H_x - \frac{H_x}{|H_x|} H_1\right) \tag{8}$$

if $H_1 < |H_x| < H_2$

and

$$\Delta M = \frac{\partial H_x}{|H_x|} \tag{9}$$

if

$$|H_x| > H_2 \tag{10}$$

The record head field longitudinal component is

$$H_x(x,y,t) = \frac{H_o(t)}{\pi}\left[\tan^{-1}\left(\frac{g/2+x}{y}\right) + \tan^{-1}\left(\frac{g/2-x}{y}\right)\right] \tag{11}$$

where $H_o(t)$ is the deep gap field and g is the gap width.

The deep-gap field, $H_o(t)$ is a periodic function of time, with a period of twelve self-clocking bits. For example, $H_o(t)$ for twelve bits of the pattern 0, 0, 1, 1, 1, 0 is shown in Fig. 3. Note that if b is the time interval of one bit, then for a pattern that contains an odd number of ones (for example that shown in Fig. 3)

$$H_o(t + 6b) = -H_o(t) \tag{12}$$

and for a pattern that contains an even number of ones

$$H_o(t + 6b) = H_o(t) \tag{13}$$

Next the alogarithm simultaneously takes into account the effect of magnetic particle interaction, or demagnetization and computes the reproduce head flux. The first step toward this objective is to compute an average magnetization M_a given by

$$M_a(x_r) = \frac{1}{d'} \int_a^{a+d} M(x_r, y)\, dy \tag{14}$$

where a is the head-to-tape spacing and d is the effective thickness of the magnetic material on tape. * Following this, we represent M_a by

$$M_a(x_r) = a_o + \sum_{n=1}^{m} \left[a_n \cos(mk x_r) + b_n \sin(nk x_r) \right] \tag{15}$$

*For discussion of effective thickness of tape, see section 3. 5.

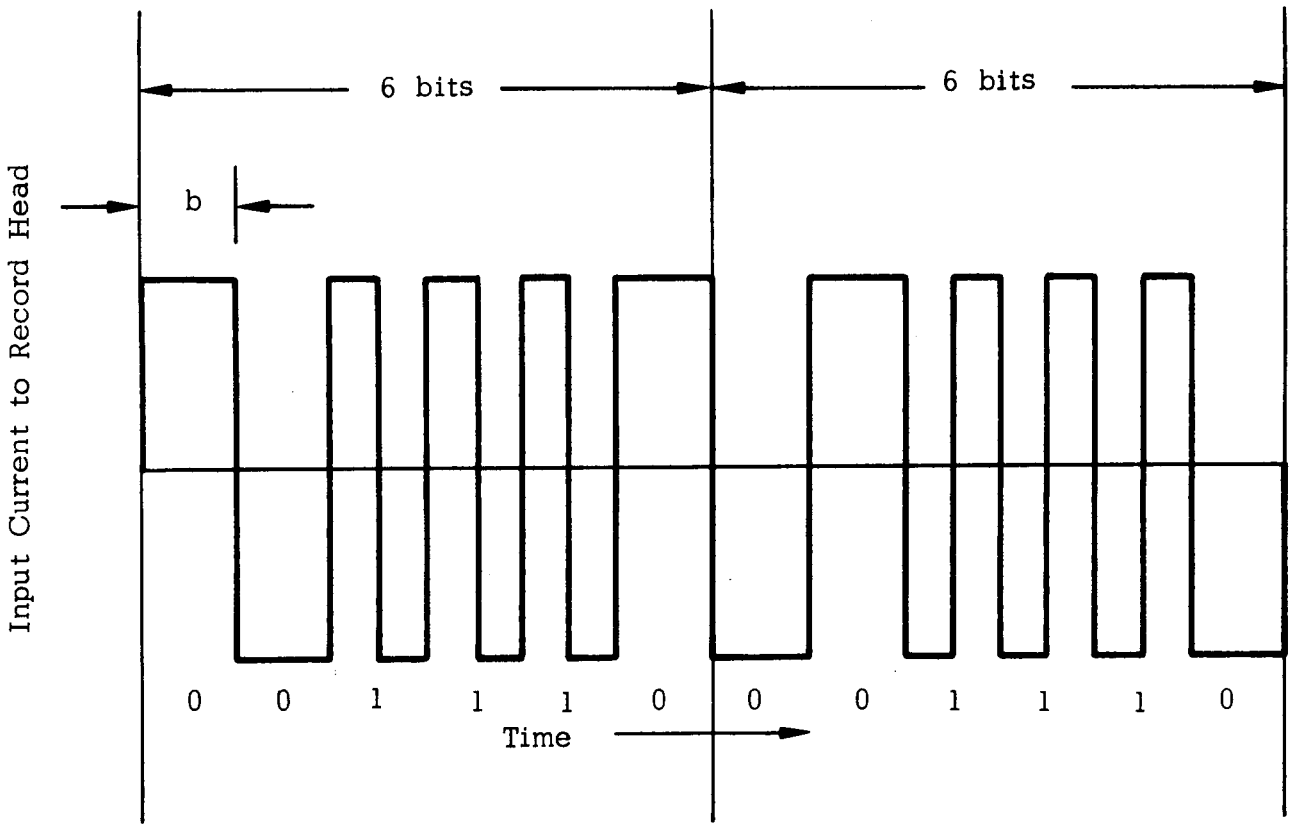

Fig. 3 Input Current Versus Time

where

$$K = \frac{2\pi}{12 X_b}$$

This Fourier series representation is possible because M_a is periodic in 12 x_b by Eq. (2) through Eq. (14). In addition, from Eq. (12) and (13), and certain other previous equations,

$$M_a(X_r + 6X_b) = -M_a(X_r)$$

if the 6 bit code contains an odd number of ones and

$$M_a(X_r + 6X_b) = M_a(X_r)$$

if the 6-bit code contains an even number of ones. As a result, M_a contains only even harmonics if the 6-bit code contains an even number of ones and M_a contains only odd harmonics if the 6-bit code contains an odd number of ones.

Mallinson[1] has shown that the flux in the reproduce head $\Phi(t)$ is given by

$$\phi(t) = e_0 + \sum_{n=1}^{m} \left[e_n \cos(nkX_r) + f_n \sin(nkX_r) \right] \tag{16}$$

where

$$e_n = D_n G_n a_n \tag{17}$$

$$f_n = D_n G_n b_n \tag{18}$$

[1] J. C. Mallinson, "Demagnetization Theory for Longitudinal Recording," IEEE Trans. on Magnetics, Vol. MAG-2, No. 3, September 1966.

In Eqs. (17) and (18)

$$D_n = \mu_2 \sinh(nkd') + \cosh(nkd') - 1 \qquad (19)$$

$$+ \frac{(\mu_1 - \mu_2)(\mu_1 \sinh(nkd') + \cosh(nkd') - 1)(\sinh(nkd') + \cosh(nkd') + \mu_2)}{\mu_1 \mu_2 (2\cosh(nkd') + (\mu_1 + 1/\mu_1)\sinh(nkd'))}$$

$$\mu_1 k n \left[\sinh(nkd')(\mu_2 \sinh(nka) + \cosh(nka)/\mu_2) + \cosh(nkd') e^{-nka}\right]$$

and $$G_n = \frac{\sin\left(nk \frac{g_r}{2}\right)}{nk g_r/2}$$

where g_r is the reproduce head gap width.

The output voltage from the reproduce head is given in terms of the flux by

$$V_r(t) = N \frac{d\phi(t)}{dt} \qquad (20)$$

where N is the number of turns on the reproduce head. From Eqs. (1), (16) and (20)

$$V_r(t) = N \sum_{n=1}^{m} nkv \left[f_n \cos(nkx_r) - e_n \sin(nkx_r)\right] \qquad (21)$$

The reproduce head output voltage is computed by Eq. (21).

2. 1. 4 Computation of Sample Signals and Cross-Correlation Functions

To compute a zero sample, we first find the output voltage from the reproduce head for a signal input to the record head that consists of six zero bits. Since for this pattern

$$H_o\ (t + B) = -H_o(t)$$

Then $M_a\ (X_r + X_b) = -\ M_a\ (X_r)$

and $V_r\ (t+b) = -\ V_r\ (t)$ (22)

From Eq. (22), we see that there must be a time t_o at which V_r is zero, and that

$$V_r\ (t_o + mb) = 0 \tag{23}$$

where m is any integer. To construct the zero sample, $S_o(t)$ we let

$$S_o(t) = V_r(t) \qquad t_o \leq t \leq t_o + 2b \tag{24}$$

$$S_o(t) = 0 \qquad t < t_o \text{ and } t > t_o + 2b \tag{25}$$

From Eqs. (23) and (24)

$$S_o(t) = S_o(t + 2b) = 0$$

and from this and Eq. (25), we see that S_o is continuous at t_o at $t_o + 2b$, as shown in Fig. 4.

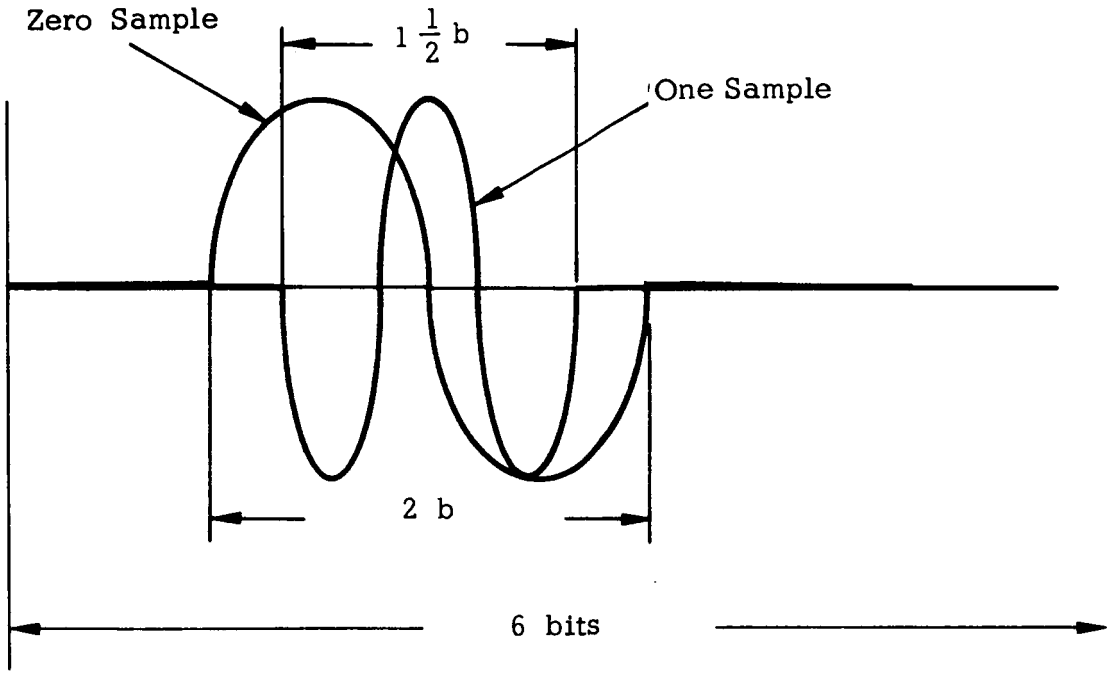

Fig. 4 Sample Signals

To compute a one sample, we first find the output voltage from the reproduce head for a signal input to the record head that consists of six one bits. Since for this pattern

$$H_o(t + b/2) = -H_o(t)$$

$$M_a(X_r + X_b/2) = -M_a(X_r) \tag{26}$$

the

and $$V_r(t + b/2) = V_r(t)$$

From Eq. (26) there must be a time t_1 at which V_r is zero, and that

$$V_r(t_1 + mb/2) = 0 \tag{27}$$

where m is any integer. To construct the one sample, $S_1(t)$ we let

$$S_1(t) = V_r(t) \qquad t_1 \leq t \leq t_1 + \tfrac{3}{2}b \tag{28}$$

$$S_1(t) = 0 \qquad t < t_0 \text{ and } t > t_1 + \tfrac{3}{2}b \tag{29}$$

From Eqs. (27) and (28)

$$S_1(t_1) = S_1(t_1 + \tfrac{3}{2}b) = 0$$

and from this and Eq. (29), we see that S_1 is continuous at t_1 and $t_1 + 3/2b$.

The cross-correlation function of the signal with respect to the zero sample, $C_o(\tau)$ and with respect to the one sample $C_1(\tau)$ are given in this application by

$$C_o(\tau) = \int_{t=t_o}^{t=t_o+2b} X(t) S_o(t+\tau)\, dt \tag{30}$$

$$C_1(\tau) = \int_{t=t_1}^{t=t_1+2b} X(t) S_1(t-\tau)\, dt \tag{31}$$

where X(t) is the signal. In the computer program, the integrals in Eqs. (30) and (31) are computed using the trapezoidal rule.

Note that t_o and t_1 are each chosen from a multiplicity of values. Furthermore, from Eqs. (30) and (31) the phase relationship between $C_o(\tau)$ and $C_1(\tau)$ changes if

$$t_1 - t_o$$

is changed as a result of a new selection of t_1 or t_o or both. The program has a provision to keep this phase relationship from changing, and to insure that $S_o(t)$ and $S_1(t)$ are orthogonal. After $S_o(t)$ and $S_1(t)$ are computed by Eqs. (26) through (29), $S_1(t)$ is slid along the time axis so that its first at absolute maximum occurs at the same value of t as the first absolute maximum of $S_o(t)$. Then $S_o(t)$ and $S_1(t)$ have the time relationship shown in Fig. 3.

We define the "detectability", $\delta(\tau)$ to be

$$\delta(\tau) = |C_1(\tau)| - |C_o(\tau)| \tag{32}$$

and compute $\delta(\tau)$ from $\tau = 0$ to $\tau = 6b$. Then the detector performance is computed using the following algorithm:

1. Let $\tau_o = 0$

2. For i = 1, 2,...6 find τ_i such that

$$|\delta(\tau_i)| = \max_{\tau_{i-1} - b/8 \le \tau \le \tau_{i-1} + b/8} |\delta(\tau)| \tag{33}$$

3. Let S + be the set of integers i for which

$$\delta(\tau_i) > \alpha$$

and S - be the set of integers i for which

$$\delta(\tau_i) < \alpha$$

where $$\alpha = \frac{1}{2}\left[\int_{t=0}^{t=6b} S_1^2(t)dt - \int_{t=0}^{t=6b} S_0^2(t)dt\right] \tag{34}$$

Then compute P and Q from

$$P = \max_{i \text{ in } S_+} |\delta(\tau_i)| \tag{35}$$

$$Q = \max_{i \text{ in } S_-} |\delta(\tau_i)| \tag{36}$$

The quantities P and Q are then used in error rate calculations.

Another parameter required for the error rate compilations is ρ, defined as

$$\rho = \sqrt{\frac{1}{2}\left[\int_{t=0}^{t=6b} S_1^2(t)\,dt + \int_{t=0}^{t=6b} S_0^2(t)\,dt\right]} \qquad (37)$$

and computed by this equation. Finally, the ratio P/ρ and Q/ρ are computed and printed out.

2.1.5 Comparison of Variable Names in Text and Computer Program

Table 2.2 shows the variable names in the computer program opposite the corresponding symbols from the text.

2.2 Description of the Computer Error-Rate Calculation (JPL-6)

2.2.1 General Description

This deck is used to compute error rates in digital detection. The error rate is computed on the basis of the detected zero and one signal P and Q, (computed in JPL-4 B), the noise power per unit bandwidth, N_o, and the parameter β, defined by

$$p(a) = \beta e^{-\beta(a-20)} \qquad (38)$$

where a is the head-to-tape spacing, and p(a) is the probability that the head-to-tape spacing will have the value "a".

Table 2.2 Comparison of Varible Names in Text and in Computer Program JPL-4B

Name of Program or Subroutine	Name in Computer Program	Symbol in Text	Number of Equation in which Symbol is Used
Main Program	A	a	14
	ALPH	α	34
	ALPHA	n	15
	C	a_n	15
	CROSS	$C_o(\tau)$	30
	CROSS1	$C_1(\tau)$	31
	D	$a + d'$	14
	DFA	D_n	19
	G	$g/2$	11
	H0	H_o	11
	HMIN	H_1	3
	RESX	$M_a(x_r)$	14
	RESX2	$V_r(t)$	21
	RESX3	$\delta(\tau)$	32
	RHO	ρ	37
	RK	k	16
	B	b_n	15
	SAMPLE 0	$S_o(t)$	24
	SAMPLE 1	$S_1(t)$	28
	X	X_r	21
	Y	y	11
Subroutine MAGCAL3	H	H_x	11
	H0	H_o	11
	RES	$M(x_n, y)$	2
	X	x	11
	Y	y	11
Function DEMAG	A	a	19
	D	$a + d'$	19
	DEMAG	$D_n\ G_n$	19
	GR	$g_r/2$	
	RK	k	19
	RMU1	μ_1	19
	RMU2	μ_2	19
Subroutine DETECT	CROSS	$\delta(\tau)$	32
	PPLUS	P	35
	PMINUS	Q	35
	PP	P/ρ	
	PM	Q/ρ	
	RHO	ρ	37

2. 2. 2 Input - Output

Table 2.3 shows the format of the data cards used for this program. The deep-in-gap magnetic field and the number of bits per inch (both which are input) are not used in the computation but appear in the printed output as an aid to identification of the computed error rate values that are printed out. For each error rate computation, the computer prints out, on a single line, the values of β, N_o, H_o, the bits per inch, and finally, the error rate. The program prints out the values of N_o, β, A (head-to-tape spacing), P/ρ, and Q/ρ, in the order in which they are read in. To permit the computation of a number of error rates, the program returns to read data card No. 4 (in Table 2.3) at the completion of each computation.

2. 2. 3 Error Function Complement

The algorithm for error rate computation employ the computation of the error function complement. The error function complement is computed in the subroutine named ERROR. This subroutine uses algorithms, provided by Abramowitz and Stegun.[1] If the argument exceeds 2. 5, the algorithm of paragraph 7. 1. 26 of this reference is used; otherwise, the algorithm of paragraph 7. 1. 23 is used.

2. 2. 4 Computation of Error Rate

The quantity ER(a) is computed by

$$ER(a) = \frac{1}{4}\left[\operatorname{erfc}\left(\frac{P}{\sqrt{2N_o P}}\right) + \operatorname{erfc}\left(\frac{Q}{\sqrt{2N_o P}}\right)\right] \qquad (39)$$

where the ratios P/ρ and Q/ρ were computed by means of the program deck JPL-4B. Note that ER(a) is a function of a because P and Q are functions of a. Finally, the error rate, ER is computed by

[1] Milton Abramowitz and Irene A. Stegun "Handbook of Mathematical Functions," National Bureau of Standards, Applied Mathematics, Series No. 55, June 1964 pp. 298-299.

$$ER = \int_{a=20}^{a=a_1} p(a)\,ER(a)\,da + \frac{1}{2} e^{-\beta(a_1,-20)} \qquad (40)$$

where $\rho(a)$ is given by Eq. (38), ER(a) is given by Eq. (39) and a_1 is the head-to-tape spacing beyond which errors occur even in the absence of noise. The first term on the right of Eq. (40) is the probability that noise will cause error, and the second term on the right of this equation is the probability that error will result only from excessive head-to-tape spacing. This integration is carried out in the computer program by use of the trapezoidal rule.

2.2.5 Comparison of Variable Names in Text and in Computer Program (JPL-6)

Table 2.4 gives the names used in computer program JPL-6 for the variables used in the above discussion of the error rate computation.

Table 2.3 Data Card Description for JPL-6 Computer Program

Data Card No.	Format	Variable	Type	Description
1	8I10	NN	INTEGER	This is the number of values of N_o to use in the computation.
		NEX	INTEGER	This is the number of values if β (see Eq. 38)) to be used in the computation.
2	8F10.0	RNO	REAL	This is an array that contains the values of N_o to be used.
3	8F10.0	EX	REAL	This is an array that contains the values of β to be used.
4	8F10.0	HO	REAL	This is the value of the deep-in-gap field.
		BPI	REAL	This is the number of bits per inch to which the computation pertains.
5	8I10	NA	INTEGER	NA is the number of value head-to-tape spacing to be used in this computation.
6	8F10.0	A		This is an array that contains the head-to-tape spacing used in this computation.
7	8F10.0	P	REAL	P is an array that contains the values of P/ρ (see Eq. (39)) for the values of head-to-tape spacing just read in.
8	8F10.0	Q	REAL	Q is an array that contains the value of Q/ρ for the values of head-to-tape spacing read in.

Table 2.4 Comparison of Variable Names in Text and in Computer Program JPL6

Name in Computer Program	Symbol in Text
A	a
ERFCP	$\operatorname{erfc}\left(P/(\rho\sqrt{2N_o})\right)$
ERFCQ	$\operatorname{erfc}\left(Q/(\rho\sqrt{2N_o})\right)$
EX	β
P	P/ρ
PA	$P(a)$
PROD	$P(a)\ ER(a)$
Q	Q/ρ
RNO	N_o
SUM	ER

3. 0 PRE-DETECTION STUDIES

3. 1 Absolute Output Voltage Multiplier

With the sole exception of program JPL-2, the original Fourier transform deck, all the computer outputs are now subject to the same calibration factor on voltage.

If the number of turns on the reproduce head is N and the maximum tape remanence is $4\pi M_r$ gauss and the track width is ω mils and the tape velocity is V ips, then the correct output voltage is derived by multiplying the computer output by the factor;

$$6.25 \cdot 10^{-11} \; (N) \; (4\pi M_r) \; (\omega) \; (V)$$

For example if; N = 250 turns, $4\pi M_r$ = 1000 gauss ω = 80 mils and V = 60 ips (these typical figures being close to IBM compatible practice),

$$(\epsilon)_{true} = (\epsilon)_{calc} \; 6.25 \cdot 10^{-11} \; . \; 250 \; . \; 1000 \; . \; 80 \; . \; 60$$

or

$$(\epsilon)_{true} = (\epsilon)_{calc} \times 7.5 \cdot 10^{-3} \text{ volts}$$

Since $(\epsilon)_{calc}$ is approximately 1 unit, we have $(\epsilon)_{true} \simeq 7.5$ milli-volts for this example.

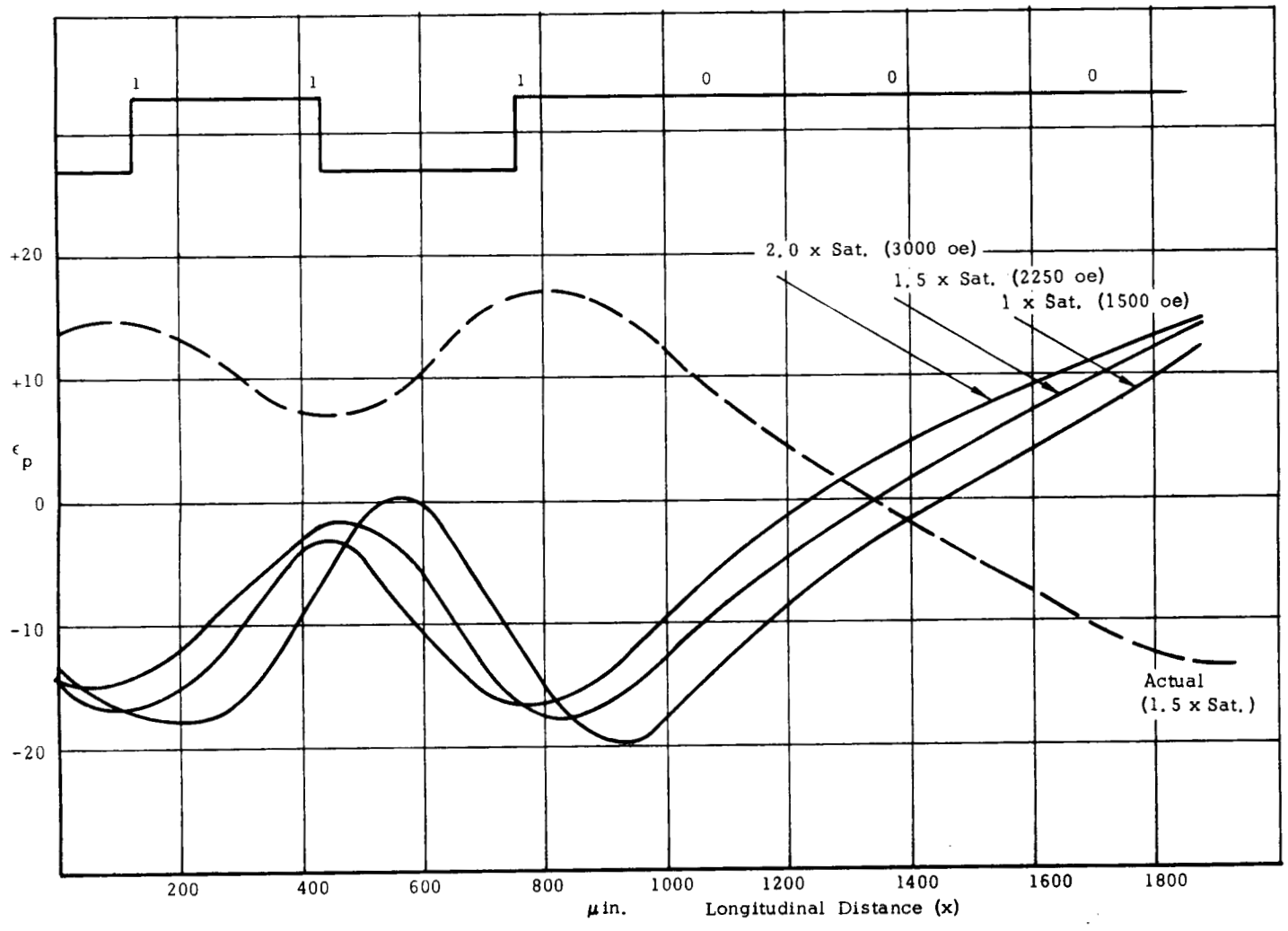

Fig. 5 Output From 1 1 1 0 0 0 (NRS) at 3200 BPI

As another example, let us consider an audio recorder of the type used in the calculation of the noise power figures.* Here we will typically have; N = 1000 turns, $4\pi M_r$ = 1250 gauss, ω = 50 mils, V = 10 ips, which yields a conversion factor of $4.\ 10^{-4}$. The tape background noise level of 10^{-11} units^2/cycle thus becomes $10^{-11}\ (4.10^{-4})^2$ volts^2/cycle which equals 160 (nanovolts)^2/cycle.

Finally, it must be remembered that none of the programs include any allowance for the well-known flux "shunting" effects in reproduce heads. Since typical head efficiencies (i. e., the ratio of flux threading the output coil to total tape flux) are approximately 20 to 40%, the computer outputs may be anticipated to be proportionately high.

3. 2 Comparison of the Fourier Series Program Output Voltage with Experiment

A test was made of the ability of the six bit program (Fourier Series) to duplicate pulse crowding or bit interaction effects correctly. Typical results at 3200 BPI are shown in Fig. 5, where the reproduce head output voltage for the six bit NRZ work 111000 is plotted against tape longitudinal distance for three values of the deep gap record field (H_o = 1500, 2250 and 3000 oe). Other parameters in the calculations, which correspond closely with the actual case shown dotted, are:

head to tape spacing	$a = 20\ \mu"$
tape coating thickness	$d = 400\ \mu"$
record gap length	$g_{rec} = 500\ \mu"$
reproduce gap length	$g_{reprod} = 250\ \mu"$
range of switching fields	$H_1/H_2 = 100/500$ oe
permeabilities	$\mu_1/\mu_2 = 5/2$

*See section 4.

It will be observed that all the essential features of the actual signal are reproduced by the computer. A small discrepancy is apparent in that the 2. 0 X SAT computer curve matches the actual curve better than the 1. 5 X SAT curve which should show the best match. The computer is in fact slightly underestimating pulse crowding. At BPI less than about 2000, pulse crowding is due simply to the superposition of adjacent pulses. At BPI greater than 2000 as is the case here, additional pulse crowding, due to the interference of the record zones, occurs. Such crowding is , of course, non-linear and non-super-imposable, and is dependent critically upon the record gap length, record deep gap field and the specific record head field function being used. The present computation error is most probably due to the use of the Karlquist head field expressions.

No additional work upon the problem will be performed during the present contract. It may be safely concluded that no worse match than that shown will occur, for any bit pattern, providing the BPI < 3000 for the 400 μ" thick media or BPI < 6000 for the 200 μ" media.

A more exhaustive program of experimental validation was undertaken as an extension to the work reported here. The details may be found in Appendix II. Suffice it to say that, upon such close examination, the program was found to be useable to higher bit densities than indicated above. In the saturation record level case, the program is good to at least 5, 000 BPI; at lower record levels, (which would be used) good agreements are found to be at least 10, 000 BPI.

3.3 The Effect of Record Current Finite Rise Times

A test was made of the effect of non-zero record current (or more pertinently record field) rise times. This investigation was made for the reason that the actual experimental waveforms, taken at a tape speed of 75 IPS, used a waveform generator with 0.5 μ sec rise time. The rise distance along the tape is thus 37 μ", to which may be added perhaps another 30μ" due to the limited frequency response (eddy currents) of the record head structure. The total rise distance of the record field is then probably about 70 μ", which is an appreciable fraction of the bit length at 3200 BPI (315 μ"). It was felt to be worthwhile to establish that the rise time effect was not contributing to the discrepancies observed.

The Fourier Series program was modified to permit exponential behaviour of deep gap field (see Fig. 6 below).

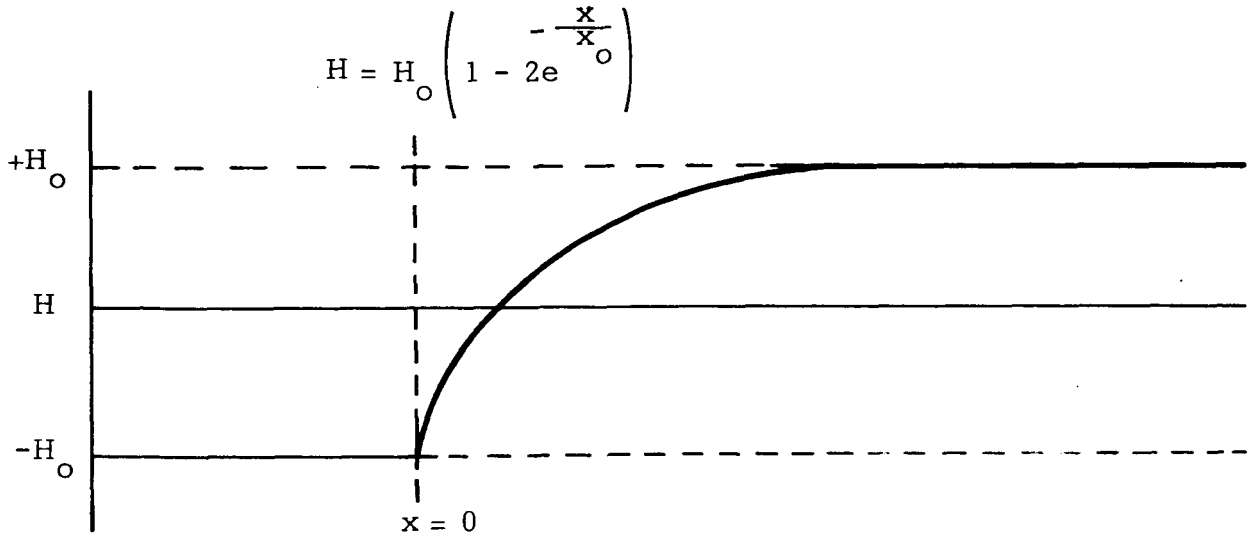

Fig. 6 Exponential Behavior of Deep Gap Field

The factor x_o is simply the exponential time constant multiplied by the tape velocity. Because mathematical complications arise if the rise distance is long compared to the bit interval, the program is restricted to $x_o \leq 1/2$ X BPI. Figure 7 shows two waveforms produced for the six bit word (NRZ) - 111000 at a deep gap field H_o of 1500 oe with two rise distances, 0 and 156 μ". The latter distance is one-half the bit interval at 3200 BPI.

It will be observed that, apart from a phase shift, wherein the finite rise distance case is moved upstream on the tape with respect to the zero rise distance case, there is indeed very little effect. It is concluded, then, that providing the rise distances are not sufficiently long to cause severe "staircasing" (i. e., incomplete switching) of the record field, the effects are negligible.

This conclusion is not surprising, in view of our previous finding that the isolated pulse output waveform was virtually independent of the precise (saturation) recording conditions. The written transition relaxes (i. e., demagnetizes) and retains little information at wavelengths less than the coating thickness. A corollary of this conclusion is that, of course, nothing useful can be gained by any of the more or less elaborate schemes of pre-shaping the input record current.

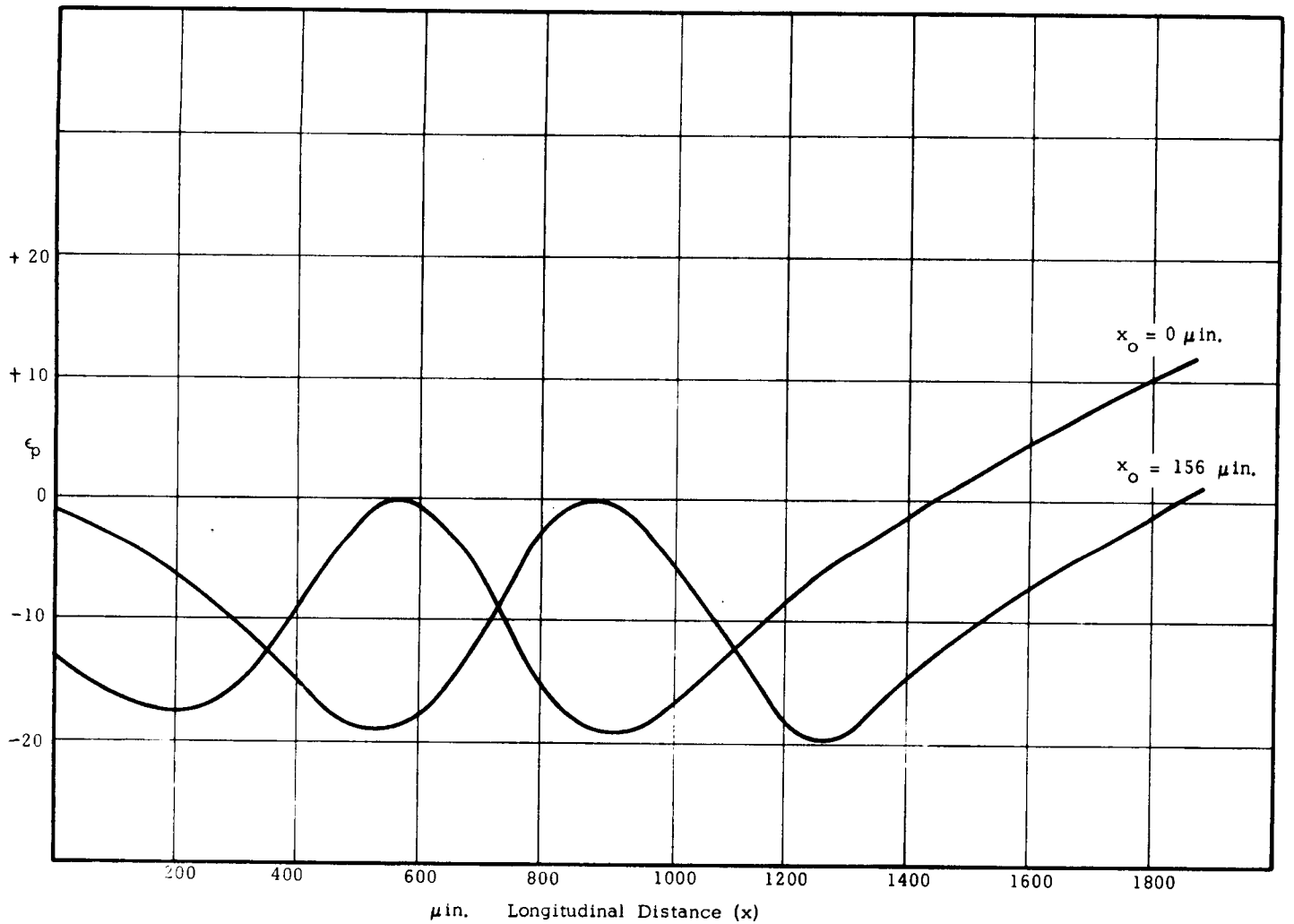

Fig. 7 Effect of Varying Rise Distance Upon 1 1 1 0 0 0 (NRZ) at 3200 BPI and at 1 x Saturation

3.4 Output Anomalies

In the course of a series of over 100 runs investigating the peak-to-peak output voltage of an "all ones" pattern on a function of deep gap field (H_o), BPI and head-to-tape spacing, it was found, whenever the record head-to-tape spacing was comparable with the bit interval being used, and whenever the record-head field was below the level required to saturate the tape (8. e., 500 oe contour beyond the the back side of the tape), that the output voltage was an oscillatory function of the deep-gap field. (See Fig. 8 .)

This oscillatory behaviour was not foreseen; neither could any reference to it be discovered in the literature. It was assumed, erroneously that some mistake in the computer program was causing the effect, and nearly ten days (and almost 20 computer runs) were spent examining a variety of possibilities. A slight computer program error was discovered (concerning the algebraic sign of the increments in remanent magnetization acquired by tape elements) but rectification of this fault did not stop the oscillations. It was finally found, by hand claculation, that the oscillations occur as a direct consequence of the noninteracting remanence loop model [see MTPR #1, (Eq. 1)]. The phenomenon only occurs when several field reversals occur during the time (or distance) that a tape element is passing through the critical range of field strengths (H_1 and H_2) on the downstream side of the record head.

It is not known, at this time, whether such oscillation really occurs in practical systems. A point worth noting is that it is predicted to occur only under conditions where the output signal is already at least 20 db (factor of ten) below the peak level possible. It may, therefore, have easily escaped observation. The whole phenomenon is closely related to the old hi-fi buff's technique of d. c. erasing tape with a "horse shoe" permanent magnet which is placed obliquely against the tape. In this case, the tape experiences a large longitudinal field, followed by a smaller field in the opposite direction, and can thus be left with zero remanence.

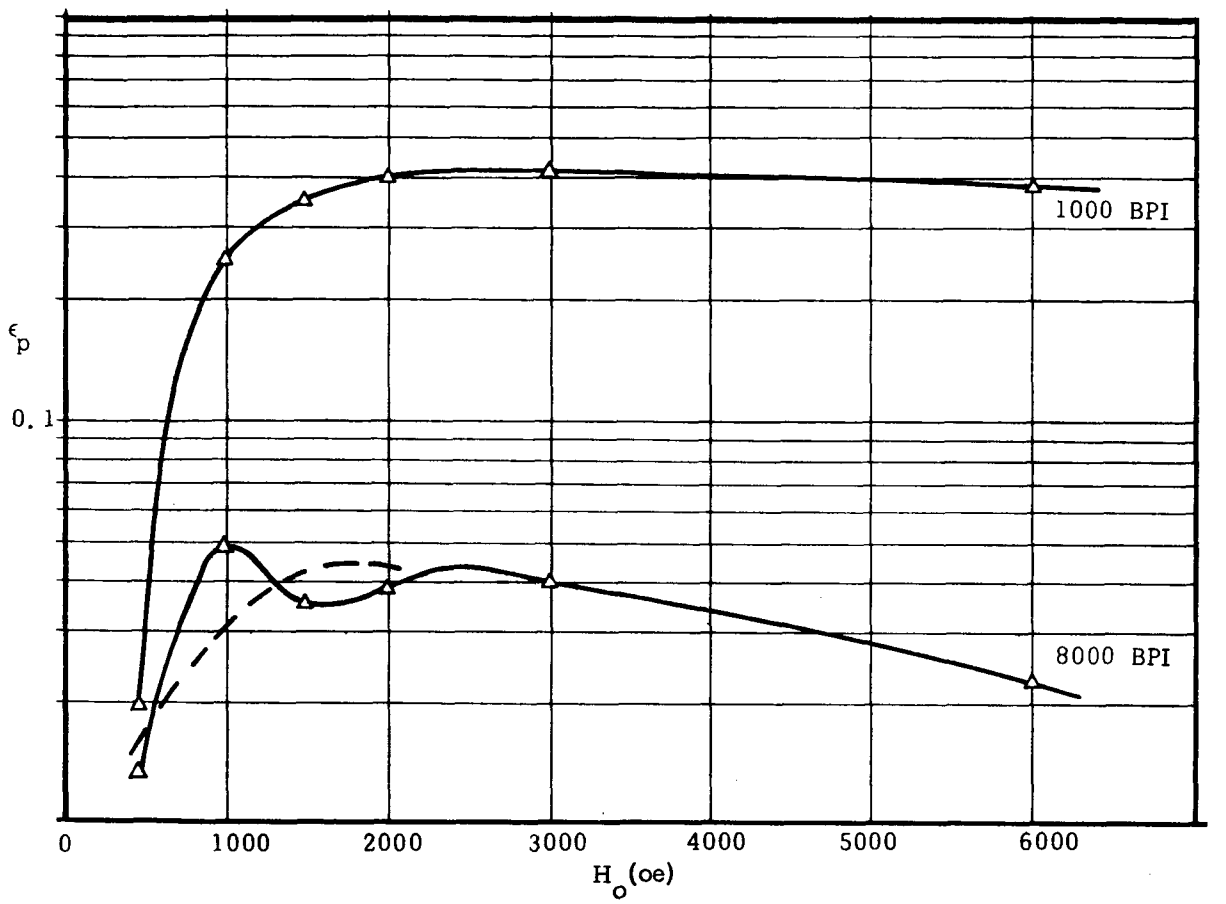

Record Head-to-Tape Spacing = 50 μin.
Reproduce Head-to-Tape Spacing = 50 μin.
Coating Thickness = 200 μin.
Record Gap Length = 150 μin.
Reproduce Gap Length = 25 μin.
Tape Switching Fields = 100/500 oe
Permeabilities = 4/2
Six Bit Word - All Ones NRZ(M).

Fig. 8 Output Voltage Versus Deep Gap Field

It is of interest that if the non-interacting M_r-H model were to be replaced by an empirical model of remanence acquisition, the effect would still persist.

It is concluded, then, that the effect calculated most probably would be found in practice but is not of any great consequence. It was decided, therefore, to leave the computer program unaltered.

3.5 Modification of the Program to Correct the Depth of Recording

It will be recalled that after each lamina of tape has been recorded upon, the next step in the computer program is the computation of the average magnetization;

$$\overline{M} = \frac{1}{d'} \int_a^{a+d'} M \, dy \quad \text{(See section 2.1)}$$

The points of concern here are the value of the upper limit of integration $(a+d')$ and the effective tape thickness d' to be used when the whole depth of the coating is not completely magnetized (i.e., saturated).

Previously, this effective tape depth (d') has been calculated according to the smaller of

$$d' = d$$

or $a + d'$ = depth of 100 oe contour on head center plane.

Thus any material which did not experience even the minimum switching field (100 oe) was merely ignored throughout the remainder of the calculation. This procedure obviously gives the maximum reasonable value for d'. The minimum reasonable value would be given by ignoring all material which is not saturated, i.e.:

$d' = d$

or, $a + d'$ = depth of 500 oe contour

It will be appreciated that much of the remaining program is critically dependent (at low values of the deep-gap field H_o) on the particular criterion chosen. This occurs mainly because the demagnetization and remagnetization processes are very sensitive to the product k d (or k d') (see page 5, MTPR #3). The old criterion (100 oe contour depth) led to the pulse width being almost independent of deep-gap field (see Table IV, page 5, MTPR #3), because even at H_o = 500 oe, the 100 oe contour still penetrates a 200 μ" coating completely. The result is the over-estimation of pulse crowding at low record currents.

Obviously no single correct criterion can be decided upon. This unfortunate situation is forced upon us by our desire to use the closed form solutions of the demag-remag problem. The alternative procedure using iteration is believed to be of virtually astronomical magnitude (200 x 200 calculations per bit cell per iteration).

It has been decided to resolve this problem by using an "engineering" approximation. The effective depth shall be considered to be half way between the maximum and minimum values possible; i. e., we take d' to be the smaller of

$d' = d$

or $a + d'$ = depth of the 300 oe contour

It is noted, in passing, that Kostyshyn (IEEE Trans. Mag. 2 3, page 236, Sept. 1966) assumed the minimum reasonable depth. In other words, he ignores completely the partially magnetized material.

3.6 Head to Tape Spacing Effects

Previously, investigations have been made (see MTPR #2 and 3) of the effects of varying the head-to-tape spacing on the amplitude (and 20% pulse width) of isolated transitions. Here we report similar data applied to the case of repetitive transitions. The six-bit word chosen is "all ones" (NRZ) i.e., the record current changes sign after each bit interval. It will be realized that, even though an isolated pulse is insensitive to head-to-tape spacing because it is not rich in harmonics of wavelength shorter than the coating thickness, this simple conclusion need not hold in the repetitive pulse case. Here all the low [<2/BPI] harmonics are forbidden and only the high harmonics, which are very sensitive to head-to-tape spacing remain. Typical data is shown in Fig. 9, in which figure is shown the output voltage, at 8000 BPI, versus deep-gap field, for four cases;

a) record and reproduce spacing = 100 μ"

b) record spacing = 100 μ", reproduce spacing = 20 μ"

c) record spacing = 20 μ", reproduce spacing = 100 μ"

d) record and reproduce spacing = 20 μ"

The curves are labeled (a_1, a_2) where a_1 is the record-head spacing and a_2 is the reproduce-head spacing.

Several comments may be made about these results.

a) Any spacing greater than the standard 20 μ" at either head causes losses which cannot be recovered completely by adjustments of H_o.

b) Whenever the record head-to-tape spacing is large, some recovery of signal is possible by increasing the record current (i.e., H_o). Note that the (100, 20) and (100, 100) curves both peak at $H_o \simeq 3500$ oe, whereas (20, 20) and (20, 100) both peak at $H_o \simeq 1500$ oe. This recovery of signal is approximately 6 db, where as the loss of signal due to 100 μ" record-head spacing is approximately 10 db.

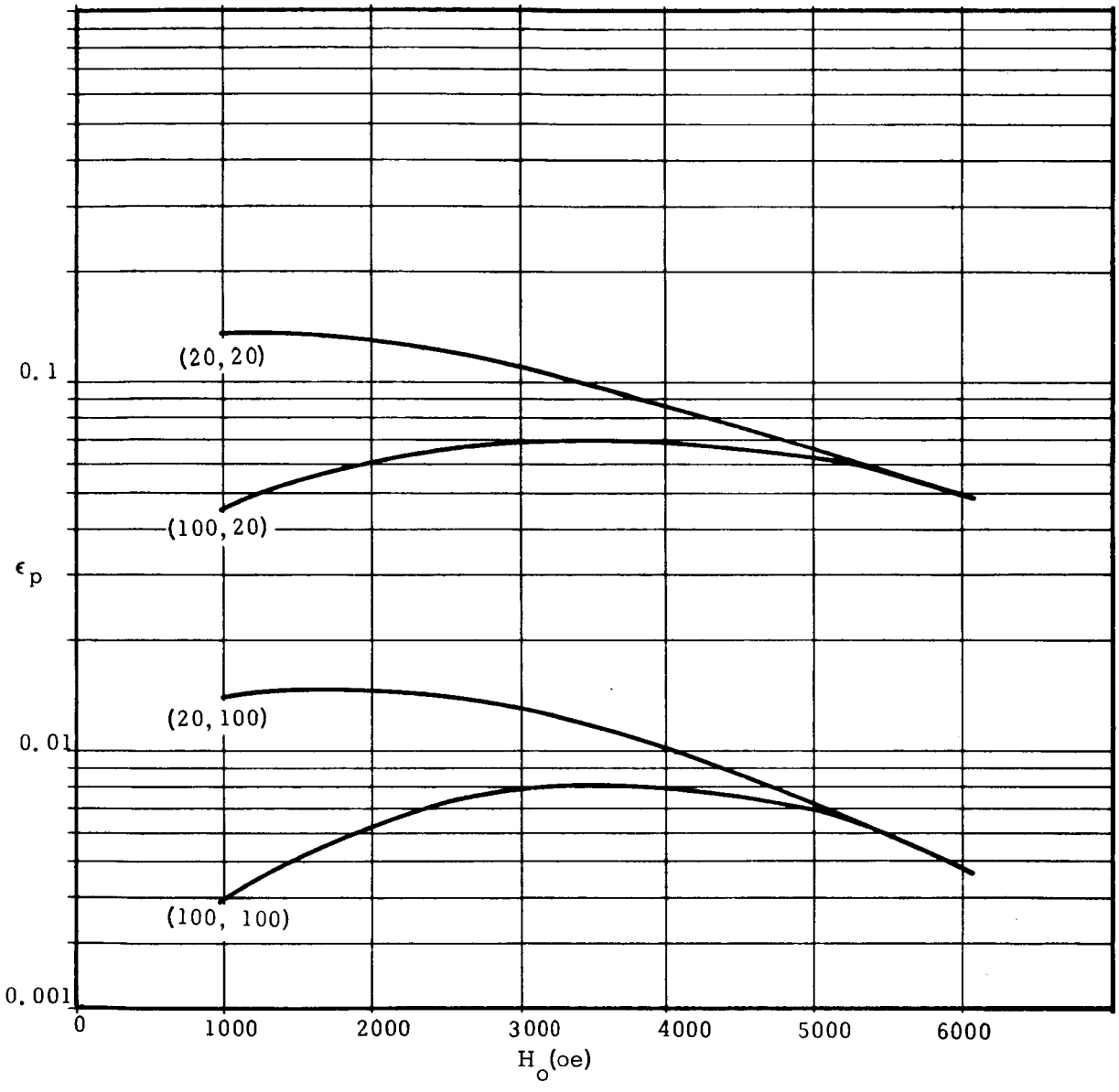

Head-Tape Spacing as noted. 8000 BPI 111111 NRZ
d = 200 μin. H_1/H_2 = 100/500 oe
g_{record} = 150 μin. μ_1/μ_2 = 4/2
g_{reprod} = 25 μin.

Fig. 9. Output Voltage Versus H_o at Various Head Tape Spacings

c) Whenever the reproduce head-to-tape spacing is large, a very large loss in signal occurs. This signal loss is approximately 20 db regardless of the record current level. This is not unexpected, since at 8000 BPI the output signal is almost purely sinusoidal, of wavelength 250μ", and consequently the increase in reproduce spacing loss is:

$$\frac{55\left[(a_2)_1 - (a_2)_2\right]}{\lambda} = \frac{55\left[100 - 20\right]}{250} = 17.5 \text{ db}$$

We conclude, therefore, that at high bit densities the "uncompensated" record-head spacing loss is about one third the reproduce spacing loss. If the record current is readjusted, the "compensated" record-head spacing loss need only be about one fifth the reproduce spacing loss. The reproduce spacing loss is closely approximated by the usual 55 a/λ type expression.

3.7 Pulse Crowding Graphs

As called for in the contract, sufficient computer runs have been made to derive graphs of output voltage versus bit density. Each of the graphs shows the computer peak output voltage (i. e., not adjusted to yield absolute volts) versus deep gap field for five bit densities, those corresponding to 500, 1000, 2000, 5000 and 10,000 BPI respectively. The data is shown in Figs. 10 through 13 each figure applying to a different pair of heads. In Fig. 10, the record gap is 250 μ", the reproduce gap zero, Fig. 11 250, 75 μ", Fig 12, 150, 0, and Fig. 13, 150, 75μ". The head-to-tape spacing on all runs was equal to 20 μ" (the nominal contact value), the tape coating thickness was 200 μ", the range of switching fields 100/500 oe and permeabilities 4/2. An additional piece of information, included in all the graphs, is whether or not super-position (of output pulses) applies or not. Super-position only applies when the original recorded magnetization patterns are completely separate and distinct, and thus pulse crowding (or bit interaction) only occurs during the (linearly super-imposable) demagnetization, remagnetization, flux collecting and differentiating processes.

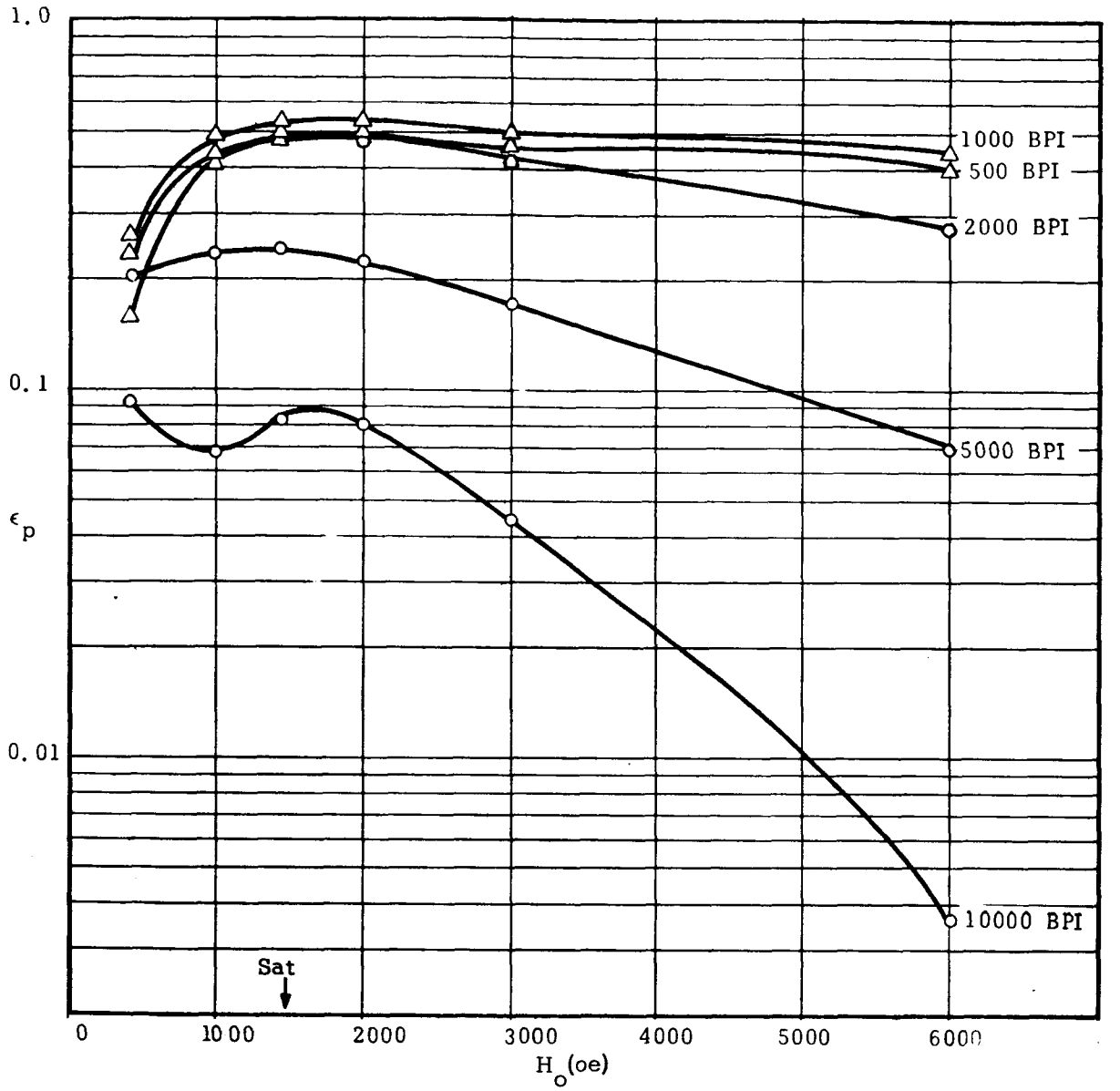

a = 20 μin. H_1/H_2 = 100/500 μ_1/μ_2 = 4/2

d = 200 μin. H_o variable as noted

g_{record} = 250 μin. BPI variable as noted

g_{reprod} = 0 μin.

All-ones pattern - peak voltage noted.

△ superposition valid

○ superposition invalid

Fig. 10 Pulse Data Crowding

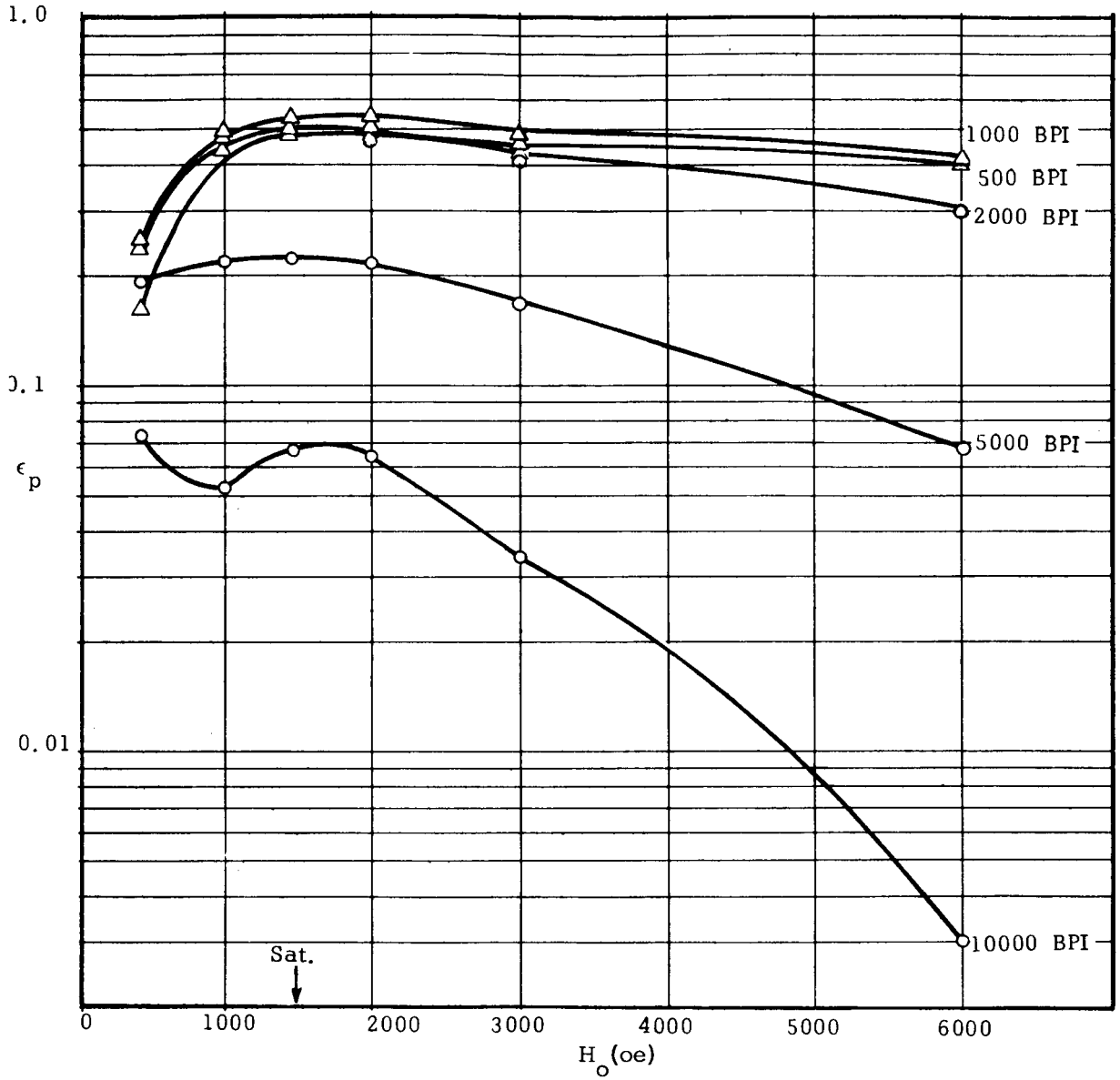

a = 20 μin.

d = 200 μin.

g_{record} = 250 μin.

g_{reprod} = 75 μin.

H_1/H_2 = 100/500

μ_1/μ_2 = 4/2

Δ Superposition valid

○ Superposition invalid

Fig. 11 Pulse Data Crowding

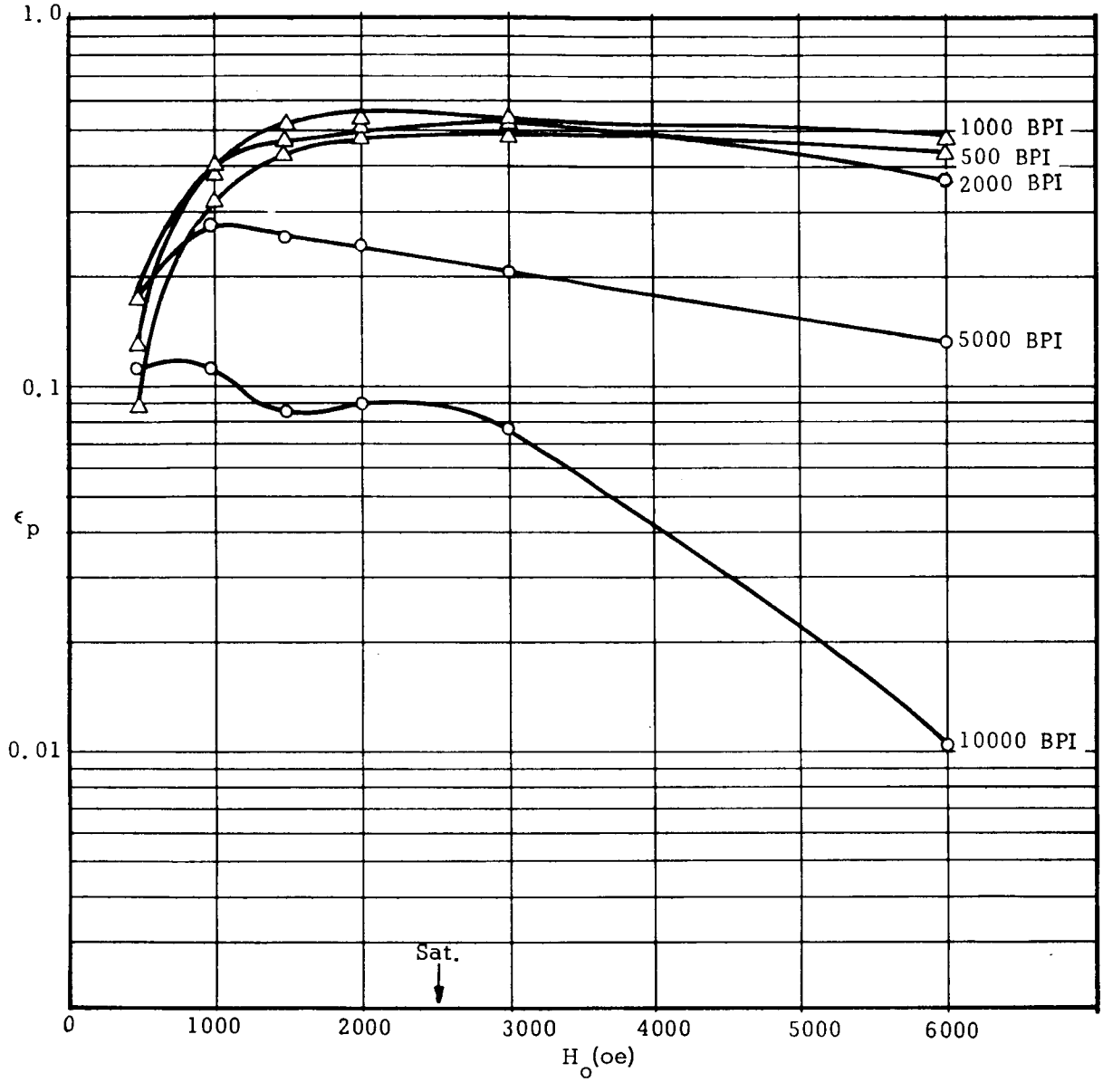

a = 20 μin.

d = 200 μin.

g_{record} = 150 μin.

g_{reprod} = 0 μin.

△ Superposition valid

○ Superposition invalid

H_1/H_2 = 100/500 μ_1/μ_2 = 4/2

Fig. 12 Pulse Crowding Data

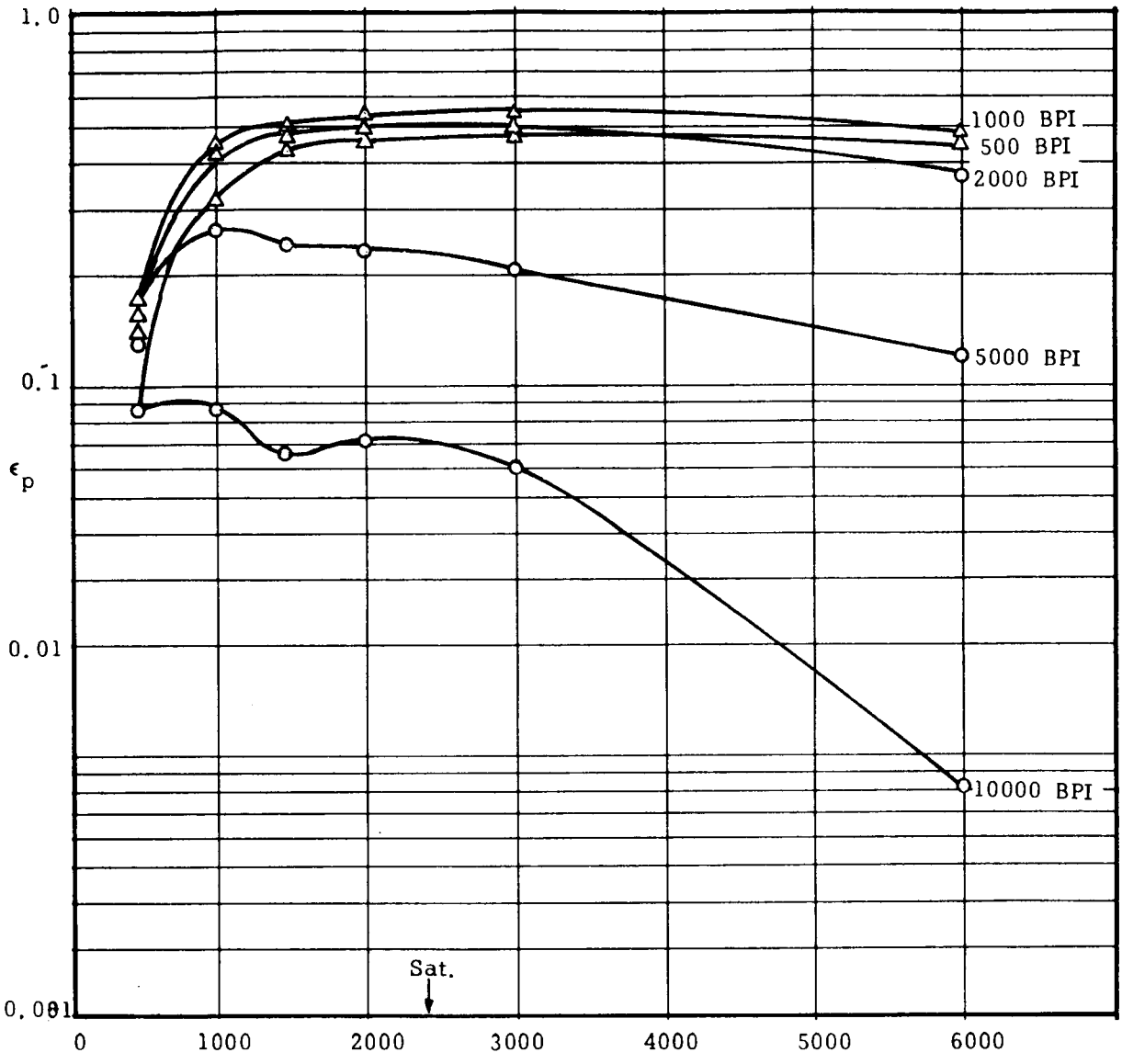

a = 20 μin. H_1/H_2 = 100/500 oe μ_1/μ_2 = 4/2

d = 200 μin.

g_{record} = 150 μin.

g_{reprod} = 75 μin.

△ superposition valid

O superposition invalid

Fig. 13 Pulse Crowding Data

The following comments may be made.

a. In all cases the effects of bit crowding do not become severe until above 2000 BPI. This "break point" is, with standard γFe_2O_3 tape, principally dependent upon the coating thickness used. If standard digital 400 μ" thick tape were to be substituted for the present 200 μ" tape, the effects of crowding would then become severe above 1000 BPI.

b. Very little difference is to be noted at deep gap fields near the saturation level between the record gap equals 250 μ" and 150 μ" data. This is, of course not unexpected.

At low bit densities, the output voltage is governed almost entirely by the demagnetization effects discussed in MTPR #1. The details of the recording process are essentially forgotten.

At high bit densities the recording takes place in a narrow zone downstream of the record gap center line (trailing edge effect). The geometry of this zone is not simply related to the record gap length. It is a function of the deep gap field, the depth into the tape, the tape particle switching fields, as well as the gap length.

The only region in which appreciable differences occur between the two record gap lenghts is at very high record levels (greater than two times saturation) and very high BPI. It will be noticed that, at H_o = 6000 oe and at 10,000 BPI, the g_{record} = 250 μ" data is about a factor of three (10 db) lower than in the 150 μ" case.

We may conclude that smaller gap lengths are better only in poorly designed regions of operation.

c. As was mentioned in MTRP #4, at the higher BPI's, it pays increasing dividends to operate below the saturation (i. e., self-erasing) level.

d. Super-position is valid for all the 500 and 1000 BPI data.

At 2000 BPI the 250 μ" record gap data is not super-imposable above 1500 oe deep gap field. The 150 μ" record gap data is super-imposable at 3000 oe deep gap field.

Above 2000 BPI neither head yields super-imposable results at any deep gap field.

e. The effect of reproduce gap is seen to be very slight in the region investigated. The zero length gap obviously will show no interference effects, the 75 μ" case will have a null at λ = 75 μ", corresponding to 26, 666 BPI and will show negligible gap losses below λ = 150 μ" (i. e., 13, 333 BPI). This is borne out in the data where even at 10, 000 BPI there exists less than 2 db difference.

A practical rule emerges concerning the selection of reproduce gap lengths. The gap length should be as large as possible but no larger than the smaller of:

a. the thickness (low BPI limit)

b. 4/BPI (high BPI limit)

3.8 Peak Shift Calculation

In accordance with the contract, calculations of peak shift have been made. The computer recorded a single pair of transitions under the following conditions:

Coating thickness	d = 200 μ"
Head-to-tape spacing	a = 20 μ"
Switching fields H_1/H_2	= 100/500 oe
Permeabilities μ_1/μ_2	= 4/2
Record gap Reproduce gap	as noted
Deep Gap field	as noted
Bit pattern	0 0 1 1 0 0 NRZ

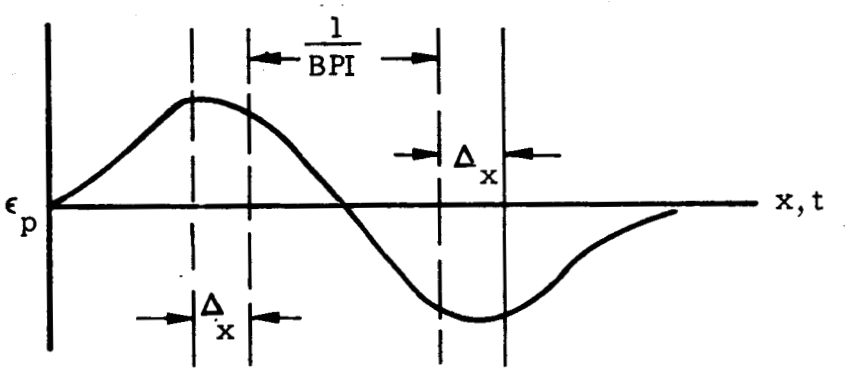

Percentage peak shift equals 100 Δx/BPI

Table 3.1 Percentage Peak Shift as a Function of BPI, Deep Gap Field, Record and Reproduce Gaps

BPI	H_o	$g_{record} = 150$ $g_{reproduce} = 75$	150 0	250 75	250 0
2,000	500	0.15	--	--	0.25
	1500	0.5	0.65	0.75	0.75
	3000	1	0.55	1.6	1.75
5,000	500	1.4	0.9	4.0	2.7
	1500	10.0	9.0	12.2	11.0
	3000	14.0	13.5	18.8	17.5
10,000	500	12.6	7.5	23.2	17.1
	1500	37.7	32.5	39.1	34.2
	3000	43.8	39.0	142.0	151.0

Several, not unexpected, trends are evident:

a. The percentage peak shift increases with increasing BPI.

b. The percentage peak shift increases with increasing deep gap field.

c. The percentage peak shift increases with increasing record gap field.

d. The percentage peak shift increases with increasing reproduce gap length.

The practical rules which emerge are:

a. Peak shift is negligible below 2000 BPI.

b. In the neighborhood of 5000 BPI the use of saturation* record current leads to peak shifts of order 10% - 20%, the precise value being dependent upon the gap lengths used. The peak shift can be rendered negligible (< 5%) by adjusting the record current appropriately.

c. In the neighborhood of 10,000 BPI the use of saturation* record currents leads to large peak shifts (>30%). The use of two times saturation currents causes over 100% peak shift. The situation may be largely corrected, however, by the combination of smaller record gaps (<150μ") and lower record currents (about one-third of saturation).

*Saturation means self erasing (H_o = 1500 oe for record gap = 150 μ"
(H_o = 2350 oe for record gap = 250 μ")

4.0 DETECTION OF SIGNALS OF KNOWN SHAPE IN THE PRESENCE OF WHITE GAUSSIAN NOISE

4.1 Signal Representation

4.1.1 Restrictions

We consider only signals of finite duration T and finite bandwidth W.

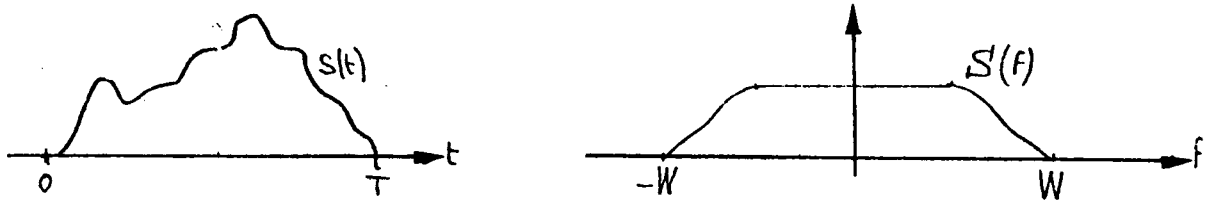

In this case the signal s(t) is completely described by a finite set of points.

4.1.1 Sampling Theorem

Fourier integral: $s(t) = \int_{-\infty}^{+\infty} S(f) e^{j2\pi ft}\, df$

The signal is bandlimited; the spectrum can be developed in Fourier series:

Complex Fourier coefficients (C_n^* : conjugate of C_n):

$$C_n^* = \frac{1}{2W} \int_{-W}^{W} S(f) e^{+j2\pi n\tau f}\, df; \quad \tau = \frac{1}{2W}$$

Comparing with the Fourier integral of s(t):

$$s(n\tau) = \int S(f) e^{j2\pi fn\tau}\, df = 2W \cdot C_n^*$$

The spectrum is determined by the values $s(n\tau)$, and from the spectrum the time-function s(t) can be computed. We need only know sampled values $\tau = \frac{1}{2W}$ seconds apart to reconstruct the complete signal. Since the signal is of duration T, s(t) is given by a set of $T/\tau = 2WT$ points. The signal could be represented by a point in a 2WT-dimensional space.

4.1.3 Ideal Lowpass

We determine the impulse response of an ideal lowpass:

$$h(t) = \frac{1}{2W} \int_{-W}^{W} e^{j2\pi ft}\, dt$$

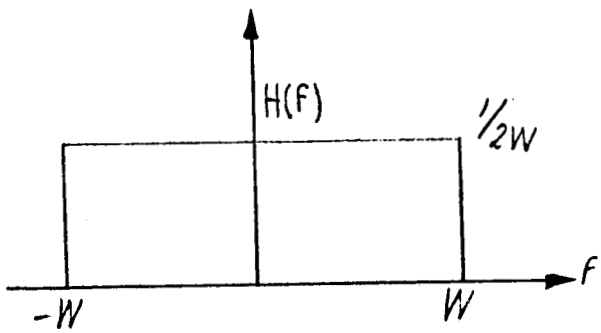

$$h(t) = \frac{\sin 2\pi Wt}{2\pi Wt}$$

4.1.4 Representation of s(t)

$$s(t) = \sum_n s(n\tau)\, h\,(t - n\tau)$$

$$= \Sigma\, s(n\tau)\, \frac{\sin 2\pi W(t - n\tau)}{2\pi W(t - n\tau)} \qquad \tau = \frac{1}{2W}$$

Total number of points: 2WT

$$s(t) = \sum_{n=1}^{2WT} s_n \frac{\sin \pi(2Wt-n)}{\pi(2Wt-n)} \qquad (4.1)$$

That this represents the signal s(t) is readily seen:

-The constructed signal consitsts of a superposition of impulse responses from a lowpass filter of bandwidth W; hence s(t) has a bandwidth W.

-For $t = m \cdot \tau = m \cdot \frac{1}{2W}$ equation (1) becomes an identity.

The functions $q_n = \frac{\sin \pi (2Wt-n)}{\pi (2Wt-n)}$ constitute a set of orthogonal functions:

$$\int_{-\infty}^{+\infty} q_n(t) q_m(t)\, dt = \begin{cases} 0 & n \neq m \\ \frac{1}{2W} & = m \end{cases} \qquad (4.2)$$

Proof:

Parceval's equation: $\int_{-\infty}^{+\infty} q_n(t)\, q_m(t)\, dt = \int_{-\infty}^{+\infty} Q_n(f) \cdot Q_m^*(f)\, df$

*) conjugate value

$q_n(t) = h(t-n\tau)$ $\qquad Q_n(f) = H(f) \cdot e^{j2\pi fn\tau}$

H(f): ideal lowpass

$$\int_{-\infty}^{\infty} Q_n(f) \cdot Q_m^*(f)\, df = \frac{1}{2W} \int_{-W}^{W} e^{j2\pi f(n-m)\tau}\, df = \frac{1}{2W} \cdot \frac{\sin \pi (n-m)}{\pi (n-m)}$$

This is $\frac{1}{2W}$ for n = m, 0 else.

4.1.5 Integration of Signals

$s_o(t)$; $s_1(t)$ are two signals with same restrictions as stated in 1.1.

$$\int_{-\infty}^{+\infty} s_o(t)\, s_1(t)\, dt = \int_{-\infty}^{+\infty} \left(\sum_n s_{on} \cdot q_n \right) \left(\sum_m s_{1m}\, q_m \right) dt \qquad \text{(see (4.1))}$$

applying the orthogonality (2):

$$\int_{-\infty}^{+\infty} s_o(t)s_1(t)dt = \frac{1}{2W}\sum_{n=1}^{2WT} s_{on} \cdot s_{1n} \qquad (4.3)$$

$$= \frac{1}{2W}\left[\underline{s_o} \cdot \underline{s_1}\right], \text{ if } \underline{s_o}, \underline{s_1} \text{ are vectors}$$

in the 2WT dimensional space:

$$s_o = \left\{s_{o1}, s_{02}, \ldots s_{o2WT}\right\}; \quad s_1 = \left\{s_{11}, s_{12}, \ldots s_{12WT}\right\}$$

4.2 Signal Detection

4.2.1 Distortion of a Signal by White Gaussian Noise n(t)

$$p(n) = \frac{1}{\sqrt{2\pi}\sigma} e^{-\frac{n^2}{2\sigma^2}}; \text{ spectral density } G_n(f) = N_o$$

In the system signal and noise are assumed to have the same bandwidth W: mean noise power $\overline{n^2} = N_o \cdot W$.

$\overline{n^2}$ equals the variance σ^2.

Since we have white noise, n is statistically independent at different points in time. The probability of a certain deformation x(t) of s(t) is easily computed:

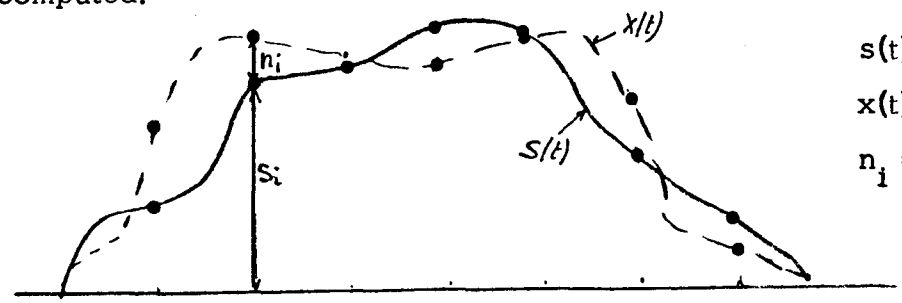

s(t): original signal

x(t): distorted signal

$n_i = x_i - s_i$

If x(t) is represented by the vector $\underline{x} = \left\{x_1, x_2, \ldots x_{2WT}\right\}$, then the probability of the signal being in the interval $\underline{x}$, $\underline{x} + d\underline{x}$ is

$$p(x_1, x_2, \ldots x_{2WT}) \cdot dx_1, dx_2 \ldots dx_{2WT}$$

$$p(x_1, x_2, \ldots x_{2WT}) = \left(\frac{1}{2\pi N_o W}\right)^{2WT/2} \cdot e^{-\frac{1}{2N_o W} \sum_{i=1}^{2WT} (x_i - s_i)^2}$$

The joint probability is the product of the individual probabilities. This holds for white gaussian noise.

4.2.2 Likelihood Test

Given an observation x(t) we have to decide which signal $s_k(t)$ of a given alphabet is the most likely one. Emitting a signal $s_k(t)$, the probability of receiving x(t) is proportional to

$$p(x_1, x_2, \ldots x_{2WT} \mid s_k(t)) = \left(\frac{1}{2\pi N_o W}\right)^{2WT/2} e^{-\frac{1}{2N_o W} \Sigma (x_i - s_{ki})^2} \quad (4.4)$$

Assuming that each $s_k(t)$ is equally likely emitted, we have to choose that s_k, which gives the maximum $p(\underline{x} \mid s_k)$.

Taking the logarithm of (4):

$$C' - \frac{1}{2N_o W} \sum_i (x_i - s_{ki})^2 = C - \frac{1}{2N_o W} \sum_i s_{ki}^2 + \frac{2}{2N_o W} \Sigma x_i s_{ki}$$

C is a constant, independent of index k.

Applying equation (3):

$$\left\{C - \frac{1}{N_o} \int s_k(t)^2 \, dt + \frac{2}{N_o} \int x(t)\, s_k(t) \, dt\right\}_{max} \Longrightarrow s_k$$

Interpretation:

$\int s_k^2(t)\,dt$ = Energy E_k of alphabet signal s_k

$\int x(t)\,s_k(t)\,dt$ = Peak output of a correlator or matched filter.

$\left(\phi_k(\tau) = \int x(t)\,s_k(t+\tau)\,dt;\ \text{Peak} = \phi_k(0)\right)$

Decision criterion:

$$\max_k \left\{ \frac{2}{N_o} \int x(t)\,s_k(t)\,dt - \frac{E_k}{N_o} \right\} \Longrightarrow s_k \qquad (4.5)$$

4.2.3 Error Probability; k = 2

We have to choose between two signals $s_o(t)$, $s_1(t)$. To find the maximum (4.5) we may consider the difference of the two expressions

$$\frac{2}{N_o} \int x(t)\,s_1(t)\,dt - \frac{E_1}{N_o} \quad , \quad \frac{2}{N_o} \int x(t)\,s_o(t)\,dt - \frac{E_o}{N_o}$$

$$u = \frac{2}{N_o} \int x(t)\,(s_1 - s_o)\,dt - \frac{1}{N_o}\,(E_1 - E_o)$$

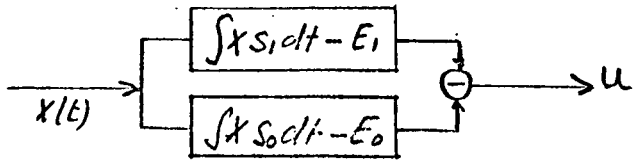

Decision: $u > 0 : s_1$

$u < 0 : s_o$

x(t) can be 1) $x_1 = s_1(t) + n(t)$

2) $x_o = s_o(t) + n(t)$

We make a false decision if:

1) x_1 and $u < 0$

2) x_o and $u > 0$

Both cases are completely symmetric; it suffices to study one. (The chance of having one of the two cases is 50%, because s_o, s_1 has been assumed to be equally likely).

We search for the probability of having x_1 and $u < 0$

$$u = \frac{2}{N_o} \int (s_1 + n)(s_1 - s_o)\, dt - \frac{1}{N_o}(E_1 - E_o),$$

$$= \frac{1}{N_o W} \sum_i (s_{1i} + n_i)(s_{1i} - s_{oi}) - \frac{1}{N_o}(E_1 - E_o) \qquad \{(4.3)\}$$

with

$$\Delta s = s_1 - s_o$$

$$\Delta E = E_1 - E_o$$

$$u = \frac{1}{N_o W} \sum_i (s_{1i} + n_i)\, \Delta s_i - \frac{\Delta E}{N_o}$$

We know the probability density function of the n_i: $p_n(n_i)$; we have to find $p_u(u)$.

u is a linear combination of the random variable n_i; like n_i, u will therefore have gaussian distribution. Mean and variance for u have to be calculated:

$$\bar{u} = \frac{1}{N_o W} \sum_i (s_{1i} \Delta s_i + \bar{n}_i \cdot \Delta s_i) - \frac{\Delta E}{N_o} \quad \therefore \quad \bar{n}_i = 0$$

$$\bar{u} = \frac{1}{N_o W} \sum_i s_{1i} \Delta s_i - \frac{\Delta E}{N_o} = \frac{2}{N_o} \int s_1(t) \, \Delta s(t) \, dt - \frac{\Delta E}{N_o}$$

$$(u - \bar{u})^2 = \left(\frac{1}{N_o W}\right)^2 \Sigma \Delta s_i^2 \overline{n_i^2} \text{ , because } \overline{n_i n_j} = \bar{n}_i \cdot \bar{n}_j = 0$$

$$\overline{n_i^2} = N_o \cdot W$$

$$\sigma_u^2 = \frac{1}{N_o W} \Sigma \Delta S_i^2 = \frac{2}{N_o} \int \Delta s^2(t) \, dt \text{ and}$$

$$p(u) = \frac{1}{\sqrt{2\pi}\sigma_u} e^{-\frac{1}{2\sigma_u^2}(u - \bar{u})^2}$$

The error probability is:

$$ER = \int_{-\infty}^{0} p(u) \, du = \frac{1}{\sqrt{2\pi}\sigma_u} \int_{-\infty}^{0} e^{-\frac{1}{2\sigma_u^2}(u - \bar{u})^2} du$$

Defining $\text{erf}_c(\beta) = \frac{1}{2\pi} \int_{-\infty}^{+\beta} e^{-\frac{1}{2}x^2} dx$ we find

$$ER = \text{erf}_c(\beta) \; ; \; \beta = -\frac{\bar{u}}{\sigma_n} \qquad (4.6)$$

$$\bar{u} = \frac{2}{N_o} \int s_1 \cdot \Delta s \, dt - \frac{\Delta E}{N_o} = \frac{1}{N_o} \int \Delta s^2(t) \, dt$$

$$\sigma_u^2 = \frac{2}{N_o} \int \Delta s^2(t) \, dt$$

$$\beta = -\sqrt{\frac{\frac{1}{2}\int \Delta s^2(t)\, dt}{N_o}} \qquad (4.7)$$

Using (3):

$$\beta = -\frac{1}{2}\,\frac{\sqrt{\Sigma \Delta s^2}}{\sqrt{N_o W}}\,,$$ which can be interpreted as follows:

$\sqrt{N_o W} = \tilde{n}$: rms value of noise

$\sqrt{\Sigma \Delta s^2}$ = "length" of the distance vector $\underline{s_1} - \underline{s_o}$ in the 2WT-dimensional space

Defining $|\Delta e_1|$ and $|\Delta e_o|$ as the peak amplitudes for $x = s_1$, and $x = s_o$ respectively

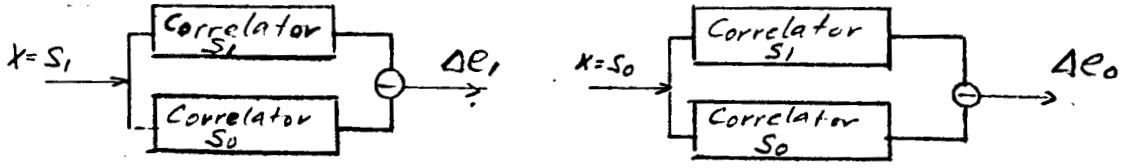

$$|\Delta e_1| = \int s_1 \Delta s\, dt \qquad |\Delta e_o| = -\int s_o \Delta s\, dt$$

$$\frac{1}{2}\left\{|\Delta e_1| + |\Delta e_o|\right\} = \frac{1}{2}\int \Delta s^2 dt$$

$$|\overline{\Delta e}| = \frac{1}{2}\left\{|\Delta e_1| + |\Delta e_o|\right\};$$

(7) yields:

$ER = \operatorname{erf}\beta$, $\quad \beta = -\sqrt{\frac{|\overline{\Delta e}|}{N_o}}$ $\quad |\overline{\Delta e}|$: Detectability

$$\text{erf}_t^{\beta} = \frac{1}{\sqrt{2\pi}} \int_{-\infty}^{\beta} e^{-\frac{1}{2}x^2}\, dx \qquad (4.8)$$

$|\Delta e_1|$ and $|\Delta e_o|$ can be computed from the correlation functions:

$$\phi_{oo}(0) = \int x_o(t)\, s_o(t)\, dt \qquad \phi_{10}(0) = \int x_1(t)\, s_o(t)\, dt$$

$$\phi_{o1}(0) = \int x_o(t)\, s_1(t)\, dt \qquad \phi_{11}(0) = \int x_1(t)\, s_1(t)\, dt$$

$$|\Delta e_1| = |\phi_{11}(0) - \phi_{10}(0)|; \qquad |\Delta e_o| = |\phi_{oo}(0) - \phi_{01}(0)|$$

$x_o(t)$, $x_1(t)$ are the actually received signals for a "0" and a "1" respectively.

4.3 Concerning Dropouts: Conclusions and Plan of Action

(a) The differences in drop-out behavior are sufficiently great between different reels of tape to preclude any meaningful statistical analysis. This comment applies even if one restricts testing to samples of one manufacturer, or indeed, to samples slit from the same original doff.

(b) The drop-out count on any one reel of tape is extremely dependent upon the method of testing. Track width, head contours, tape tension, tape speed are all factors which can alter the drop-out count by several orders of magnitude.

(c) There exists evidence that, despite the foregoing, the actual drop-out behavior observed on some particular sample of tape being tested in some particular manner, is almost 100% repeatable between consecutive runs. By far the majority (>90%) of drop-outs occur at specific tape

locations and can, upon microscopic examination, be associated with physical defects. The number and position of such defects change only slowly with repeated passes of the tape. It is, therefore, reasonable to assume, in the computer-simulation of drop-out behavior, that the head-to-tape spacing is perturbed equally during both the record and reproduce cycles.

(d) In fact, there is no physical distinction between drop-outs and the so-called surface noise. The complete noise spectrum of tape shows broad-band, almost white noise to which is added, at low frequencies, surface noise. A drop-out is nothing more or less than an instance of the surface noise exceeding some arbitrary level and/or duration.

For the purpose of computation, however, it is a great simplification to assume that the drop-outs are long in duration compared to the six bit word. This means that the head to tape spacing may be considered to be constant during the whole six bit word calculation. This simplification which will be adopted for the remainder of this programe is shown below

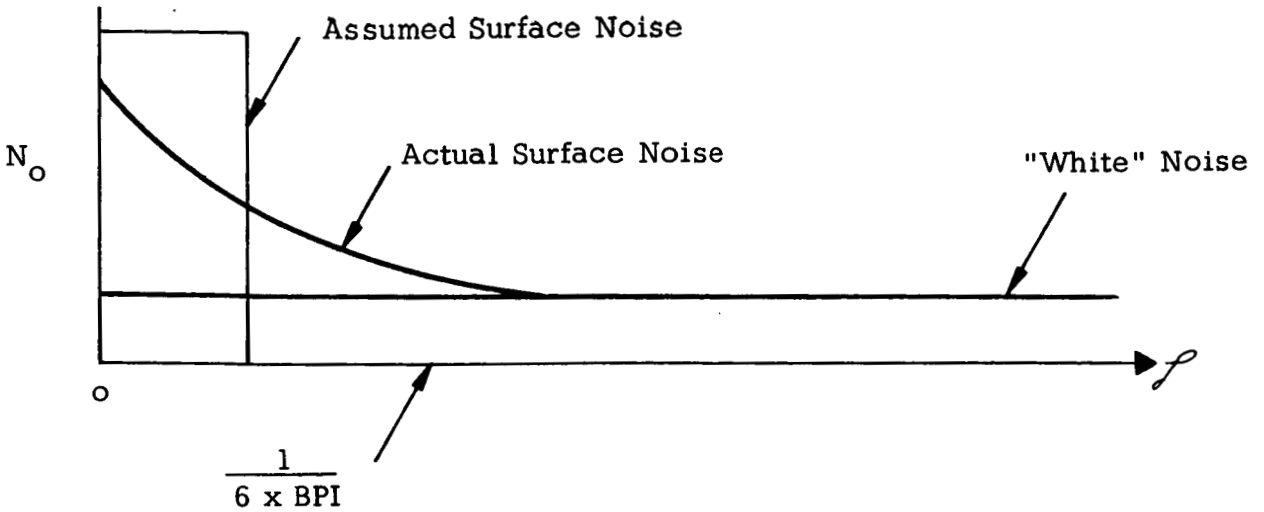

(e) Similarly, while there is no a priori physical justification for assuming that a drop-out extends uniformly across the whole track width, such will be assumed in the computer program. This is, of course, a considerably more restrictive assumption than that in (d) above. Intuitively one expects the longitudinal and transverse dimensions of a drop-out to be comparable. What we are really presuming here is that an effective head-to-tape spacing exists, in which the tape and head planes are exactly parallel for dimensions greater than the track width. The validity of this approximation will shortly be tested (see below).

(f) We seek a typical probability density versus effective head to tape spacing curve.

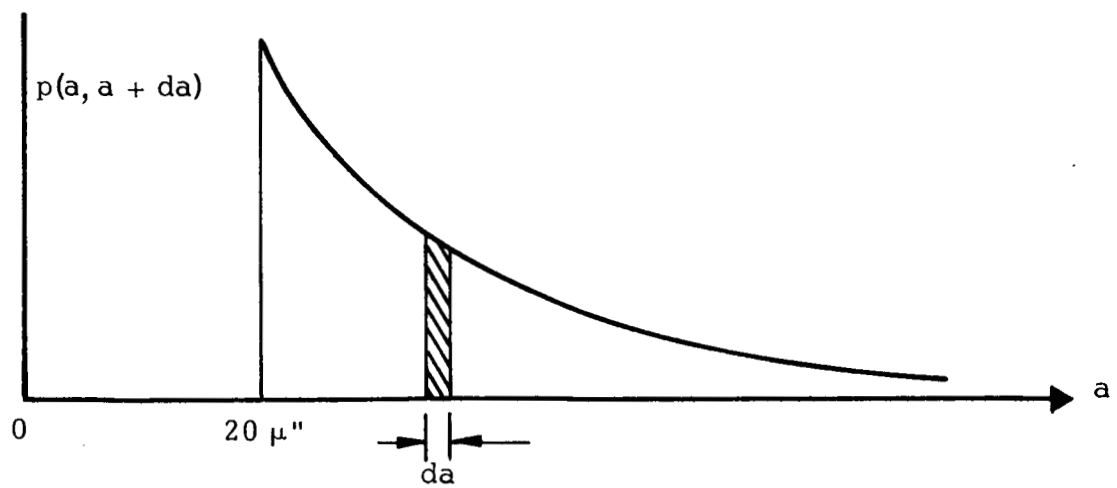

In such a graph the probability that the head-to-tape spacing is between value a and a + da is p da (i.e. the shaded area).

Purely in the interests of simplicity, the function p(a) will be assumed to be an exponential of the type:

$$p(a) = \alpha\, e^{-\alpha(a-20)}$$

The value of the constant α is determined in section 4.3 of this report.

(g) Finally, the effect of drop-outs upon the eventual error rate will be calculated according to:

$$\overline{ER} = \int_{20\,\mu"}^{\infty} ER\,(a)\; p\;(a)\; da$$

The determination of ER (a) has been considered in the previous section.

4.4 The Head-to-Tape Spacing Probability Density Distribution Function

As discussed in the previous section, we shall assume a simple exponential. It had been hoped that the exponent could be derived unequivocally from existing data. Unfortunately, it transpires that only an upper bound can be found.

The raw data falls into two classes, both of which were taken on an Ampex FR-1400 (longitudinal instrumentation recorder) at a tape speed of 60 ips and at a wavelength of 300 μin., using standard high-quality instrumentation tape. The first class of data, shown below in Table No. 4.1 gives the number of dropouts per 100 ft of tape lasting more than 20 μsec versus their amplitude.

The raw data falls into two classes, both of which were taken on an Ampex FR-1400 (longitudinal instrumentation recorder) at a tape speed of 60 ips and at a wavelength of 300 μin., using standard high-quality instrumentation tape. The first class of data shown below in Table No.4.1 gives the number of dropouts per 100 ft of tape lasting more than 20 μsec versus their amplitude.

Table 4.1

Loss of Signal	No. of Events/100 ft.	$\therefore \int_{a'}^{\infty} p(a)da$	a'
3-6 db	181	$\geq 181 \times 10^{-6}$	40 μin.
6-10 db	4.8	$\geq 4.8 \times 10^{-6}$	60 μin.
> 10 db	0.4	$\geq 0.4 \times 10^{-6}$	80 μin.

We seek to fit this data to an exponential which is generally:

$$p(a) = \alpha e^{-\beta(a - 20)}$$

If we normalize so that $\int_{20}^{\infty} p(a)\, da = 1$, then $\alpha = \beta$

The data in Table No. 4.1 yields, for the three cases:

$$\alpha \leq 0.43$$
$$\alpha \leq 0.30$$
$$\alpha \leq 0.25$$

The fit to an exponential is not particularly good but it is not felt to be worthwhile introducing more sophisticated models. Note also, since the original data applied to dropouts of duration greater than or equal to 20 μsec, we are left only with an upper bound on α.

The second class of raw data gives the number of dropouts of magnitude greater than 6 db versus their duration.

Table 4.2

Duration	No. of Events/100 ft	$\therefore \int_{a'}^{\infty} p(a)da$	a'
5-20 μs	57	710 μs	60 μin.
20-40 μs	6	180 μs	60 μin.
$\geq$ 40 μs	12	-	60 μin.

Whereas in the previous case the amplitude was well defined and the duration more or less arbitrary, here we have the converse. The values of α derived from Table No. 4.2 are:

$$\alpha \leq 0.25$$

$$\alpha \leq 0.33$$

We conclude that the function p(a) is bounded by:

$$p(a) = 0.25\ e^{-0.25(a-20)}$$

The actual value of the constant α is therefore, a matter of some conjecture. In the hand calculation demonstrated in the following sections of this report a value of 0.05 is used. The machine calculations of the overall error rate (section 4.7) have used a value of 0.08.

4.5 Worst Case Error Rates

We present below tables of the error rate anticipated for seven levels of clipping. All the errors are assumed to be due to "noise-free dropouts" as defined below*. The errors are worst case in the sense

*If the head-to-tape spacing momentarily increases sufficiently that the "one" signal amplitude falls below the clipping level, errors can occur even in the absence of noise. It is clear therefore that the choice of clipping level is critical and should be related to the noise level anticipated.

that the amplitude attenuation with spacing is assumed to be as large as is possible (i.e., the all-ones case as shown in the pulse crowding data graphs shown in section 3.7. Thus the error rates apply to a recording simulation using the JPL parameters. The head-to-tape probability density distribution function assumed for this illustration is

$$p(a) = 0.05\ e^{-0.05(a-20)}$$

Worst Case I	Clipping Level 50%
BPI	Error Rate
1000	$10^{-2.2}$
3000	$10^{-0.8}$
8000	$10^{-0.4}$

Worst Case II	Clipping Level 20%
BPI	Error Rate
1000	$10^{-5.2}$
3000	$10^{-2.2}$
8000	$10^{-1.0}$

Worst Case III	Clipping Level 15% (IBM Compatible Standard Practice)
BPI	Error Rate
1000	$10^{-6.2}$
3000	$10^{-2.6}$
8000	$10^{-1.4}$

Worst Case IV	Clipping Level 10%
BPI	Error Rate
1000	$10^{-7.5}$
3000	$10^{-3.2}$
8000	$10^{-1.6}$

Worst Case V — Clipping at RMS Noise Level

Bandpass equal to twice BPI
Noise power density = 10^{-11} units^2/cycle
Tape speed 10 ips (See next section)

BPI	Error Rate
1000	$< 10^{-20}$
3000	10^{-9}
8000	10^{-3}

Worst Case VI — Clipping at RMS Noise Level

Same as V but
$N_o = 10^{-9}$ unit^2/cycle
(see next section)

BPI	Error Rate
1000	10^{-15}
3000	$10^{-5.5}$
8000	$10^{-1.3}$

Worst Case VII — Clipping at RMS Noise Level

Same as V but
$N_o = 10^{-7}$ unit^2/cycle
(see next section)

BPI	Error Rate
1000	10^{-8}
3000	$10^{-2.2}$
8000	10^{-0}

Note that although worst cases V, VI and VII are related to the noise level, the errors computed are "noise-free dropouts" and not "noise dropouts".

It may be concluded that a simple amplitude detector employing a nonzero clipping level is not particularly useful at 8000 BPI. In section 4.6, written by H. Lienhard, the theoretical advantages of the zero clippling level usable with the correlation detector are extolled.

4.6 The White Noise Power Spectral Density Function - N_o

It is necessary to establish appropriate noise levels for the computer error calculation. It has been decided to use three levels, representing normal tape-limited background noise, one hundred times and one thousand times this level respectively.

Normal tape background noise yields (cf. standard audio practice) a wideband (25 Kcs) tape-limited signal-to-noise ratio of about 60 db, at a tape speed of about 10 IPS. This ratio is defined as:

$$\left(\frac{S}{N}\right)_{\text{wideband}} = 20 \log_{10} \frac{\epsilon}{\sqrt{\int \bar{N}_o \, df}}$$

where

ϵ is the signal output voltage

f is the frequency.

In this analysis the noise N_o is presumed to be frequency independent (so-called white noise) and the integral may be dispensed with.

$$\left(\frac{S}{N}\right)_{\omega b} = 10 \log_{10} \frac{\epsilon^2}{N_o \, \Delta_f}$$

Now the output signal level given by the computer programs is about one unit (this unit and its relationship to absolute voltage is discussed in section 3.1.

Thus the value of N_o corresponding to tape background noise is about 10^{-11} units^2/cycle.

The three noise levels to be used in the error rate calculation are then 10^{-11}, 10^{-9} and 10^{-7} units^2/cycle and they correspond to wide-band (audio) signal-to-noise ratios of 60 db, 40 db and 20 db respectively. These three levels are chosen so that the whole range from the optimum down to an extreme case of amplifier noise (which pertains to low tape playback speeds) is simulated.

4.7 Signal Detection Theory

The following questions concerning signal detection have been investigated:

Influence of head-to-tape spacing (fading)
Clocking
Equalization of signal energies
Comparison of amplitude and correlation detection
Performance of correlation detection with zero decision level for different signal-to-noise ratios.

All the mathematical derivations are found in the Appendix. We summarize the essential results:

(a) Fading and Crowding

The test signals for the correlation detector $s_o(t)$ and $s_1(t)$ are determined assuming nominal conditions (s_o: "0-signal," s_1: "1-signal"): no fading (nominal head-to-tape spacing a_o), patterns of all "ones" or all "zeros". The actual output signals (without additive noise) $s_o^*(t)$, $s_1^*(t)$ can deviate considerably from s_o and s_1 due to fading, and

crowding effects at high BPI. Equation (1) of the Appendix gives the error-probability for a false detection of the degraded signals s_o^*, s_1^* in the presence of white gaussian noise.

(b) Self-Clocking

A big difference in the signal energies of $s_o(t)$ and $s_1(t)$ means significant amplitude differences of the correlator outputs $\int x s_1 dt$ and $\int x s_o dt$. For self-clocking detection the detectability curve should show distinct maxima for both the "1" and the "0". With a large energy difference it can easily occur that, e.g., the peaks from the s_1-correlator are wiped out by deteriorations of the s_o correlator output. Hence for selfclocking the signal energies should be made approximately the same. In section 3.0 of the Appendix it is shown that, on the average, the correct clocking has to coincide with a detectability peak.

(c) Zero Decision Level

There is another strong reason to prefer equal signal energies. In section 1.0 of the Appendix we find that the decision level for the "1" and "0" is essentially determined by the difference in signal energies of $s_o(t)$ and $s_1(t)$. If this decision level α is nonzero, then the detectability peak can fall below this level due to a large head-to-tape spacing and produce a false decision even in the absence of any additive gaussian noise. For high signal-to-noise ratios the dominant error source will be the head-to-tape spacing. With equal energies for "1" and "0" the decision level is shifted to zero ($\alpha = 0$). In this case fading alone will not cause any errors at all.

(d) Equalization of Signal Energies

The highly desirable case of equal signal energies can hardly be realized in the tape recorder. However, we show in section 2.0 of the Appendix that this case is easily approximated by attenuating one correlator output. Errors may be computed with formula (1) of the Appendix.

(e) Comparison of Amplitude and Correlation Detection

By an "amplitude detector" we mean a decision scheme that operates on a fixed clipping level ℓ. The correct time for interrogation is supposed to be known. A "one" is detected if the signal is higher than ℓ. The "peak detector", widely used in digital recording, operates similarly. The exact position of the peak is irrelevant for our analysis. Equation (3) in the Appendix gives the error probability for amplitude detection. The performances of the two detection principles are compared in section 4.5 of the Appendix, assuming high signal-to-noise ratio (60 db) and low BPI (no crowding effects). With a nonzero decision level α, the correlation detector can be replaced by an amplitude detector with corresponding clipping level and signal-to-noise ratio. The decision errors are mainly caused by variations in head-to-tape spacing ("drop-outs"). Since both schemes analyzed in the Appendix work on the same effective clipping level ($\approx 16\%$), we find much the same error rates for both schemes ($\approx 2 \times 10^{-6}$). Digital tape machines are usually set on a 15% clipping level for an effective signal-to-noise ratio of approximately 26 db. This corresponds to a 5% noise level. The major part of the noise is "machine noise" (crosstalk, firing from the drive motors, etc.).

The above comparison is not valid for high BPI. If the neighboring bits are interacting, the output signals can suffer considerable d-c shifts, making amplitude detection rather impossible. (See illustration on following page.)

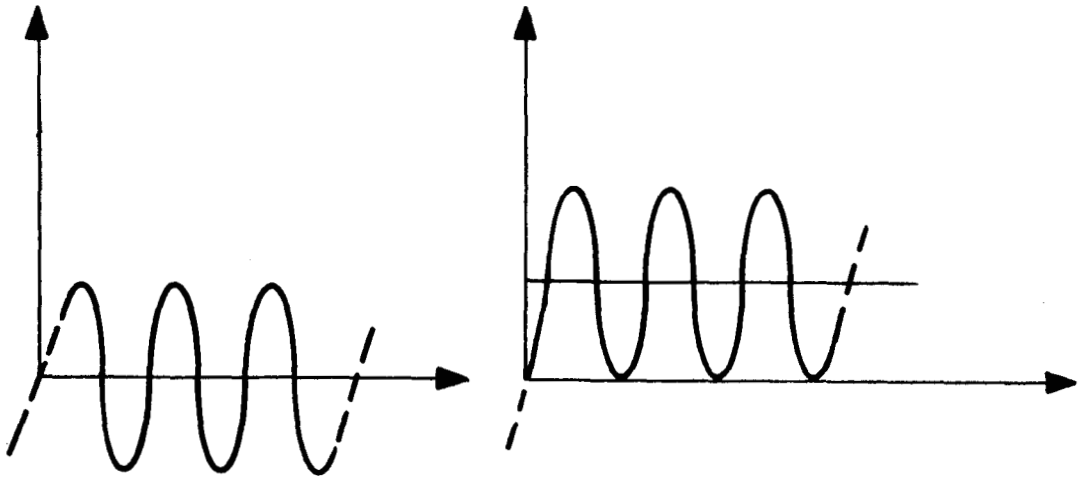

Two "1" in a string of "1" Two "1" after "0"

D-c Shift Due to Crowding

Since the correlator detector is essentially a waveform detector, it can still operate properly at high BPI.

(f) Performance of the Equalized Correlation Detector

The full potential of the matched filter approach becomes apparent when the signal energies are equalized, thus yielding a zero decision level. Approximate computations give the following error rates (see section 4.5.1 of the Appendix), for 1000 BPI.

Signal-to-Noise Ratio	Error Probability
60 db	10^{-24}
40 db	10^{-16}
30 db	10^{-12}
20 db	10^{-9}
10 db	10^{-5}
0 db	10^{-1}

For 60 db signal-to-noise, the error probability is lowered by a factor of 10^{18} compared to amplitude detection.

If the assumed drop-out model (section 4.2 of the Appendix) is essentially correct, then it has been proved that the performance of digital recorders can be tremendously increased by appropriate detection.

4.8 Computed Overall Error Rates

This section shows the overall error rates computed by JPL4 (see section 2.1) and JPL6 (see section 2.2). As has been agreed previously, we show three graphs of error rate versus BPI for differing values of the steep gap fields as illustrated in Figs. 14 through 16. Each graph has three plots appropriate to the three noise levels (N_o) discussed in section 4.5. The head-to-tape spacing function used is:

$$p(a) = 0.08\ e^{-0.08(a-20)}.$$

Other parameters are:

Tape coating thickness	200 μin.
Record gap length	150 μin.
Reproduce gap length	75 μin.
Switching fields	100/500 oe
Permeabilities	4/2
Bit pattern	000111, frequency doubling

The calculations pertain to the optimum type correlation detector, with equalization of the signal energies, as is described in sections 1.0 and 2.0 of the Appendix of this report.

Certain observations may be made concerning these graphs:

(a) The choice of H_o = 800 oe (see Fig. 14), that is one third of saturation is obviously bad. The record level is too low to measure against even small increases in the head-to-tape spacing. At a head-to-tape spacing of about 120 μin., the 300 oe longitudinal field contour of the record head is just grazing the near side of the tape. Thus for all spacings greater than 120 μin. no signal is, according to the modified program (see section 6.0) written at all. This fact would require further thought in any continuation of this study.

(b) For the case of saturation recording (H_o = 2400 oe), (see Fig. 15), no particular comments need be made except to remark that the standard IBM compatible machines have effective signal-to-noise ratios of about 26 db which falls about mid-way between the tape noise plus 20 db and plus 40 db levels. The overall error rates applicable to the IBM machine are expected to be about 10^{-8} at 500 BPI, 10^{-6} at 1000 BPI, 10^{-4} at 2000 BPI and etc., while figures sound to be very reasonable.

(c) At three times saturation level (H_o = 7200 oe), (see Fig. 16) we see two points of great interest. First at low BPI (< 1000) the error rate is decreased relative to the saturation level case. This is because of the ability of the head folt to continue to write satisfactorily on the tape even during

moments of long head-to-tape spacing. Some insurance against "drop-outs" thus occurs as is, indeed, the popularly held belief. Conversely at high BPI (> 1000), the high record current causes so much (non-linear) pulse crowding that the computer program was unable to detect the output correctly. Specifically the trouble appeared to be that "peak shift" (see section 3.8) so distorted the "detectability" curve (i.e., the difference between the moduli of the cross correlators) that the peak seeking algorithm used fails. This difficulty was not unexpected, for it has long been apparent that the use of high record currents at high BPI is an extremely bad situation which should be avoided.

In the following section, proposed topics for a continuation of the detector study are outlined.

4.9 Proposed Topics for a Continued Study of the Signal Processing in Digital Recording

We summarize a few topics that we feel essential for the optimization of the digital recording process. The main points include:

Synchronization

Signal design

Noise

Optimization with respect to dropouts

1. Reliability in Synchronization

   a) Actual flutter data have to be incorporated in the calculations.

   b) The gaussian noise will randomly shift the detectability peaks.

   c) Crowding effects result in peak shifts.

All three effects determine the probability of false synchronization.

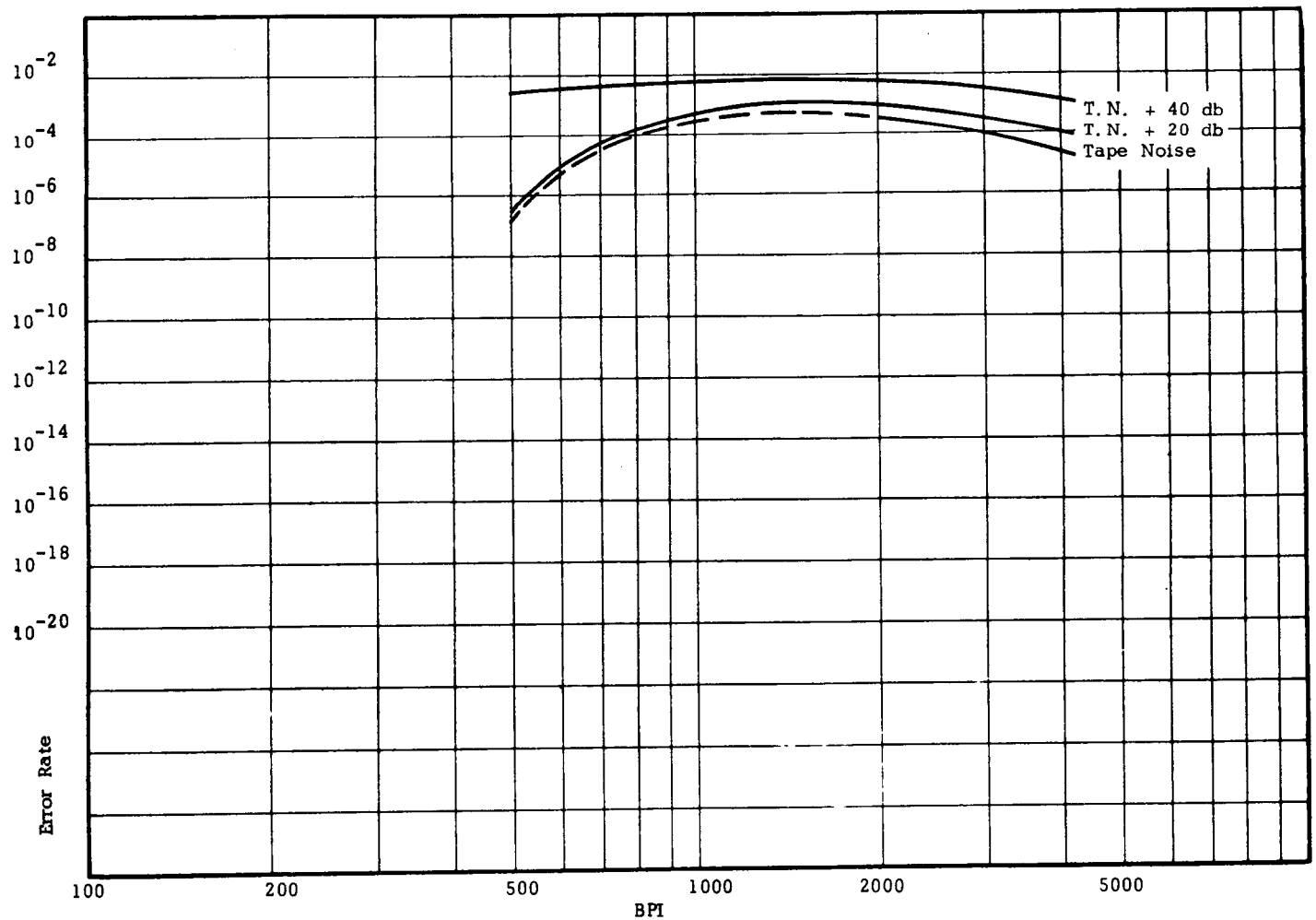

Fig. 14 Computed Error Rate Versus BPI for Deep Gap Field H_o = 800 oe (1/3 x SAT) and Three Noise Levels

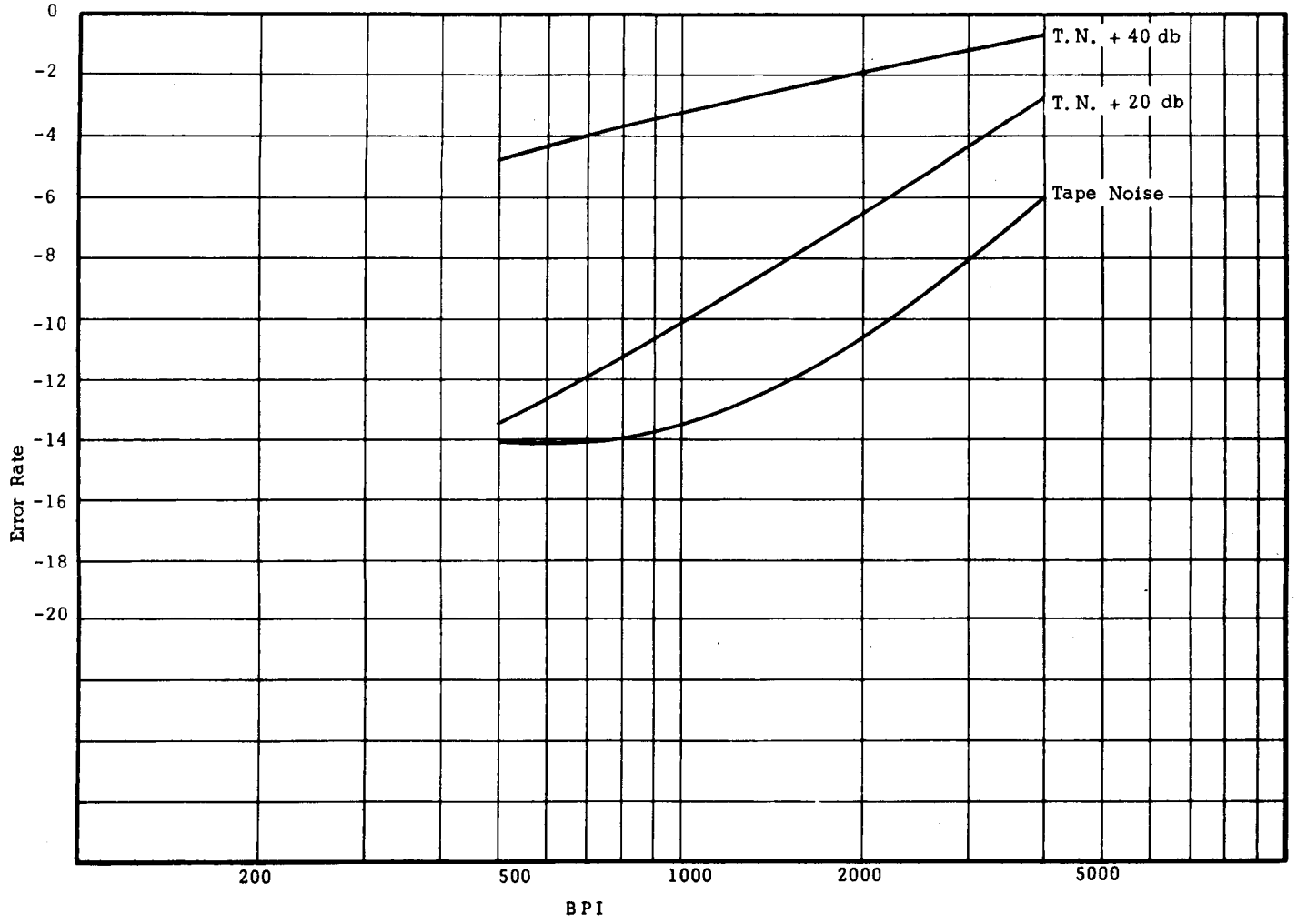

Fig. 15 Computed Error Rate Versus BPI for Deep Gap Gield H_o = 2400 oe (1 x SAT) and Three Noise Levels

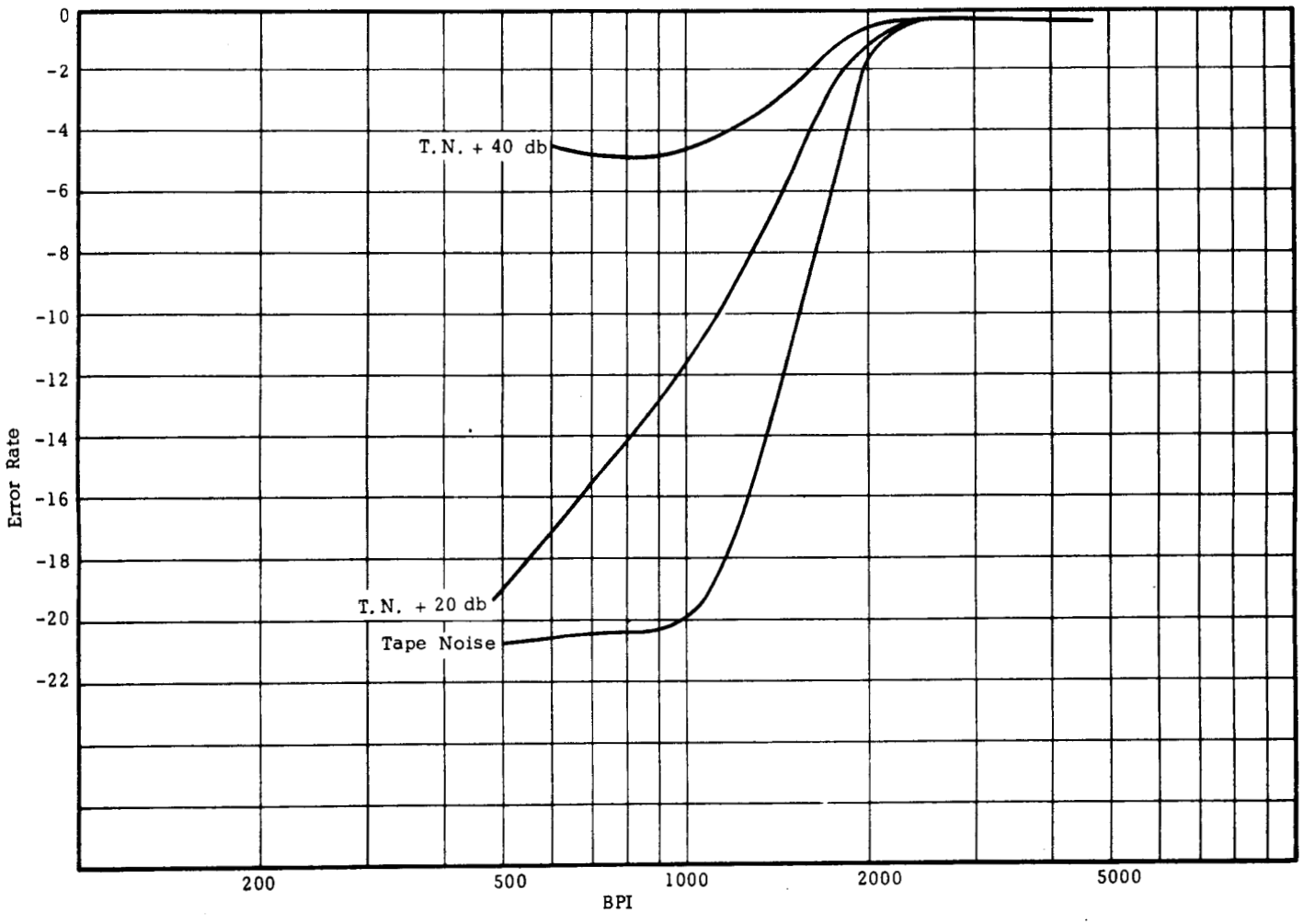

Fig. 16 Computed Error Rate Versus BPI for Geep Gap Field
H_o = 7200 oe (3 x SAT) and Three Noise Levels

2. Peak Seeking Procedures

The results of point 1) will indicate how carefully the synchronization has to be carried out. The peak location problem can be treated as a parameter estimation problem.

3. Signal Design

The record signals for "zero" and "one" should be designed to minimize crowding effects in the reproduce signal.

4. Tape, head, and electronics noise

Since the actual noise power density will not be white at the recorder output it might be necessary to include reversible "whitening filters" to equalize the noise power density. This way we are able to find the correct optimum detector for non-white gaussian noise.

5. Optimization with Respect to Dropouts

So far the decision scheme has been strictly optimized only for gaussian noise. The fading, which is due to dropouts, has been taken into consideration only by forcing the decision level to zero. A study is proposed to find proper encoding to minimize the effects of dropouts.

APPENDIX I

1. THE CORRELATION-DETECTOR IN THE PRESENCE OF FADING

The effect of the variations in head-to-tape spacing (a) will be treated as "fading." Since this fading is caused by an attenuation of the signals $s_o(t)$ and $s_1(t)$ the matched filter or correlation detector described in the appendix of the monthly report No. 3 still gives the appropriate solution. The error figures will obviously depend on the actual head-to-tape spacing.

Assuming a non-parametric detection scheme, the matched filters have to be designed for some nominal spacing a_o (and, of course, some fixed BPI).

We make the following distinctions:

$s_o(t)$, $s_1(t)$ are the optimum test signals for the "0" and "1" at nominal conditions (no fading).

$s_o^*(t)$, $s_1^*(t)$ are the actual output signals in the absence of additive noise.

For the nominal case we find the following optimum decision scheme:

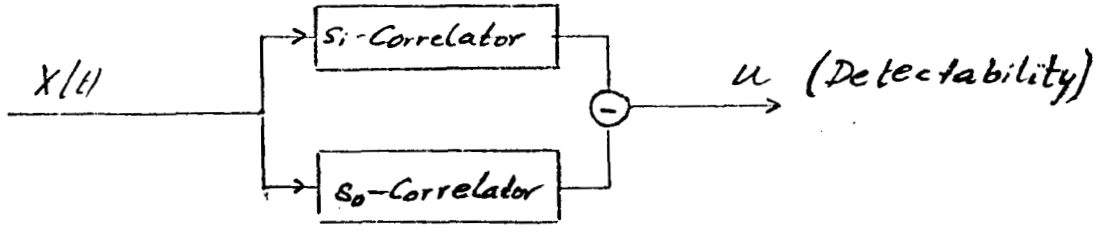

In the monthly report No. 3, page 15, we found the following decision criterion:

$$\max_k \left\{ \int X(t) S_k(t)\,dt - \tfrac{1}{2} E_k \right\} \Rightarrow S_k$$

$$E_k = \int S_k^2\,dt$$

For the two signals $s_o(t)$, $s_1(t)$ this means

$$\int x(t) s_1(t)\,dt - \frac{E_1}{2} \gtrless \int x(t) s_0(t)\,dt - \frac{E_0}{2} \Rightarrow s_1$$

or

$$\int x(t)\,\Delta s(t)\,dt \gtrless \frac{1}{2}\left\{\int s_1^2\,dt - \int s_0^2\,dt\right\} \Rightarrow s_1$$

$$\Delta s = s_1(t) - s_0(t) \qquad u \gtrless \frac{1}{2}\left\{\int s_1^2\,dt - \int s_0^2\,dt\right\} \Rightarrow \text{"1"}$$

$$u = \int x\,\Delta s\,dt \qquad u \leq \frac{1}{2}\left\{\int s_1^2\,dt - \int s_0^2\,dt\right\} \Rightarrow \text{"0"}$$

For the error computation we determine the distribution of the detectability u assuming white gaussian noise n(t):

$\overline{n(t)} = 0$ Spectral density = $N_0/2$ (For frequencies $-\infty$ and $+\infty$)

$$u = \int \Delta s\,[s^*(t) + n(t)]\,dt \qquad s^* = s_1^* \text{ or } s_0^*$$

$$\bar{u} = \int \Delta s\, s^*\,dt$$

$$\sigma_u^2 = \overline{(u-\bar{u})^2} = \frac{N_0}{2}\int \Delta s^2\,dt; \quad \bar{u}_1 = \int \Delta s\, s_1^*\,dt, \quad \bar{u}_0 = \int \Delta s\, s_0^*\,dt$$

False decision:

$$P_\varepsilon = \frac{1}{2}\frac{1}{\sqrt{2\pi}\,\sigma_u}\left\{\underbrace{\int_{-\infty}^{\alpha} e^{-\frac{1}{2\sigma_u^2}(u-\bar{u}_1)^2}\,du}_{\text{"0" instead of "1"}} + \underbrace{\int_{\alpha}^{\infty} e^{-\frac{1}{2\sigma_u^2}(u-\bar{u}_0)^2}\,du}_{\text{"1" instead of "0"}}\right.$$

α = decision level = $\frac{1}{2}\left\{\int s_1^2\,dt - \int s_0^2\,dt\right\}$

$$P_\varepsilon = \frac{1}{2} f\left[\frac{\bar{u}_1 - \alpha}{\sigma_n}\right] + \frac{1}{2} f\left[\frac{\alpha - \bar{u}_0}{\sigma_n}\right]; \quad f(x) = \frac{1}{\sqrt{2\pi}} \int_x^\infty e^{-\frac{1}{2}t^2}\,dt$$

$\bar{u}_0$, $\bar{u}_1$ are the actual detectability peaks in the absence of noise

Define

$p = \text{Min}\,(\bar{u}_1 - \alpha)$

$q = \text{Min}\,(\alpha - \bar{u}_0)$ in a "worse case" pattern

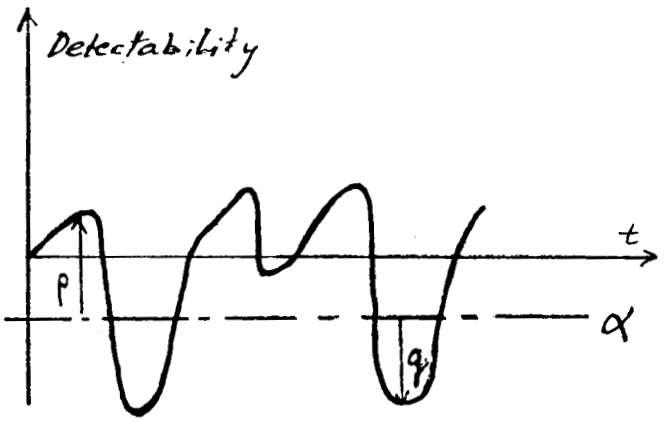

$$P_\varepsilon = \frac{1}{2} f\left(\frac{p}{\sigma_n}\right) + \frac{1}{2} f\left(\frac{q}{\sigma_n}\right) \qquad (1)$$

$\sigma_n = \sqrt{\frac{N_0}{2}\left(\int s_1^2\,dt + \int s_1^2\,dt\right)}$, assuming orthogonal test signals $\Rightarrow$ $\int s_0 s_1\,dt = 0$

P_ε = error rate for fixed spacing a

p = p(a); q = q(a).

2. EQUALIZATION OF SIGNAL ENERGIES

We modify our detector to obtain equal detectability peaks for "0" and "1" in the nominal case (no fading, no noise).

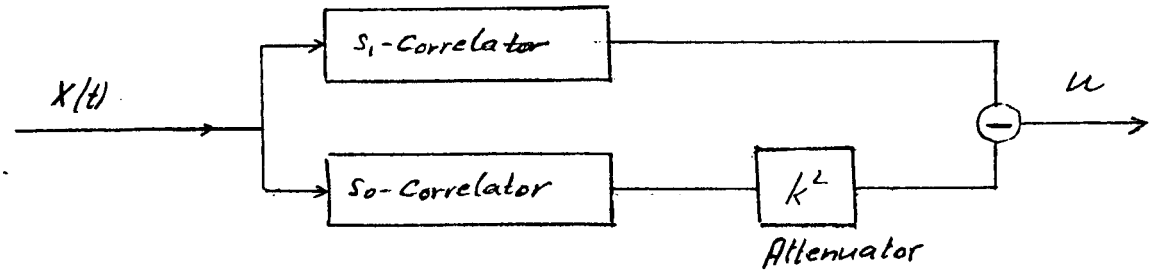

For equalization: $\int s_1^2 dt = k^2 \int s_0^2 dt$

Decision: ($\alpha = 0$) $u \geq 0 \Rightarrow$ "1"

$u < 0 \Rightarrow$ "0"

$u = \int x \, \Delta s \, dt \quad ; \quad \Delta s = s_1 - k^2 s_0$

Distribution of u:

We find in the same way as in the preceding paragraph :

$\bar{u}_1 = \int s_1 \Delta s \, dt = \int s_1^2 dt \quad$ for $\int s_0 s_1 dt = 0$

$\bar{u}_0 = -k^2 \int s_0^2 dt = -\bar{u}_1$

$\sigma^2 = \frac{N_0}{2} \int \Delta s^2 dt = N_0 \int s_1^2 dt \left(\frac{1+k^2}{2} \right)$

If the signals $s_0(t)$ and $s_1(t)$ were actually designed to give equal energies, $\int s_1^2 dt = \int s_0^2 dt$, we would find $\sigma_u^2 = N_0 \int s_1^2 dt$, hence $\sigma^2 = \sigma_u^2 \left(\frac{1+k^2}{2} \right)$

Error probability:

$$P_\Sigma = \frac{1}{2} \frac{1}{\sqrt{2\pi}\sigma} \left\{ \int_{-\infty}^{0} e^{-\frac{1}{2\sigma^2}(u-\bar{u}_1)^2} du + \int_{0}^{\infty} e^{-\frac{1}{2\sigma^2}(u-\bar{u}_0)^2} du \right\}$$

$$P_\varepsilon = \frac{1}{2} f\left(\frac{\bar{u}_1}{\sigma}\right) + \frac{1}{2} f\left(\frac{-\bar{u}_0}{\sigma}\right)$$

Since $\bar{u}_0 = -\bar{u}_1 = \bar{u}$ we find

$$P_\varepsilon = f\left(\frac{\bar{u}}{\sigma}\right) \; ; \quad f(k) = \frac{1}{\sqrt{2\pi}} \int_k^\infty e^{-\frac{1}{2}t^2} dt$$

$\bar{u}$ being the detectability peaks in the absense of noise.

For equal energies $s_0(t)$ and $s_1(t)$ we would find

$$P_\varepsilon = f\left(\frac{\bar{u}}{\sigma_u}\right) \; ; \quad \int s_0^2 dt = \int s_1^2 dt$$

$$\sigma = \sigma_u \sqrt{\frac{1+k^2}{2}} \; ; \quad 0.707 \leq \sqrt{\frac{1+k^2}{2}} \leq 1 \quad ---- (2)$$

Since σ comes close to σ_u, our attenuator scheme and the real equal energy scheme give much the same error rates. Thus for error-probability calculations formula (1) may be used.

3. EXTRACTION OF TIMING INFORMATION

Our selfclocking code should provide enough information to control the clocking. We give a short verification of the fact that the detectability peaks indicate, on the average, the correct time of the occurrence of either s_0 or s_1.

u being the output of a correlator:

$$u(t) = \int x(\tau)\, s(\tau - t)\, d\tau \quad ; \quad x(\tau) = s(\tau) + n(\tau)$$

Averaging over t:

$$\overline{u(t)} = \int s(\tau)\, s(\tau - t)\, d\tau + \underbrace{\int \overline{n(\tau)}\, s(\tau - t)\, d\tau}_{=0}$$

$$\overline{u(t)} = \int s(\tau)\, s(\tau - t)\, d\tau$$

Since $\left[s(\tau) - s(\tau - t) \right]^2 \geq 0$ it follows that

$$\int s(\tau)^2 d\tau + \int s(\tau - t)^2 d\tau - 2 \int s(\tau)\, s(\tau - t)\, d\tau \geq 0$$

or

$$\int s^2(\tau)\, d\tau \geq \int s(\tau)\, s(\tau - t)\, d\tau$$

Hence

$$\overline{u(0)} \geq \overline{u(t)}$$

t = 0 indicates the occurrence of s(t) and we have proved that at t=0 the correlator output must have, on the average, a maximum.

4. AMPLITUDE AND CORRELATION DETECTION IN THE PRESENCE OF FADING AND WHITE GAUSSIAN NOISE

4.1 Amplitude Detection:

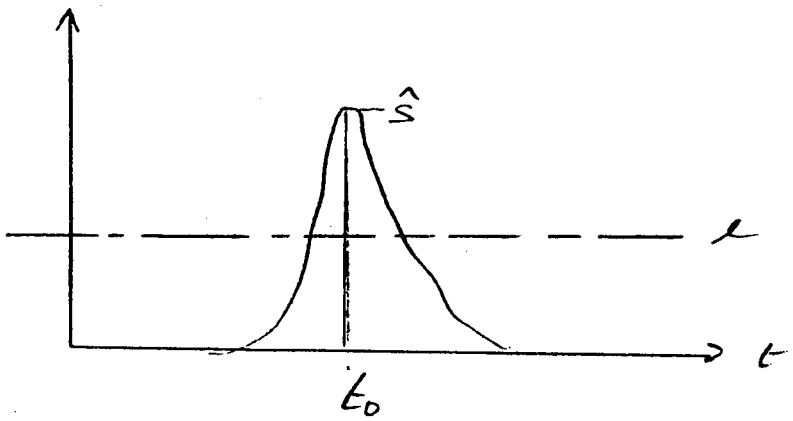

signal s(t)

ℓ = decision level

x(t) = n(t) ⇒ no signal

or

x(t) = s(t) + n(t) ⇒ signal present

Decision:

$x(t_o) \geq \ell \Rightarrow$ signal present

$s(t_o) < \ell \Rightarrow$ no signal

This would constitute an amplitude detector for NRZ - Code.

Noise n(t): $\overline{n(t)} = 0 \quad \overline{n^2} = \sigma^2$ (Bandlimited)

$p_n(\alpha) = \frac{1}{\sqrt{2\pi}\sigma} e^{-\frac{1}{2\sigma^2}\alpha^2}$

at time t_o $\quad x = \hat{s} + n(t_o)$ or $x = n(t_o)$

$p_x(\alpha) = p_n(\alpha - \hat{s})$

or

$p_x(\alpha) = p_n(\alpha)$

False decision:

$$P_s = \frac{1}{2} \frac{1}{\sqrt{2\pi}\sigma} \left\{ \underbrace{\int_{-\infty}^{\ell} e^{-\frac{1}{2\sigma^2}(\alpha-\hat{s})^2} d\alpha}_{\text{"drop out"}} + \underbrace{\int_{\ell}^{\infty} e^{-\frac{1}{2}\alpha^2} d\alpha}_{\text{"drop in"}} \right\}$$

$$P_\varepsilon = \frac{1}{2} f\left(\frac{\hat{s}-e}{\tilde{N}}\right) + \frac{1}{2} f\left(\frac{e}{\tilde{N}}\right); \quad f(x) = \frac{1}{\sqrt{2\pi}} \int_x^\infty e^{-\frac{1}{2}t^2} dt$$

$\tilde{N}$ = RMS - noise voltage $= \sigma = \sqrt{n^2}$

4.2 Fading Model

Since the output voltage of a tape recorder decreases, in a first approximation, exponentially with the spacing a, we define the fading:

$$s(t) = S_n \cdot e^{-k\xi}; \quad \xi = \frac{a-a_o}{a_o} \qquad (4)$$

S_n : voltage for nominal spacing $a = a_o$ $(\xi = 0)$

$k \approx 0.134$ for 1000 BPI

4.3 Distribution of Head-to-Tape Spacing

$$p_a(a) = c\, e^{-c(a-a_o)}$$

$$p_a(\xi) = c a_o\, e^{-c a_o \xi} \qquad (5)$$

The average error rate is

$$ER = \overline{P_\varepsilon(a)} = c a_0 \int_0^\infty P_\varepsilon(\xi) e^{-c a_0 \xi} d\xi \quad \text{------} \quad (6)$$

For the following computations we shall assume:

$c = 0.05$; $a_o = 20\ \mu$"

$p(\xi) = e^{-\xi}$

4.4 Correlation-Detector

To extimate the performance of the correlation detector, we must make certain assumptions about the waveforms of $s_o(t)$ and $s_1(t)$.

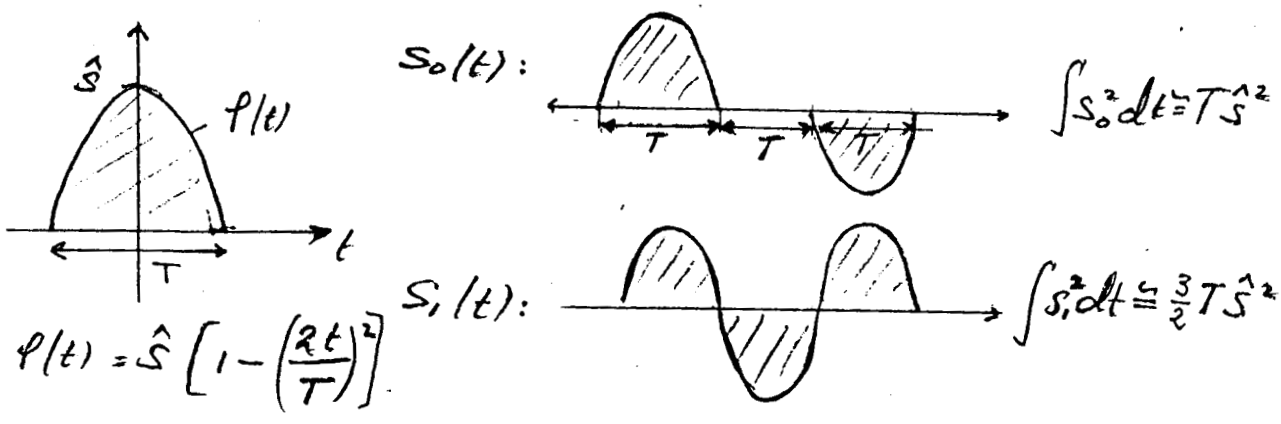

Decision level $\alpha = \frac{1}{2}\left\{\int s_1^2\,dt - \int s_o^2\,dt\right\} = \frac{1}{4}\,T\,\hat{S}^2$

Attenuated signals: $s_1^* = s_1 e^{-k\xi}$; $s_o^* = s_o e^{-k\xi}$

$$\bar{u}_1 = \int \Delta s\, s_1^*\, dt \qquad \bar{u}_o = \int \Delta s\, s_o^*\, dt$$

$$\bar{u}_1 = \frac{3}{2} T\hat{S}^2 e^{-k\xi} \; ; \quad \bar{u}_o = -T\hat{S}^2 e^{-k\xi}$$

$$p = \bar{u}_1 - \alpha = \frac{3}{2} T \hat{S}^2 \left[e^{-k\xi} - 1/6 \right]$$

$$q = \alpha - \bar{u}_0 = T \hat{S}^2 \left[e^{-k\xi} + 1/4 \right] \; ; \; W : \text{Bandwidth}$$

$$\sigma_u = \hat{S} \sqrt{\frac{5}{4} N_0 T}$$

$$\gamma = \frac{\hat{S}}{\sqrt{N_0 W}} = \frac{\text{signal}}{\text{noise}}$$

$$\beta_1 = \frac{p}{\sigma_u} = \frac{3}{\sqrt{5}} \sqrt{WT} \left[e^{-k\xi} - 1/6 \right] \cdot \gamma$$

$$\beta_2 = \frac{q}{\sigma_u} = \frac{2}{\sqrt{5}} \sqrt{WT} \left[e^{-k\xi} + 1/4 \right] \cdot \gamma$$

For the error-rate we found in Paragraph 1)

$$P_\Sigma = \frac{1}{2} f(\beta_1) + \frac{1}{2} f(\beta_2)$$

4.5 Comparison of Amplitude Detection and Correlation Detection

Amplitude detection:

$$P_\Sigma = \frac{1}{2} f\left(\frac{\hat{S}^* - e}{N} \right) + \frac{1}{2} f\left(\frac{e}{N} \right) \; ; \; \hat{S}^* = \hat{S}_n e^{-k\xi} \text{ (Fading)}$$

assuming $e = \hat{S}_n / 6$ ($\approx 16\%$ clipping)

$$P_\Sigma = \frac{1}{2} f\left[\gamma \left(e^{-k\xi} - 1/6 \right) \right] + \frac{1}{2} f\left[\frac{1}{6} \gamma \right] \; ; \; \gamma = \frac{\hat{S}_n}{N}$$

For both detection schemes:

$$P_\Sigma = \frac{1}{2} f(\beta_1) + \frac{1}{2} f(\beta_2)$$

	Amplitude Detection	Correlation Detection
$\beta_1 =$	$\gamma \left[e^{-k\xi} - 1/6 \right]$	$\frac{3}{\sqrt{5}} \sqrt{WT}\, \gamma \left[e^{-k\xi} - 1/6 \right]$ ... (7)
$\beta_2 =$	$\gamma/6$	$\frac{2}{\sqrt{5}} \sqrt{WT}\, \gamma \left[e^{-k\xi} + 1/4 \right]$

Estimate of time - bandwidth product: $W > \frac{1}{T}$ (sampling theorem)

Choose $W = \frac{3}{T}$ $\qquad \sqrt{WT} = \sqrt{3}$

For signal-to-noise ratio we choose $\gamma = 10^3$ (60 dB). If γ is large, $f(\beta_2)$ becomes negligible. Consequently:

$$P_2 \simeq \frac{1}{2} f(\beta)$$

Amplitude Detection

$$\beta = \gamma \left[e^{-k^2} - 1/6 \right]$$

Correlation detection

$$\beta = \gamma' \left[e^{-k^2} - 1/6 \right]$$

$$\gamma' = 2.32 \cdot \gamma$$

Conclusion:

To analyze the correlator detector, it can be replaced by an amplitude detector operating under a different signal-to-noise ratio γ'. This is only true for high γ and nonzero decision level α for the correlation detection.

Rough estimate of error rates:

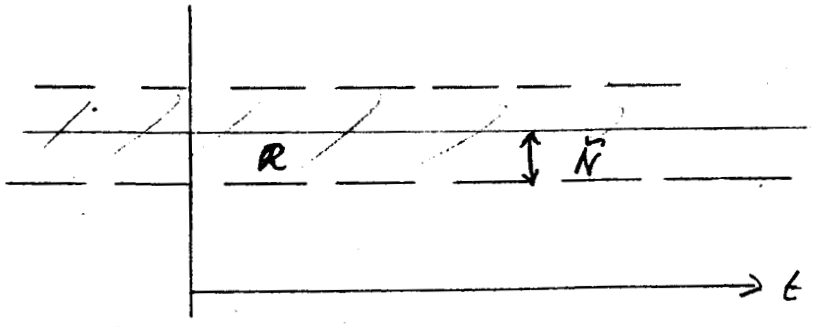

R: Uncertainty region due to gaussian noise $R = [\ell - \tilde{N}, \ell + \tilde{N}]$

False detection if S falls below $\ell + N$:

$$\hat{S}^* \leq \frac{\hat{S}}{6} + \gamma^{-1}\hat{S} = \hat{S}\left(\tfrac{1}{6} + \gamma^{-1}\right)$$

To the attenuation $\frac{\hat{S}^*}{\hat{S}}$ corresponds a critical spacing ξ_k, every $\xi \geq \xi_k$ will give rise to false detection:

$$ER = \int_{\xi_k}^{\infty} p_a(\xi)\, d\xi = e^{-\xi_k} \qquad \text{(see 4.3)}$$

With $k = 0.134$, $a_o = 20\ \mu"$, $c = 0.05$, we find

$$\text{ER (Amplitude Detection)} = e^{-13.38} \qquad (\approx 2 \cdot 10^{-6})$$

$$\text{ER (Correlation Detector)} = e^{-13.32}$$

Both schemes give almost the same error rate. This has to be the case, since both detectors have the same effective clipping level (approximately 16%) and at this clipping level the gaussian noise has a negligible effect.

4.5.1 Zero decision level for the correlation detection

We assume equal signal energies for $s_o(t)$ and $s_1(t)$: $\int s_o^2\, dt = \int s_1^2\, dt$. If this is not apriori the case, we come very close to it by applying the equalization scheme of paragraph 2). Our decision level becomes zero ($\alpha = 0$). With the assumptions of paragraph 4.4 we easily find:

$$\int s_0^2 dt = \int s_1^2 dt = T\hat{s}^2$$

$$\bar{u}_1 = p = T\hat{s}^2 e^{-k\xi} \; ; \quad q = -\bar{u}_0 - p \; ; \quad \sigma_u = \sqrt{N_0 \hat{s}^2 T}$$

$$\frac{p}{\sigma_u} = \frac{q}{\sigma_u} = \sqrt{WT} \cdot \gamma e^{-k\xi}$$

$$P_\varepsilon = f\left[\sqrt{WT}\,\gamma e^{-k\xi}\right] \qquad (8)$$

Total error rate (over all spacings ξ)

$$ER = \int_0^\infty f\left(\sqrt{WT}\, e^{-k\xi}, \gamma\right) p_a(\xi)\, d\xi \qquad (9)$$

We approximate $f(x) = \frac{1}{\sqrt{2\pi}} \int_x^\infty e^{-\frac{1}{2}t^2} dt$ by $\frac{1}{2} e^{-\frac{1}{2}x^2}$

$$ER = \frac{1}{2} \int_0^\infty \exp\left\{-\frac{1}{2}\left[WT e^{-2k\xi}\right]\gamma^2\right\} \exp(\xi)\, d\xi \; ; \quad (a_0 = 1)$$

defining $\alpha = \frac{1}{2} WT \gamma^2 = 1.5 \cdot 10^6 \quad (\gamma = 10^3, \; WT = 3)$

$$ER = \frac{1}{2} \int_0^\infty e^{-\alpha e^{-2k\xi}} \cdot e^{-\xi} d\xi$$

We change the variable of integration:

$$z = e^{-\xi} \qquad dz = -z\,d\xi$$

$$ER = \frac{1}{2}\int_0^1 e^{-\alpha z^{2k}}\,dz \quad ; \text{ Integrand } I(z) = e^{-\alpha z^{2k}}$$

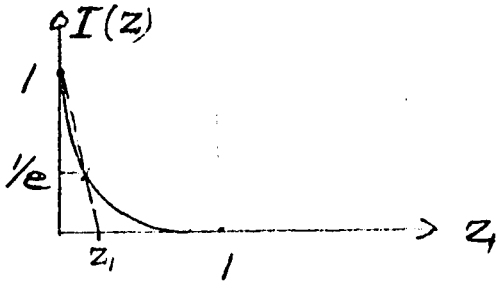

$$z = 0 \;:\; I = 1$$

$$z = 1 \;:\; I = e^{-\alpha} \approx 0$$

We approximate I(Z) by a straight line through (0, 1) and $(z_0, \frac{1}{e})$

$$e^{-\alpha z_0^{2k}} = e^{-1} \rightarrow \qquad \log z_0 = -\frac{\log 1.5 \cdot 10^6}{2k}$$

For $k = 0.134$ (1000 BPI) $\qquad \log z_0 \approx -23$

$$z_{1,0} \approx 10^{-23}$$

Linearization: $\int_0^1 I(z)\,dz \approx \frac{z_1 \cdot 1}{2}$

$$\frac{z_1}{z_0} = \frac{1}{1 - 1/e} = 1.58 \qquad \frac{z_1}{2} = 0.79 \cdot 10^{-23}$$

$$ER \approx \frac{z_1}{4} = 4 \cdot 10^{-24}$$

Comparing this to the case of nonzero decision level (see 4.5) we see that the error rate is lowered by almost a factor of 10^{18} for similar signal energies and equal signal-to-noise ratios.

Different signal-to-noise ratios:

define $\gamma_{dB} = 20 \log \gamma$

$\log Z_o = -0.373 (10 \log 1.5 + \gamma_{dB})$ for $k = 0.134$

$10 \log 1.5 = 1.761$

γ_{dB}	$\log Z_o$	$\approx Z_o$	$ER = 0.4 \cdot Z_o$
60 dB	-23	10^{-23}	$4 \cdot 10^{-24}$
40 dB	-15.5	$3 \cdot 10^{-16}$	$1.2 \cdot 10^{-16}$
30 dB	-11.85	$1.4 \cdot 10^{-12}$	$0.56 \cdot 10^{-12}$
20 dB	-8.1	$1/1.25 \cdot 10^{-8}$	$3.2 \cdot 10^{-9}$
10 dB	-4.4	$1/2.5 \cdot 10^{-4}$	$1.6 \cdot 10^{-5}$
0 dB		$2.2 \cdot 10^{-1}$	$0.88 \cdot 10^{-1}$

APPENDIX II

1. INTRODUCTION AND SUMMARY

In conformance with the extension of the contract, a short program of experimental validation was undertaken at the conclusion of the original study. The validation sought is concerned with the basic tape recorder simulation (JPL-4) and is in no way related to errors and reliability.

To this end, appropriate recording apparatus was assembled and actual output waveforms photographed. These were then compared with the computed waveforms. Although the extension contract calls for a set of four such comparisons, in fact, eighteen runs were made in order that a greater range of prarmeters might be covered.

In every case, the agreement is better than had been anticipated earlier. In the case of saturation level recording the program is found to be adequate up to at least 2500 bpi, frequency doubling (i. e. 5000 bpi NRZ). At lower levels the program is usable without serious error up to bit densities of 7500 bpi (i. e. 15, 000 bpi NRZ).

It is concluded that, since there exists no justification for operating at the saturation level at high bit densities, the existing program (JPL-4) is perfectly adequate for all foreseeable engineering purposes.

2. DESCRIPTION OF THE DIGITAL RECORDING APPARATUS

A DATAPULSE output unit 903 is connected to a specially made bistable digital record amplifier. The output is connected directly to an Ampex FR-1400, 11 turn per leg, 150 microinch gap length, 3 mil lamination Moly-permalloy record head. The amplifier is able to drive $\pm$125 mA current through the turns on one leg which may be computed to result in a deep gap field of 4400 oersteds. For a 150 microinch gap length the saturating field (i. e. that which puts the 500 oersted contour at a distance of 420 microinch above the head plane) is about 4500 oersteds. The magnitude of record current is thus adequate, a conclusion borne out by the ability of the apparatus to self-erase previously recorded information.

The tapes used are Ampex 771 and Ampex 772, of coating thickness 400 and 200 microinches respectively, both being 35% by volume γFe_2O_3 instrumentation tape on 1 mil Mylar. The maximum remanence is about 1350 guass, the intrinsic coercive force (M = 0) is 280 oersteads, giving a linearized demagnetizing permeability of about 5. The remagnetizing permeability may be assumed to be about 2. The range of switching fields is approximately 100 - 500 oersteds.

The reproduce head is an Ampex FR-1600 with 35 turns per leg, 25 microinch gap length, 3 mil lamination of Moly-permalloy which is connected to a field effect transistor pre-amplifier which provides +40 db gain, flat within 0. 5 db between 1 Kcs and 2. 0 Mcs.

The tape transport is a precision type, with vacuum column tape tension control and a lightweight capstan assembly with servo control. The machine provides 240, 120, 60, 30, 15, 7. 5, 3. 75, 1. 875 ips tape speeds, forward and reverse.

The record current, measured on the head terminals, shows a negligible rise time of less than 0.5 microsecond. The two frequencies proposed for use correspond to durations of 13.5 and 27 microseconds, viz:

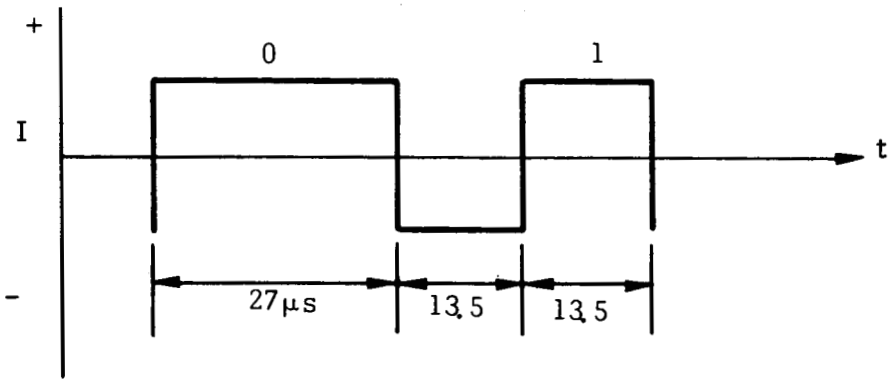

At a tape speed of 60 ips this yields 625 bpi, at 30 ips 1250 bpi, and so on through 3.75 ips yielding 10,000 bpi (i.e. 20,000 frpi maximum).

The 8 bit frequency doubling word used throughout the whole validation program is

0 1 0 1 0 0 1 1

3. COMPUTER INPUT PARAMETERS

The parameters used in the computer simulation correspond as closely as possible to the experimental situation. They are:

Head-to-tape spacing, a,	=	20 μin.
Tape coating thickness, d,	=	200 or 400 μin. as appropriate
Record gap length	=	150 μin.
Reproduce gap length	=	25 μin.
Deep gap field, H_o,	=	As appropriate (calculated on the basis 35 oe per mA of head current)

Tape permeabilities, μ_1/μ_2,	=	5/2
Tape switching fields	=	100/500 oe.
Bit densities	=	625, 1250, 2500, 5000 and 10,000 bpi (as appropriate)

In order that the experimental waveforms could be "inputed" to the computer, the following procedure was used:

a) The original polaroid oscilloscope picture was enlarged 400% and made negative.

b) The amplitude of the waveform was measured, by hand, at some 60-70 points per 8 bit word. This corresponds to a point density of about 40 per inch on the original photograph (and to about 8 points per bit length).

It may be seen by comparison of the experimental and reconstituted waveforms that this procedure is sufficiently accurate to reproduce all the essential features of the waveforms.

In addition to computing the waveform and comparing it with the experimental waveform, the computer was also programmed to compute the normalized cross-correlation between the two waveforms. This function, considered a "figure of merit" by JPL, is:

$$\text{F.O.M.} = \frac{\int_T e(t)\, c(t+\tau)\, dt}{\left[\int_T [e(t)]^2\, dt \int_T [c(t)]^2\, dt\right]^{1/2}}$$

where e (t) and c(t) are the experimental and computed waveforms, of respectively, both of period T. This FOM is plotted in each case for values of τ between O and T.

4. RESULTS

For each test we show three figures. The first is a high resolution photograph of the experimental waveform. The second is computer graph showing the computed and reconstituted experimental waveforms (i. e. compute versus measure.) The third is the cross correlation FOM graph.

The experimental conditions are:

Test No.	Coating Thickness (microinch)	Deep Gap Field (oersted)		BPI
1	400	4500		625
2	400	4500	1 x sat.	1250
3	400	4500		2500
4	400	4500		5000
5	400	2250		625
6	400	2250		1250
7	400	2250	1/2 x sat.	2500
8	400	2250		5000
9	400	2250		7500
10	400	2250		10,000
11	400	1500	1/3 x sat.	7500
12	400	1500		10,000
13	400	1100	1/4 x sat	7500
14	400	1100		10,000

15	200	2500		625
16	200	2500	1 x sat.	1250
17	200	2500		2500
18	200	2500		5000

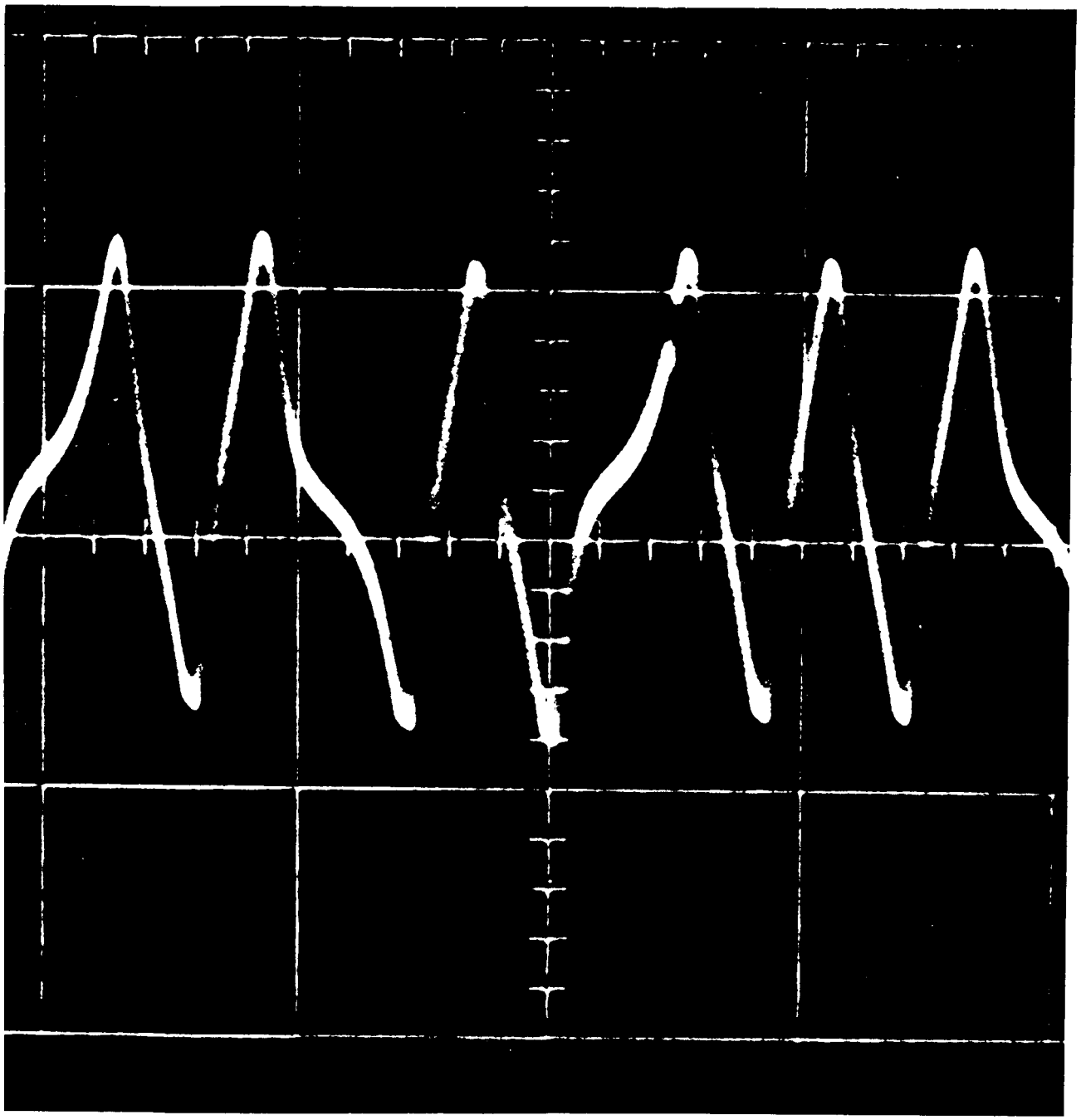

Fig. 1 Coating Thickness 400 μ in. 1A
Deep Gap Field 4500 oe (1 x saturation), 625 BPI
a) Experimental Waveform
b) Computed versus Experimental
c) Computed Cross-Correlation F. O. M

1B

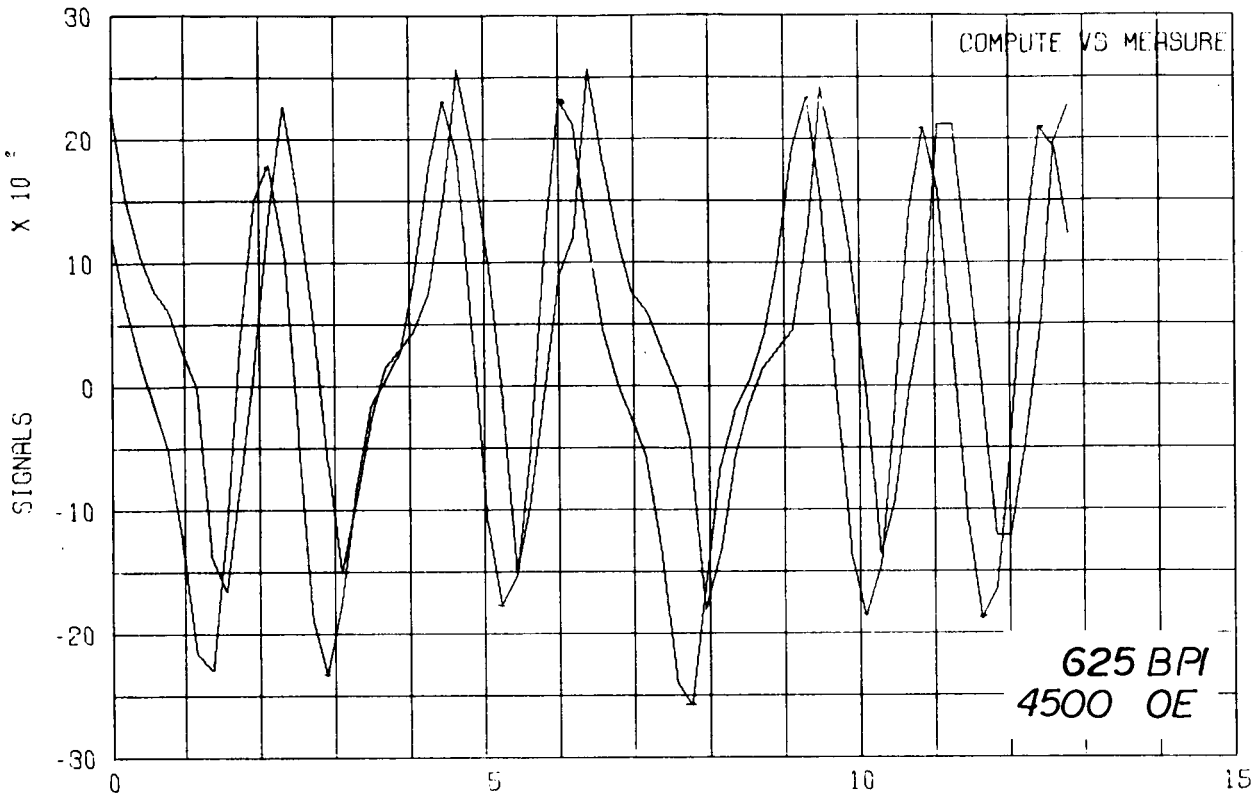
COMPUTE VS MEASURE
SIGNALS
X 10
30
20
10
0
-10
-20
-30
0
5
10
15
625 BPI
4500 OE

1C

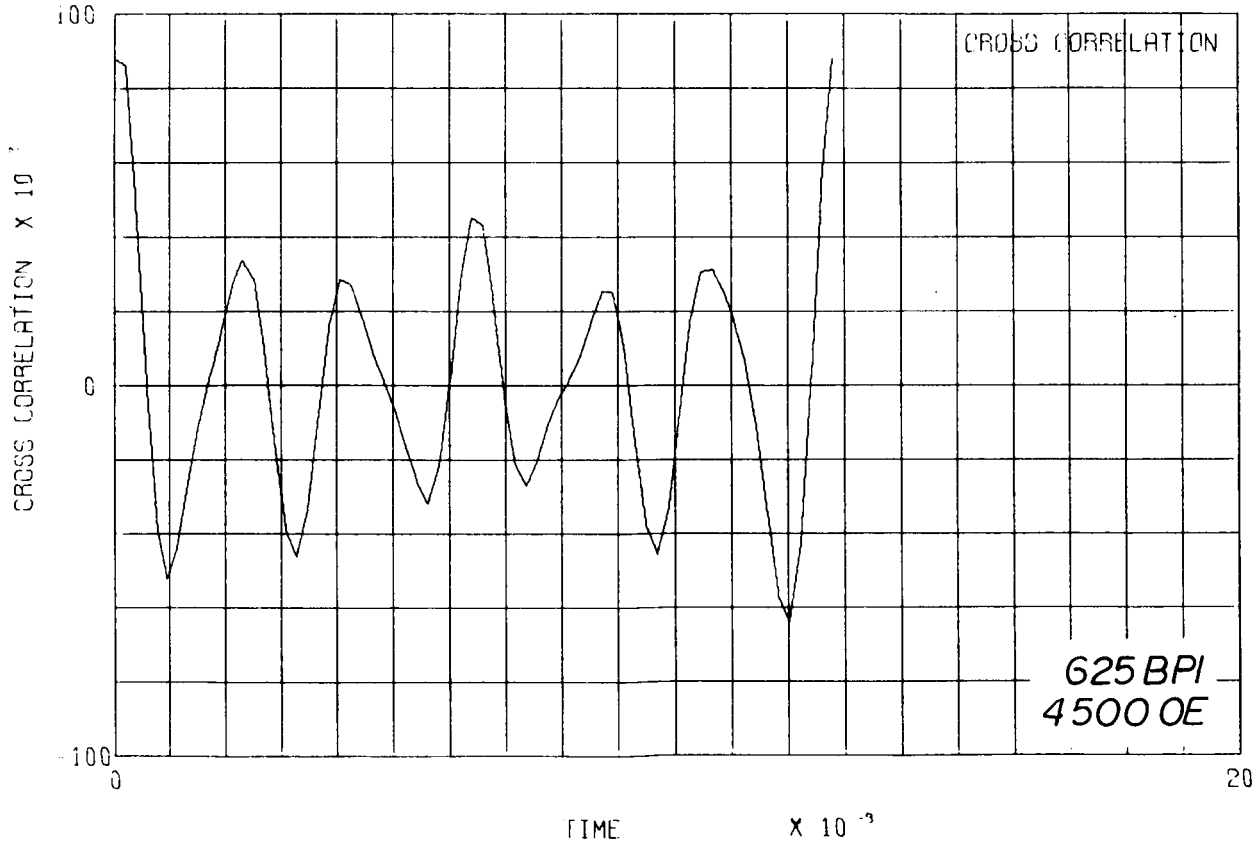
CROSS CORRELATION
CROSS CORRELATION X 10
100
0
-100
0
20
TIME
X 10
625 BPI
4500 OE

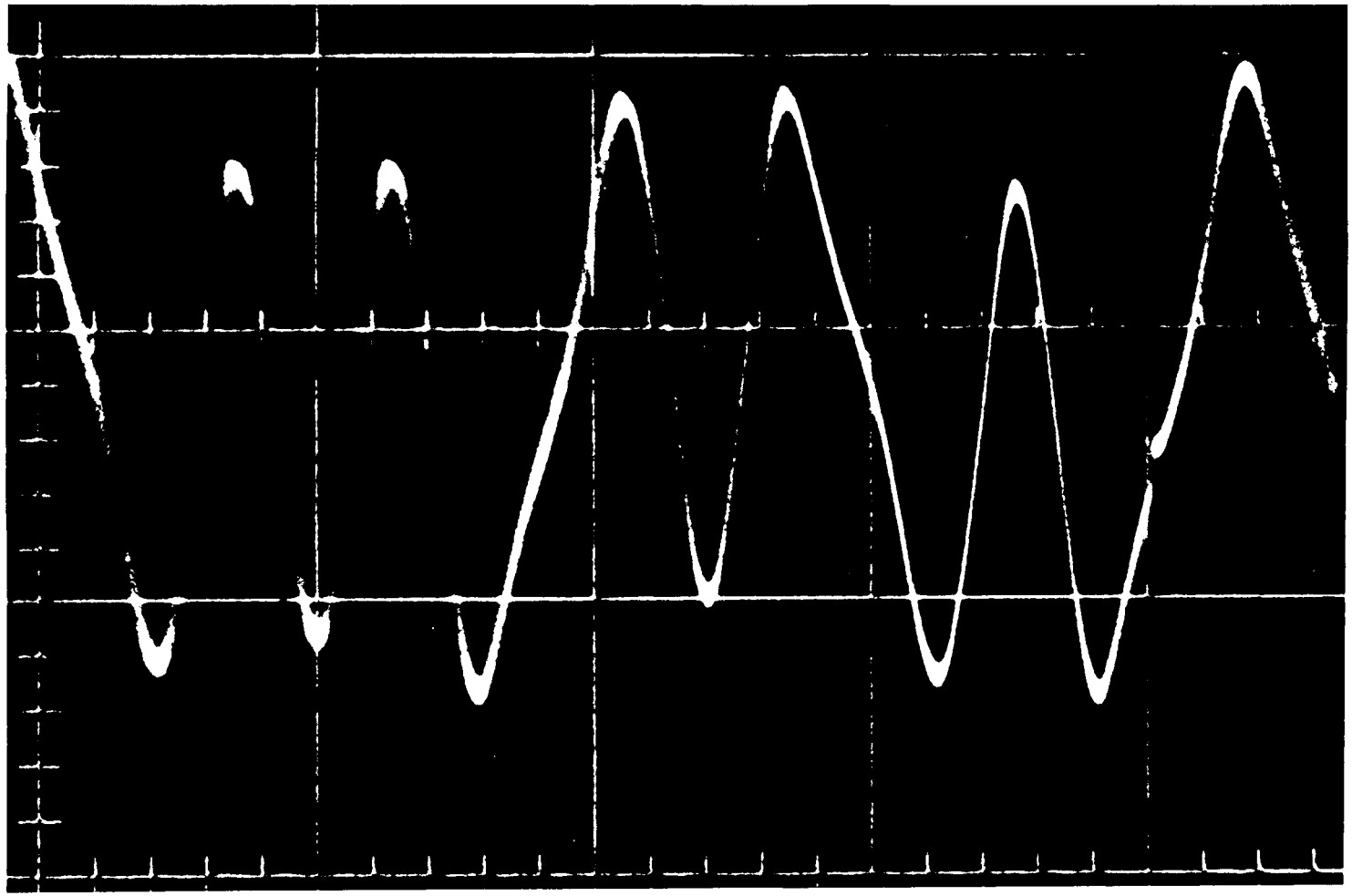

Fig. 2 Coating Thickness 400 μin.
Deep Gap Field 4500 oe (1 x saturation), 1250 BPI
a) Experimental Waveform
b) Computed versus Experimental
c) Computed Cross-Correlation F. O. M.

2A

2B

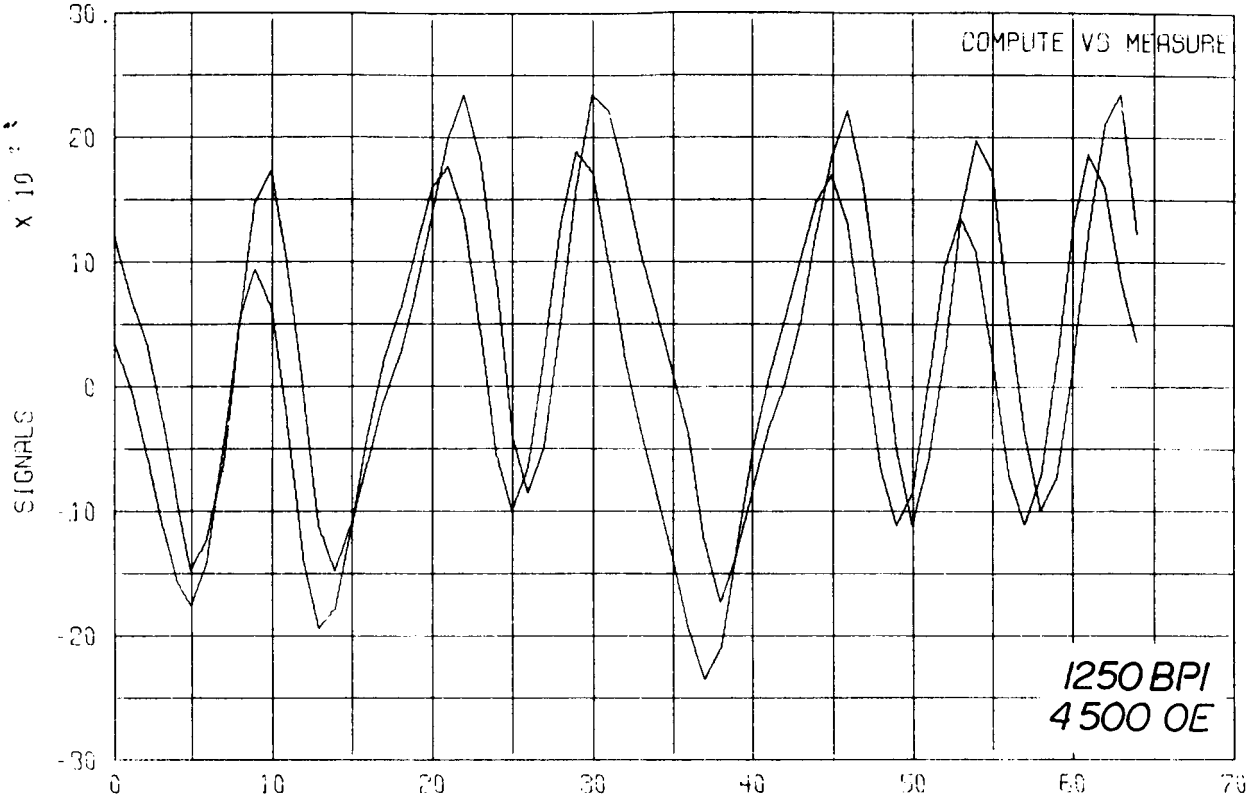
COMPUTE VS MEASURE
SIGNALS
30
20
10
0
-10
-20
-30
0
10
20
30
40
50
60
70
1250 BPI
4500 OE

2C

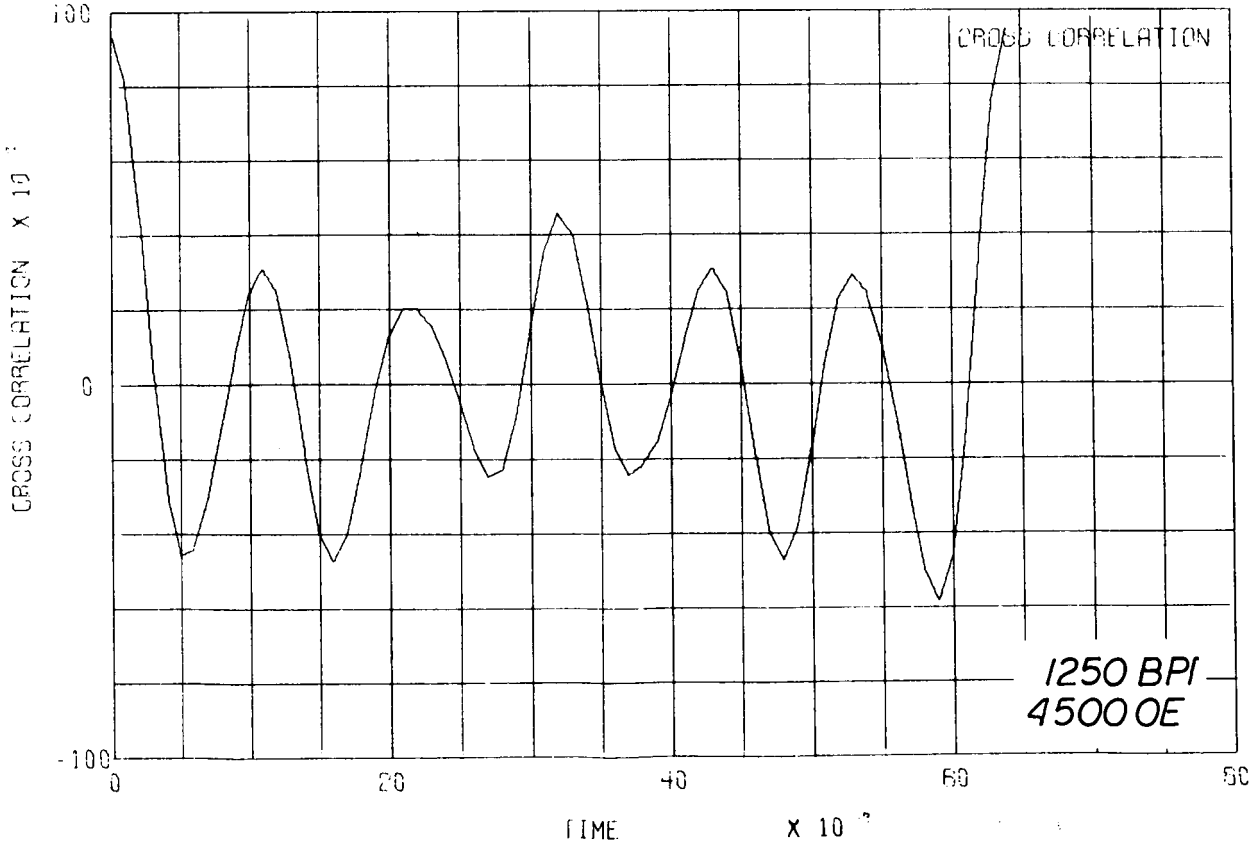
CROSS CORRELATION
CROSS CORRELATION
100
0
-100
0
20
40
60
80
TIME
1250 BPI
4500 OE

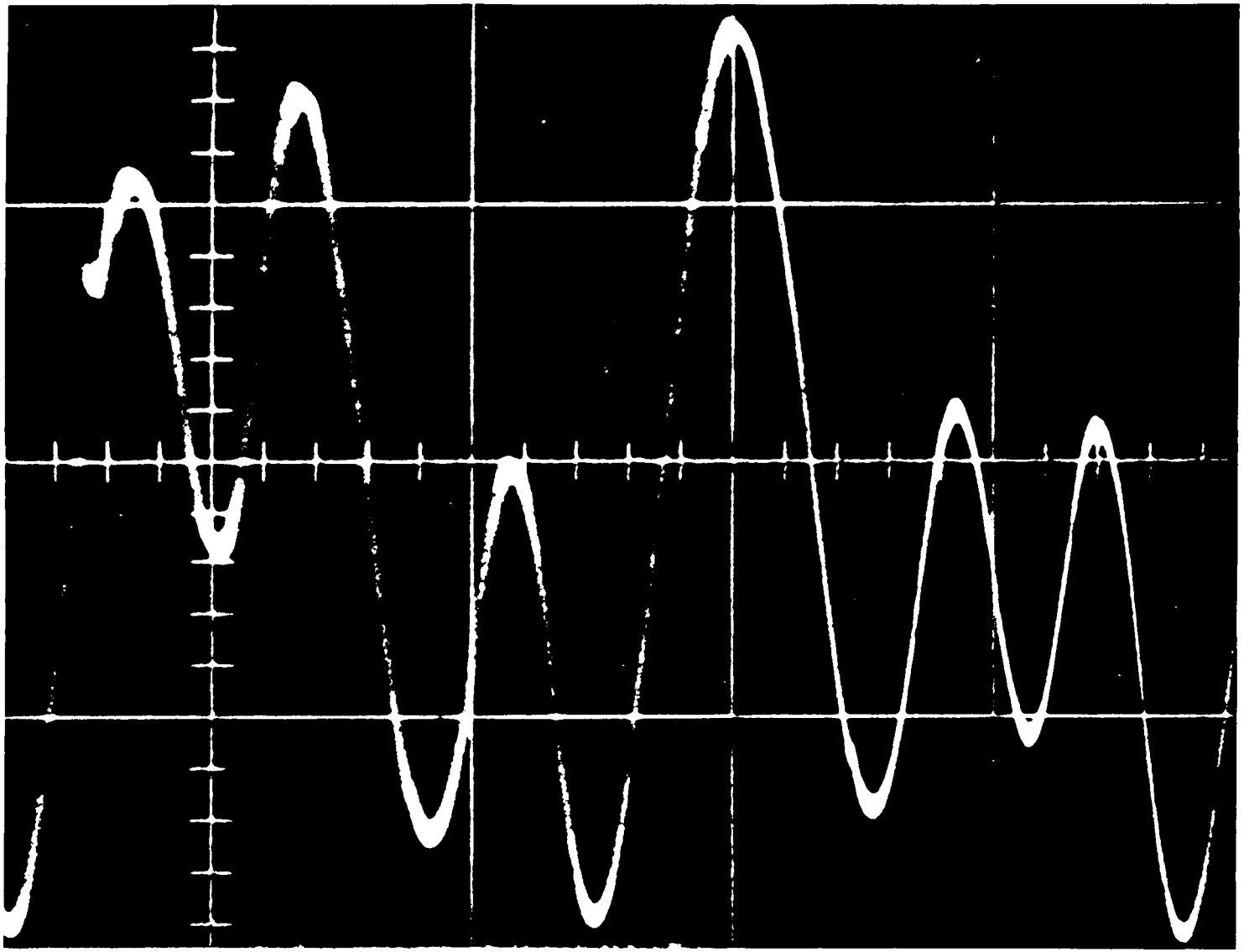

3A

Fig. 3 Coating Thickness 400 μin.
Deep Gap Field 4500 oe (1 x Saturation), 2500 BPI
a) Experimental Waveform
b) Computed versus Experimental
c) Computed Cross-Correlation F.O. M

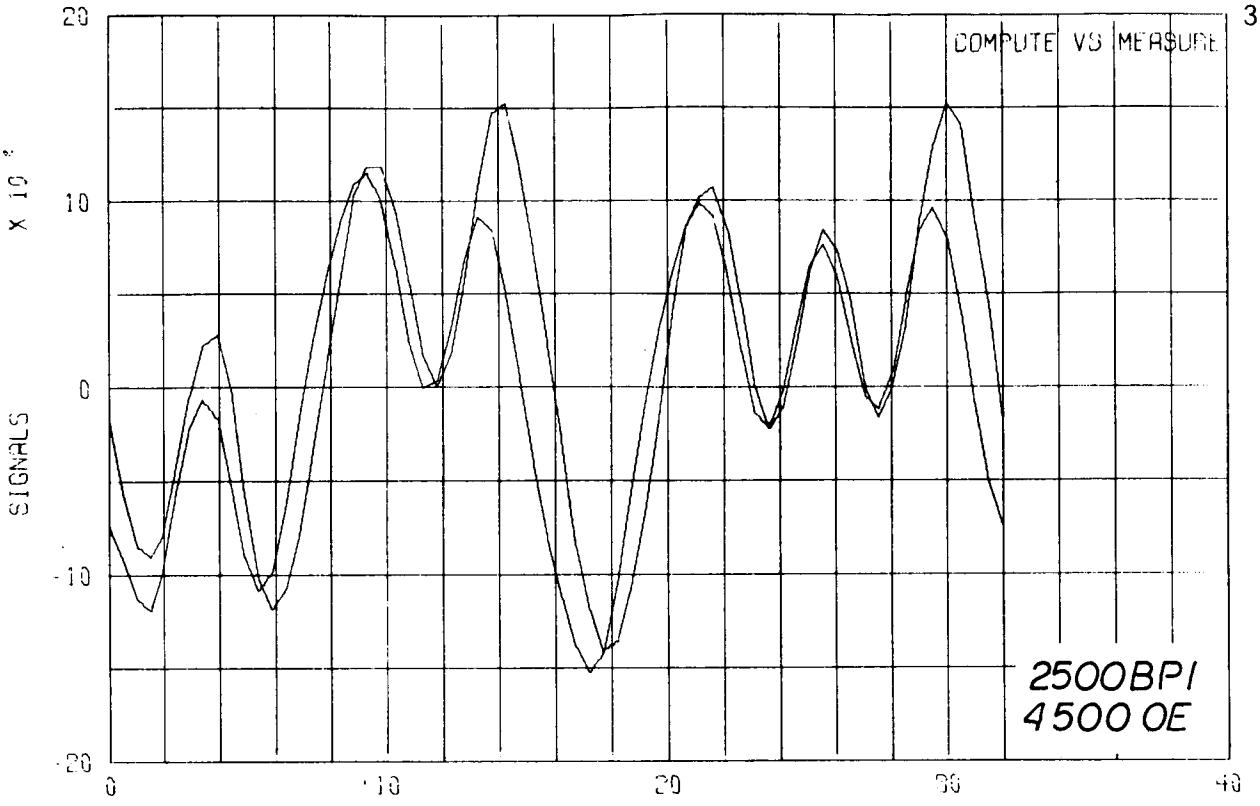
3B
COMPUTE VS MEASURE
SIGNALS
X 10
20
10
0
-10
-20
0
10
20
30
40
2500BPI
4500 OE

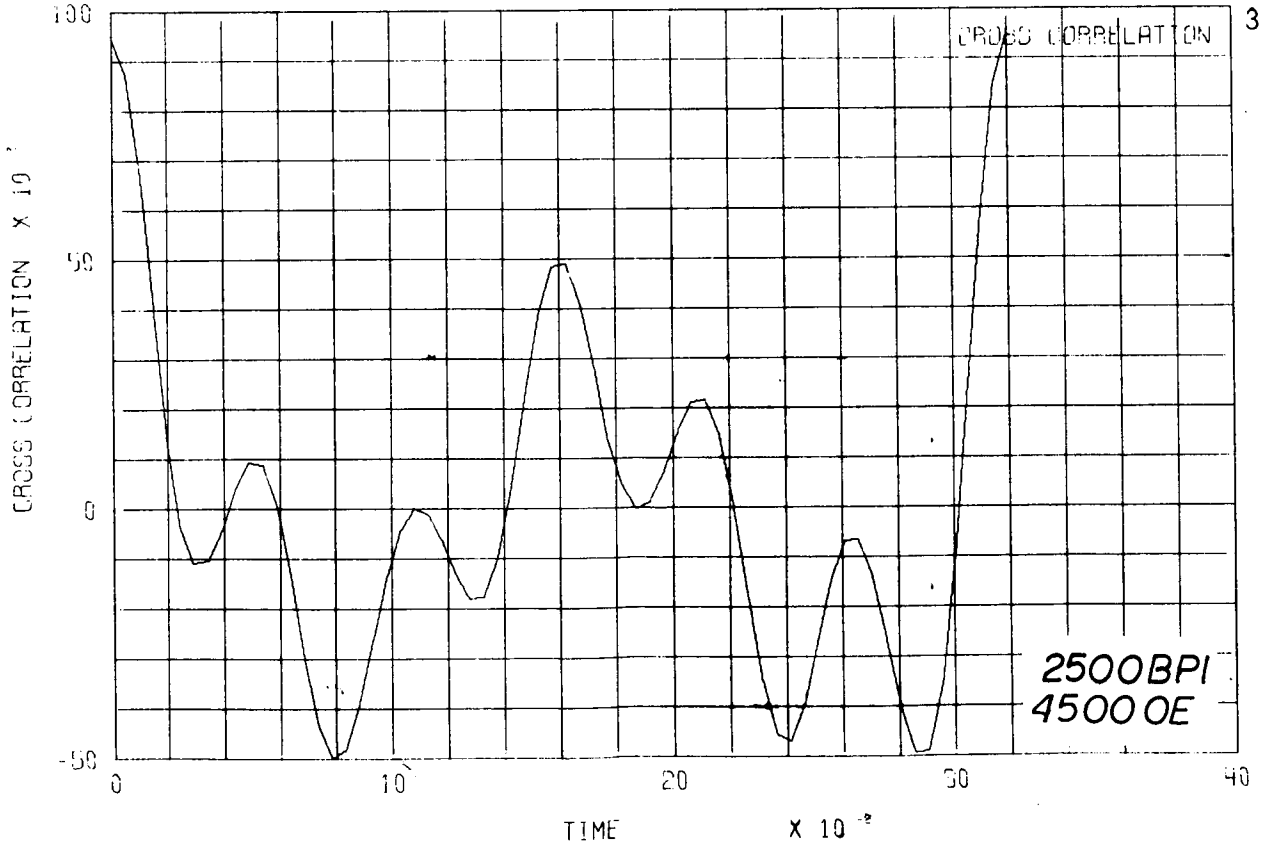
3C
CROSS CORRELATION
CROSS CORRELATION X 10
100
50
0
-50
0
10
20
30
40
TIME
X 10
2500BPI
4500 OE

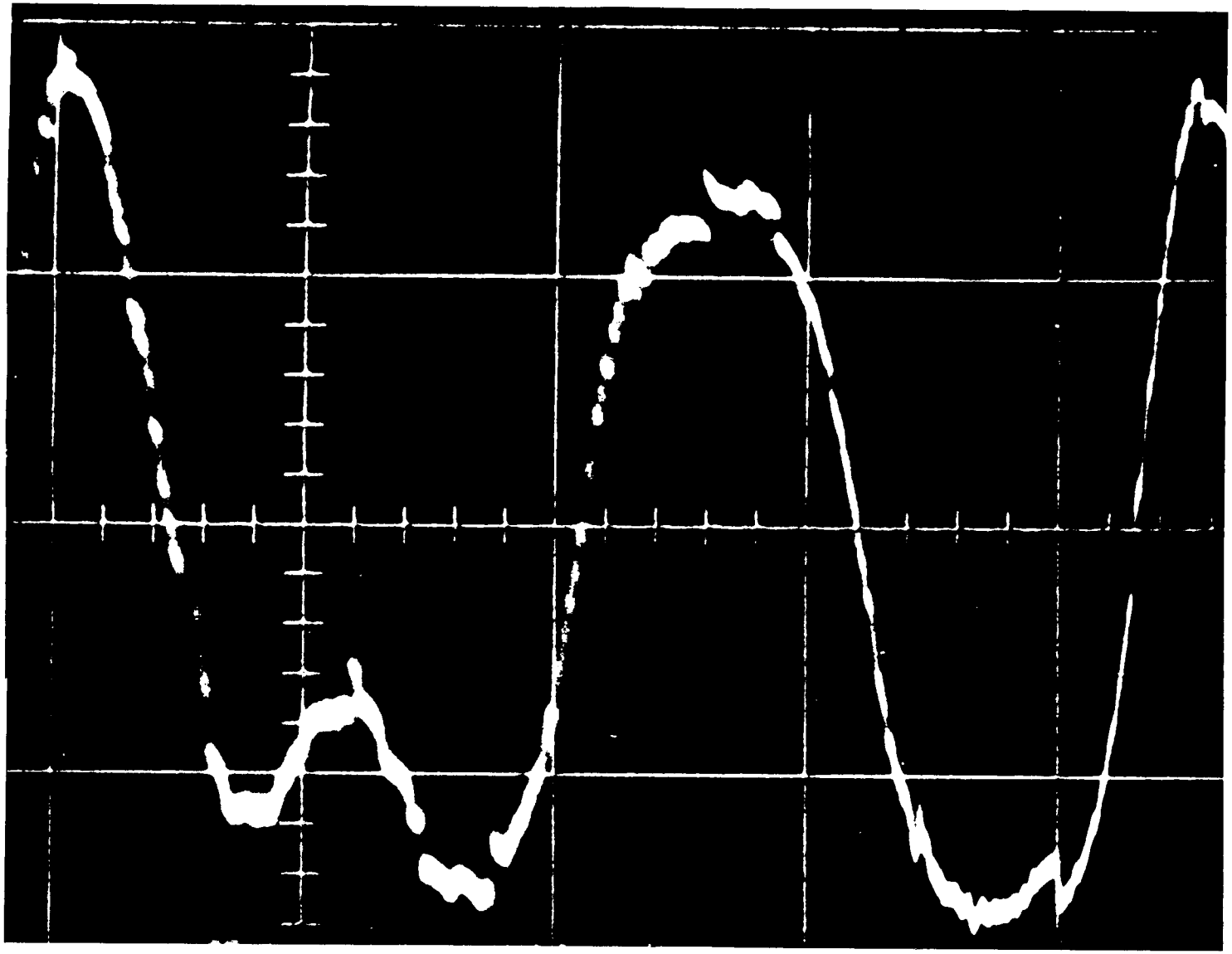

4A

Fig. 4 Coating Thickness 400 μin.
Deep Gap Field 4500 oe (1 x Saturation), 5000 BPI
a) Experimental Waveform
b) Computed versus Experimental
c) Computed Cross-Correlation F. O. M

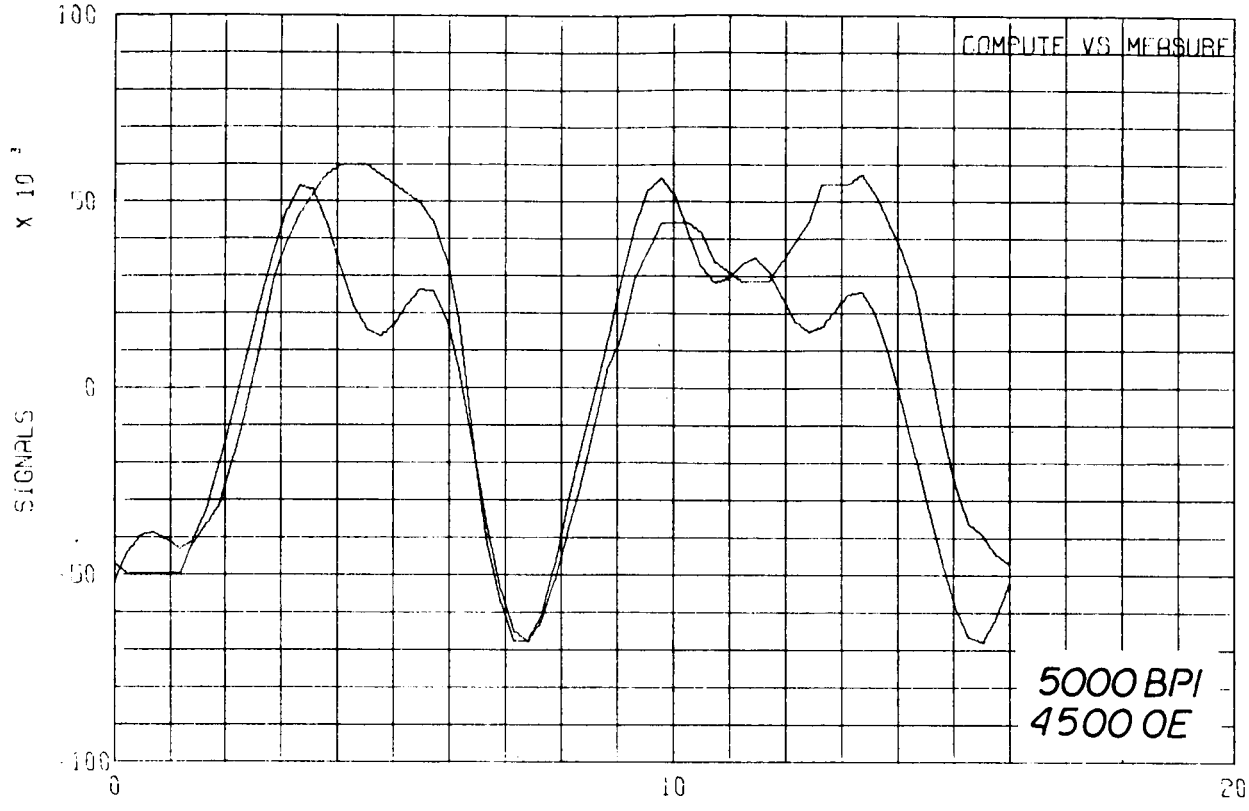
COMPUTE VS MEASURE
SIGNALS X 10 ³
100
50
0
-50
-100
0
10
20
5000 BPI
4500 OE

4B

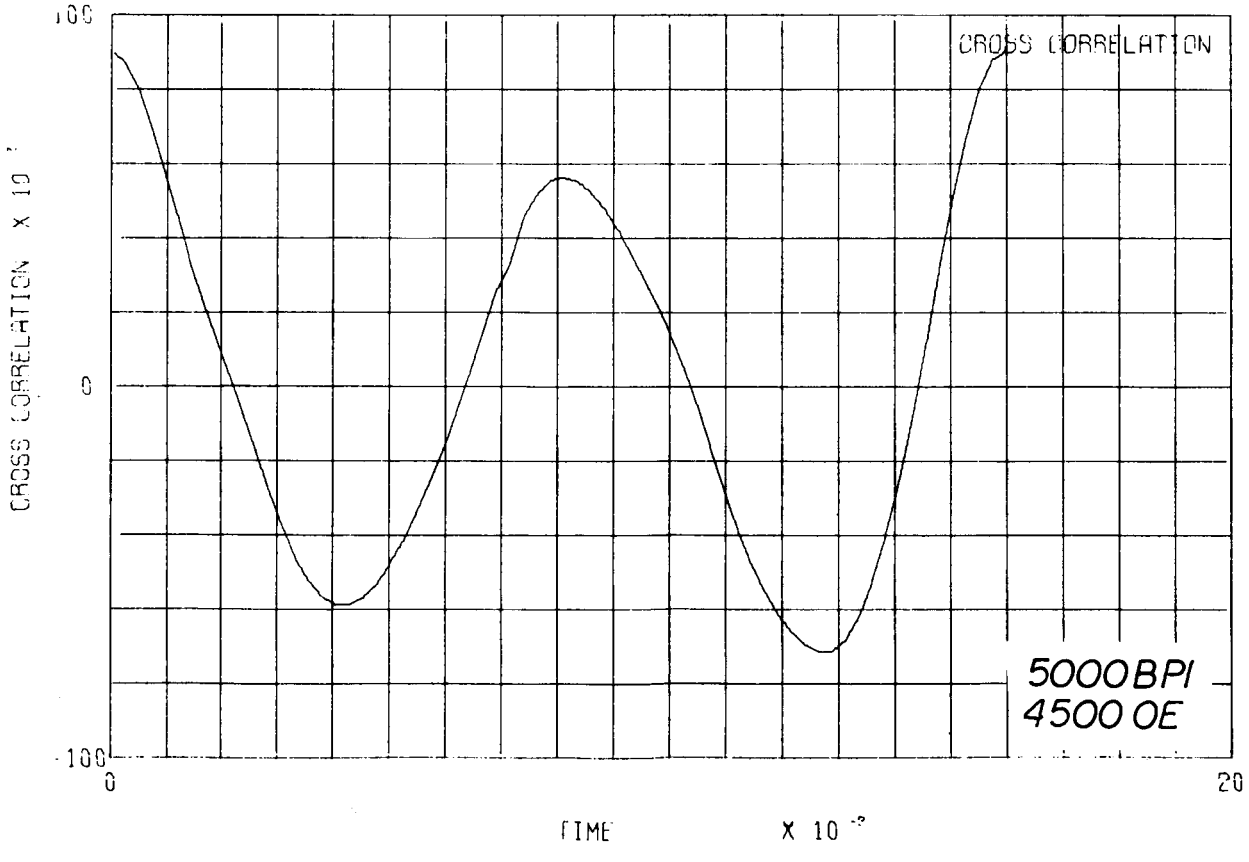
CROSS CORRELATION
CROSS CORRELATION X 10 ³
100
0
-100
0
20
TIME X 10 ⁻³
5000 BPI
4500 OE

4C

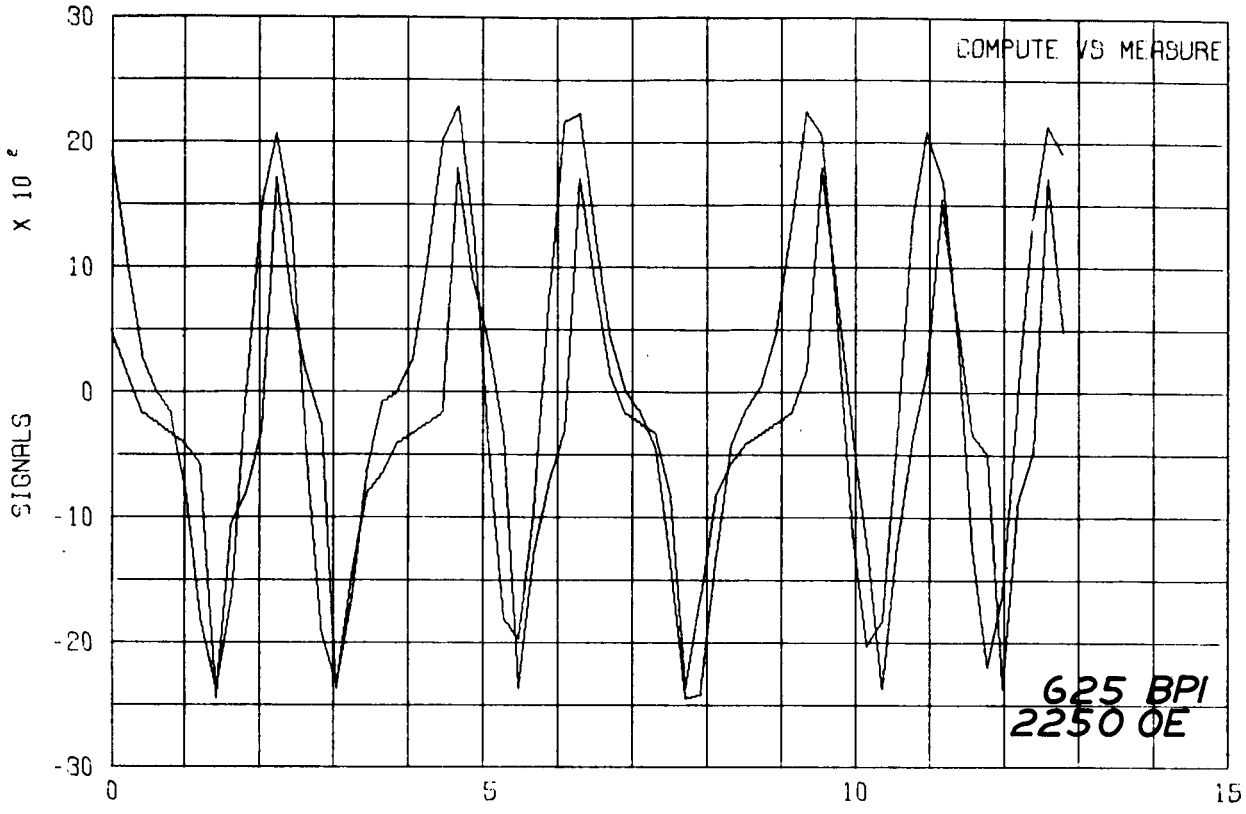
COMPUTE VS MEASURE
SIGNALS X 10 ^ e
30
20
10
0
-10
-20
-30
0
5
10
15
625 BPI
2250 OE

5B

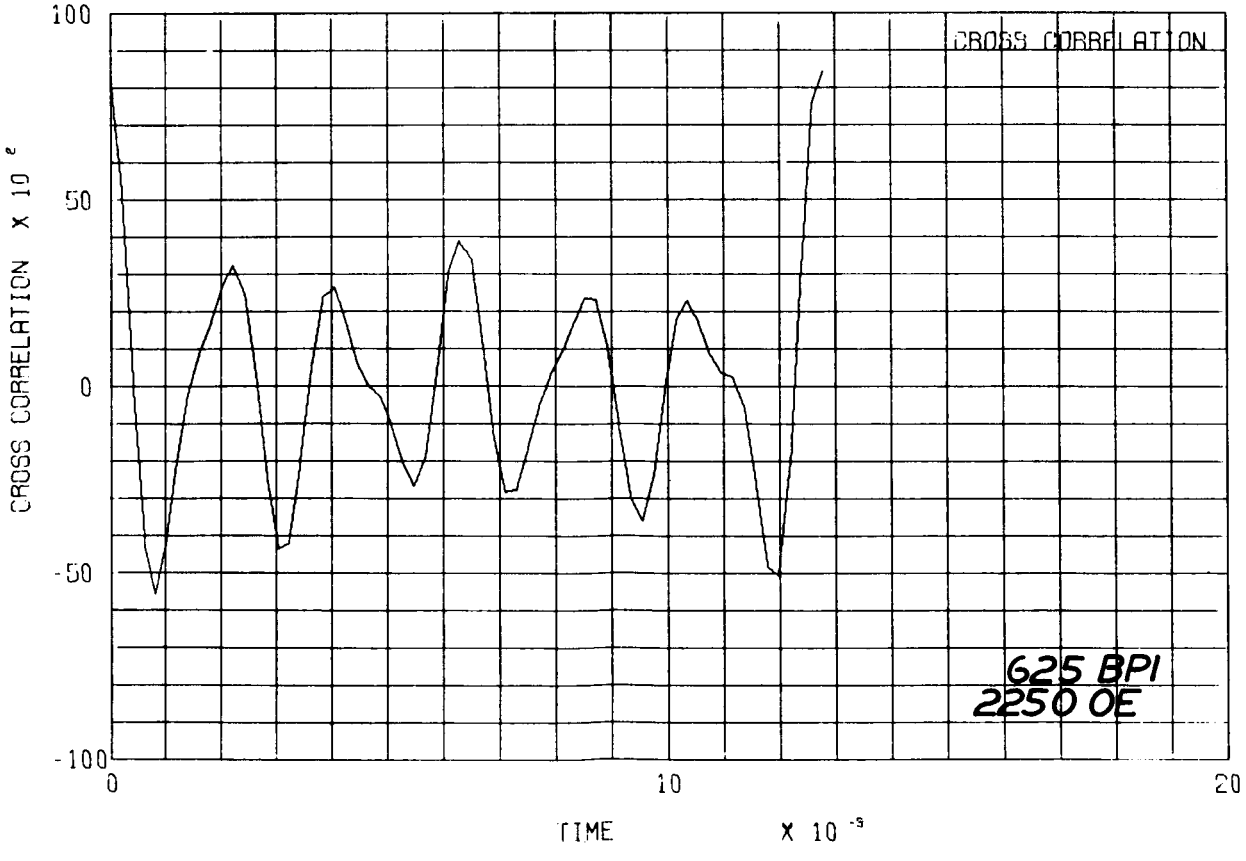
CROSS CORRELATION
CROSS CORRELATION X 10 ^ e
100
50
0
-50
-100
0
10
20
TIME X 10 ^ -3
625 BPI
2250 OE

5C

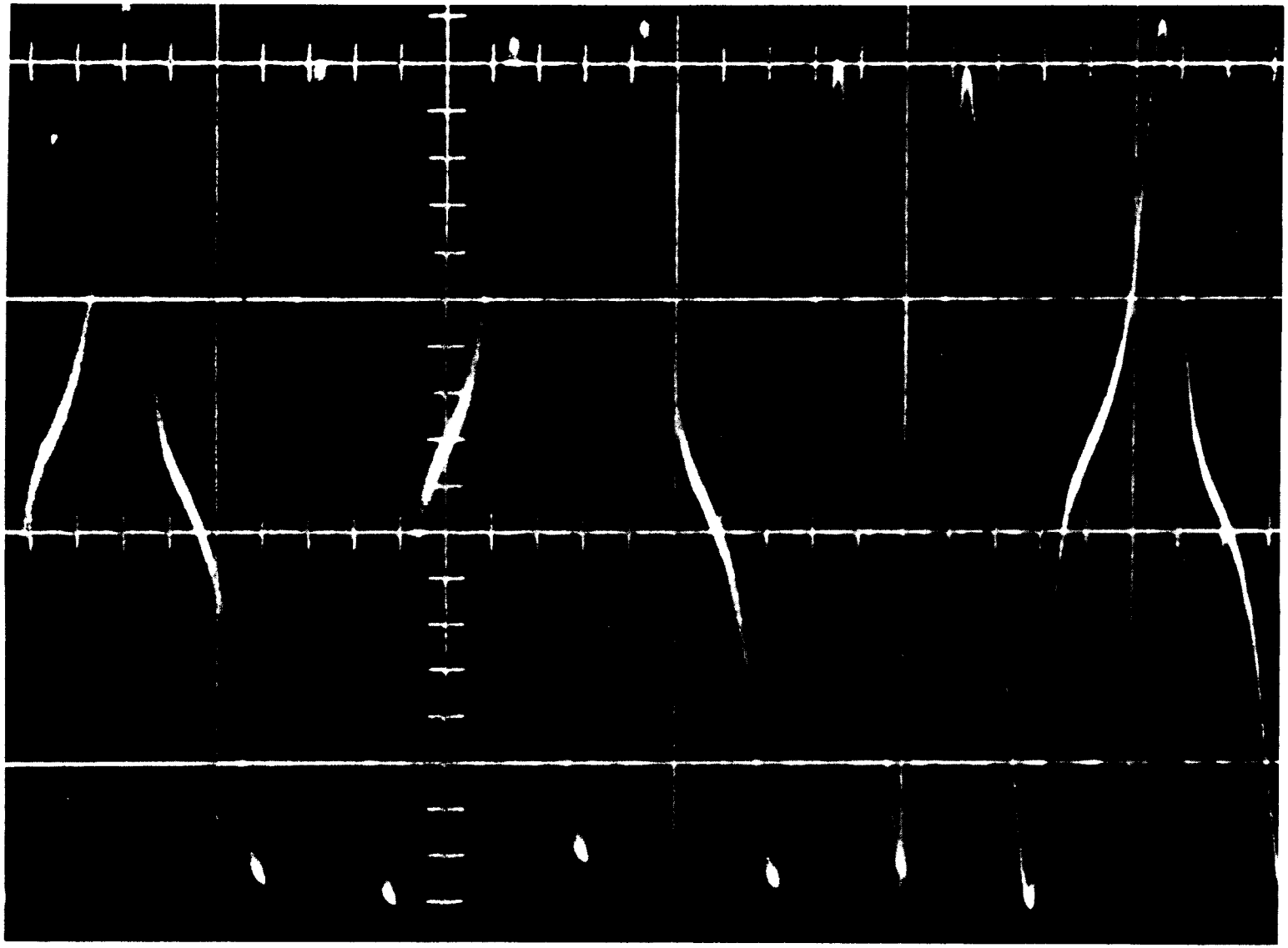

Fig. 6 Coating Thickness 400 μin.
Deep Gap Field 2250 oe (1/2 x Saturation), 1250 BPI
a) Experimental Waveform
b) Computed versus Experimental
c) Computed Cross-Correlation F. O. M

6A

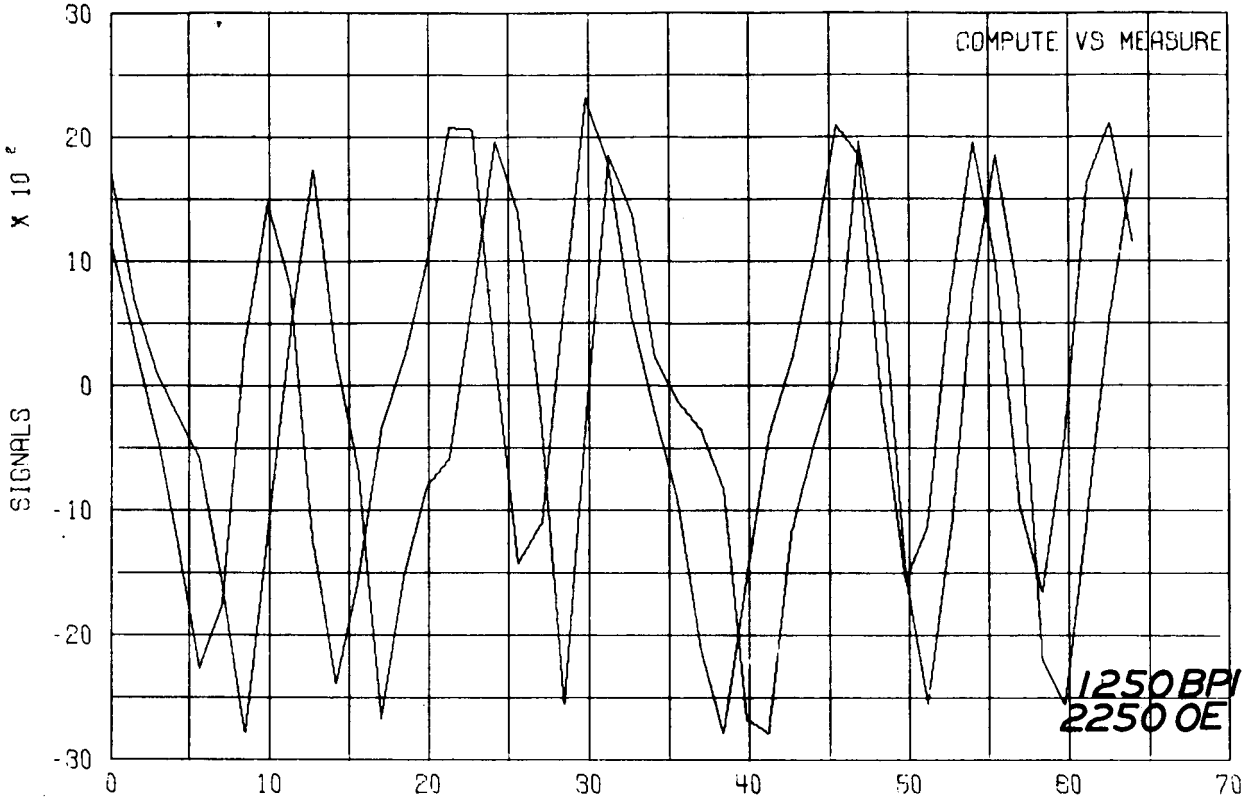
COMPUTE VS MEASURE
SIGNALS X 10 ²
30
20
10
0
-10
-20
-30
0
10
20
30
40
50
60
70
1250 BPI
2250 OE

6B

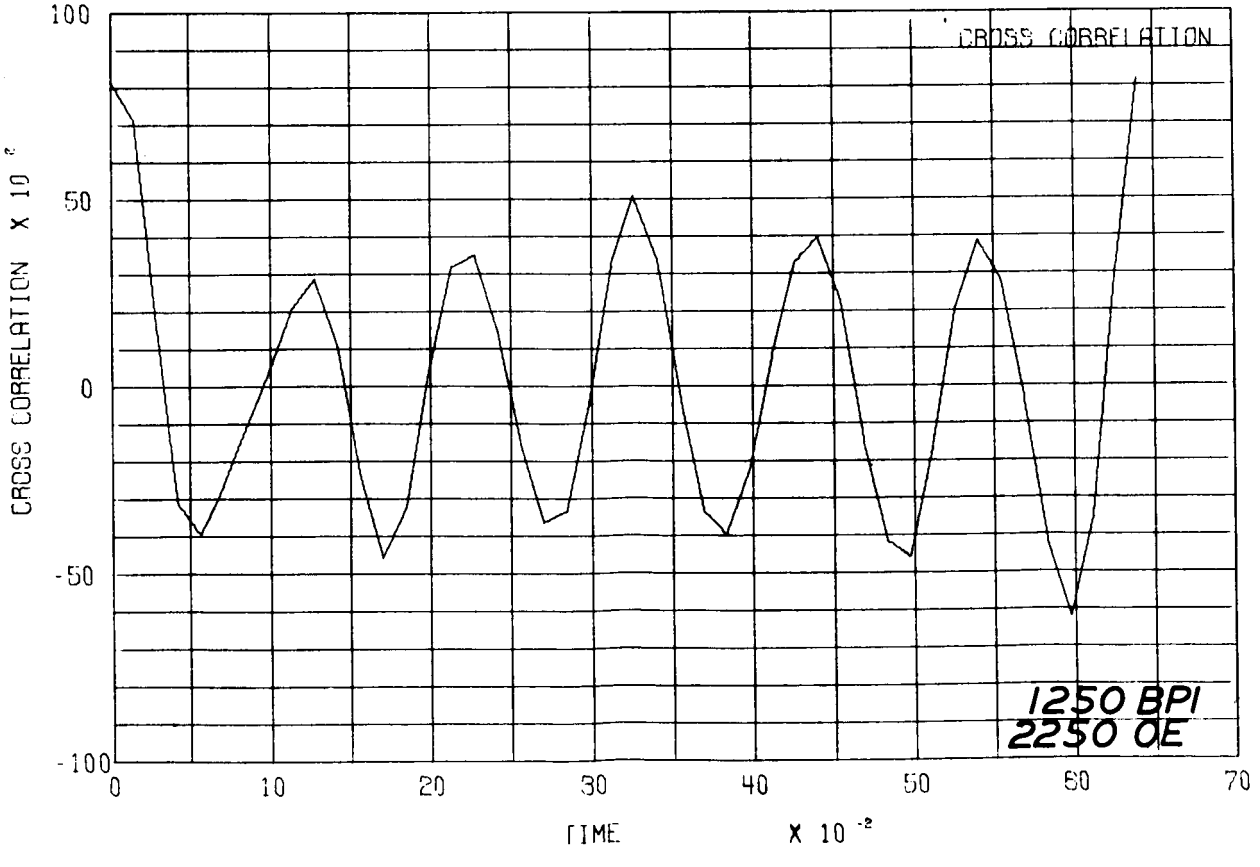
CROSS CORRELATION
CROSS CORRELATION X 10 ²
100
50
0
-50
-100
0
10
20
30
40
50
60
70
TIME X 10 ⁻²
1250 BPI
2250 OE

6C

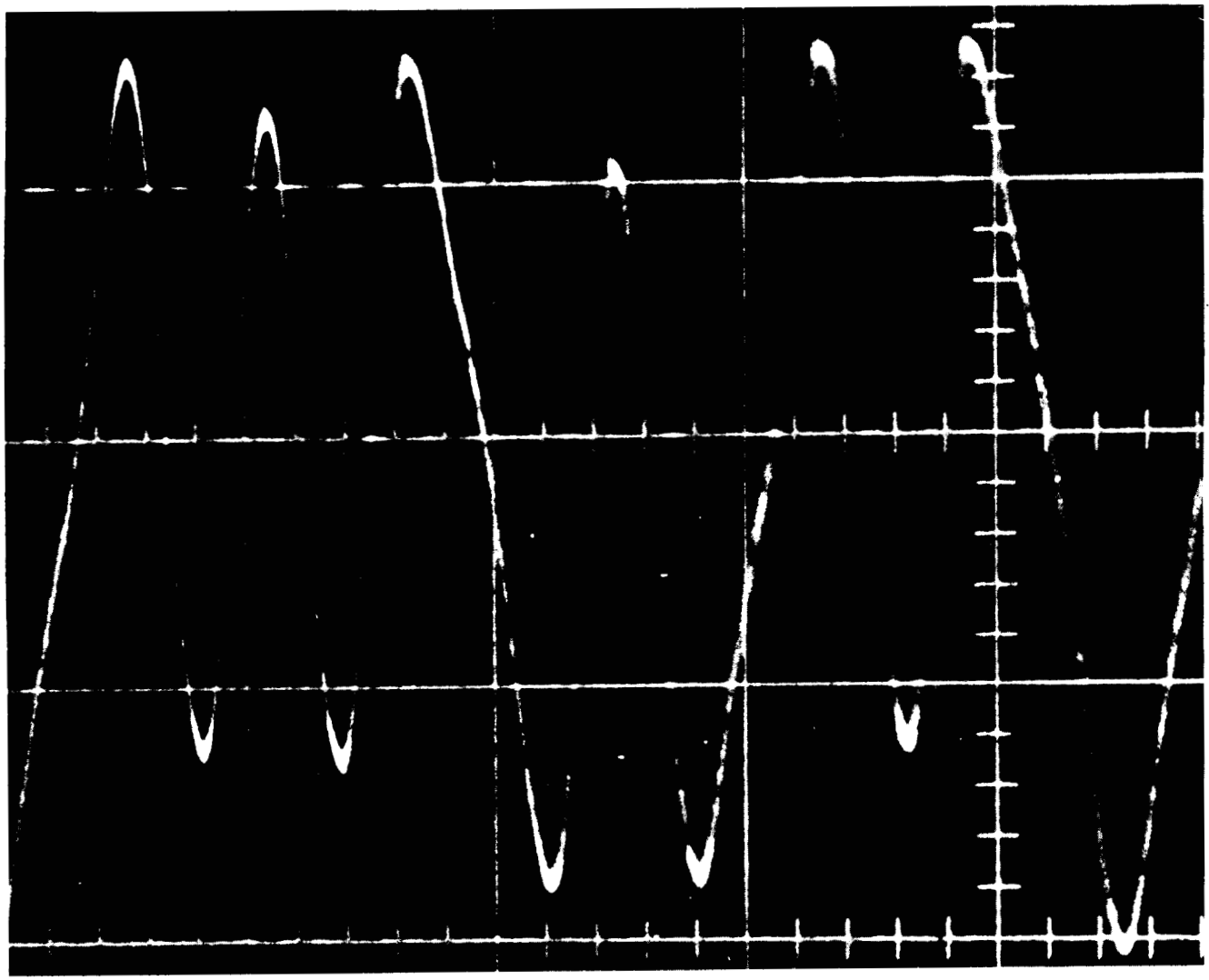

7A

Fig. 7 Coating Thickness 400 μin.
Deep Gap Field 4500 oe (1/2 x Saturation), 2500 BPI
a) Experimental Waveform
b) Computed versus Experimental
c) Computed Cross-Correlation F. O. M.

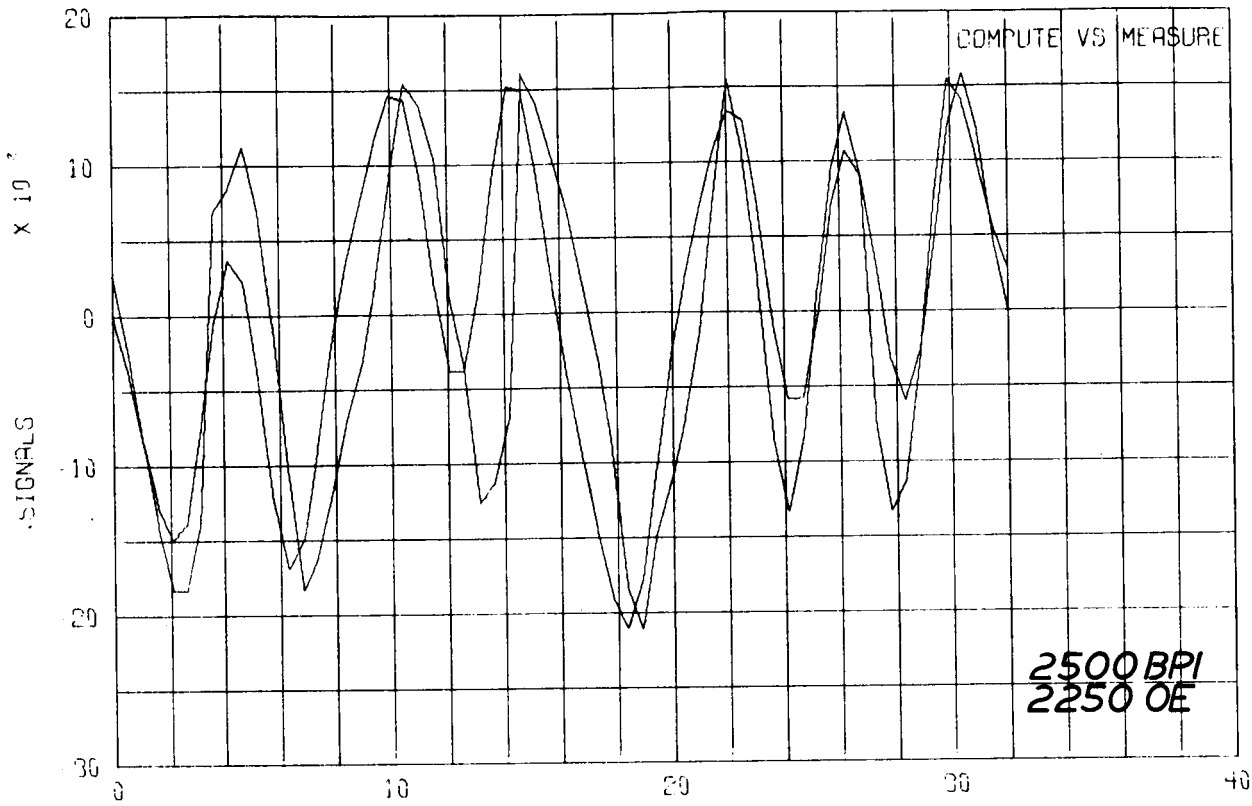
COMPUTE VS MEASURE
2500 BPI
2250 OE
SIGNALS
X 10
20
10
0
-10
-20
-30
0
10
20
30
40

7B

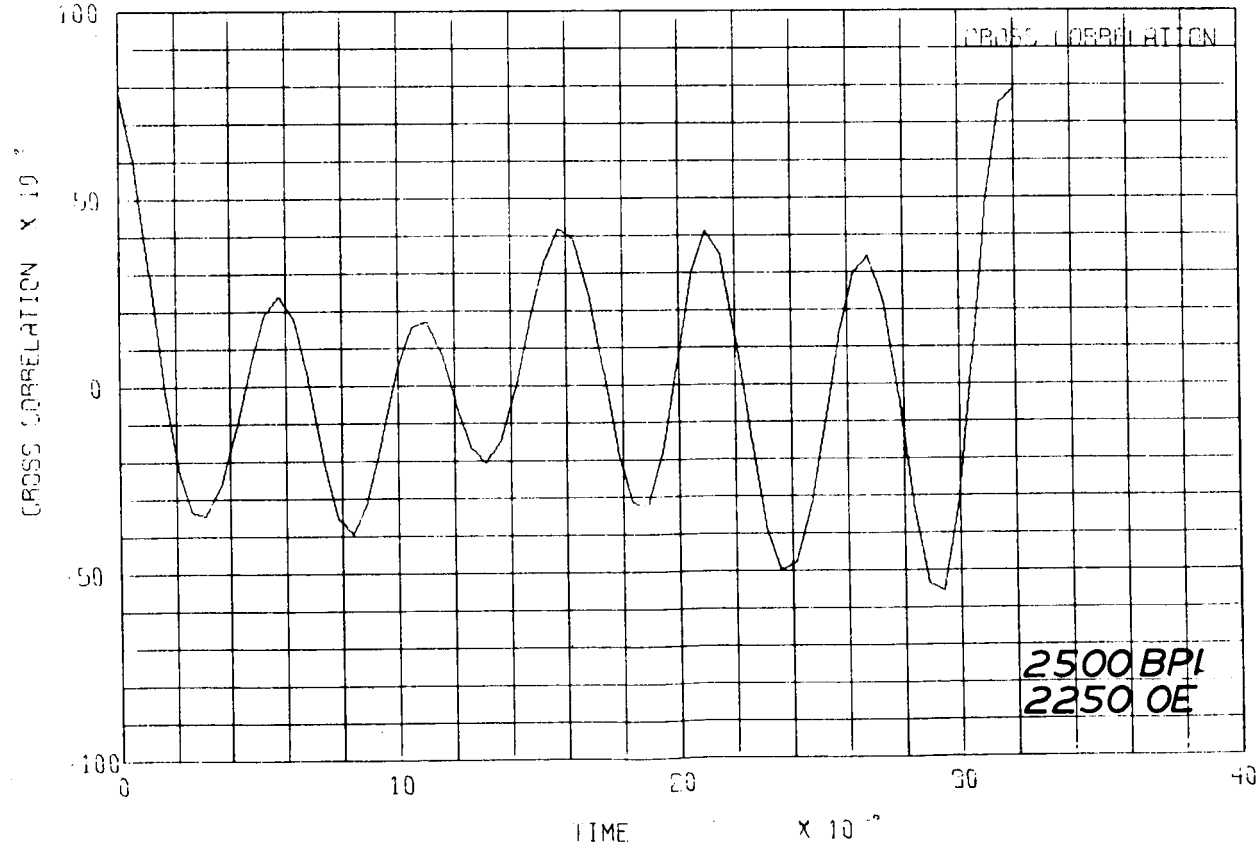
CROSS CORRELATION
2500 BPI
2250 OE
CROSS CORRELATION X 10
100
50
0
-50
-100
0
10
20
30
40
TIME X 10

7C

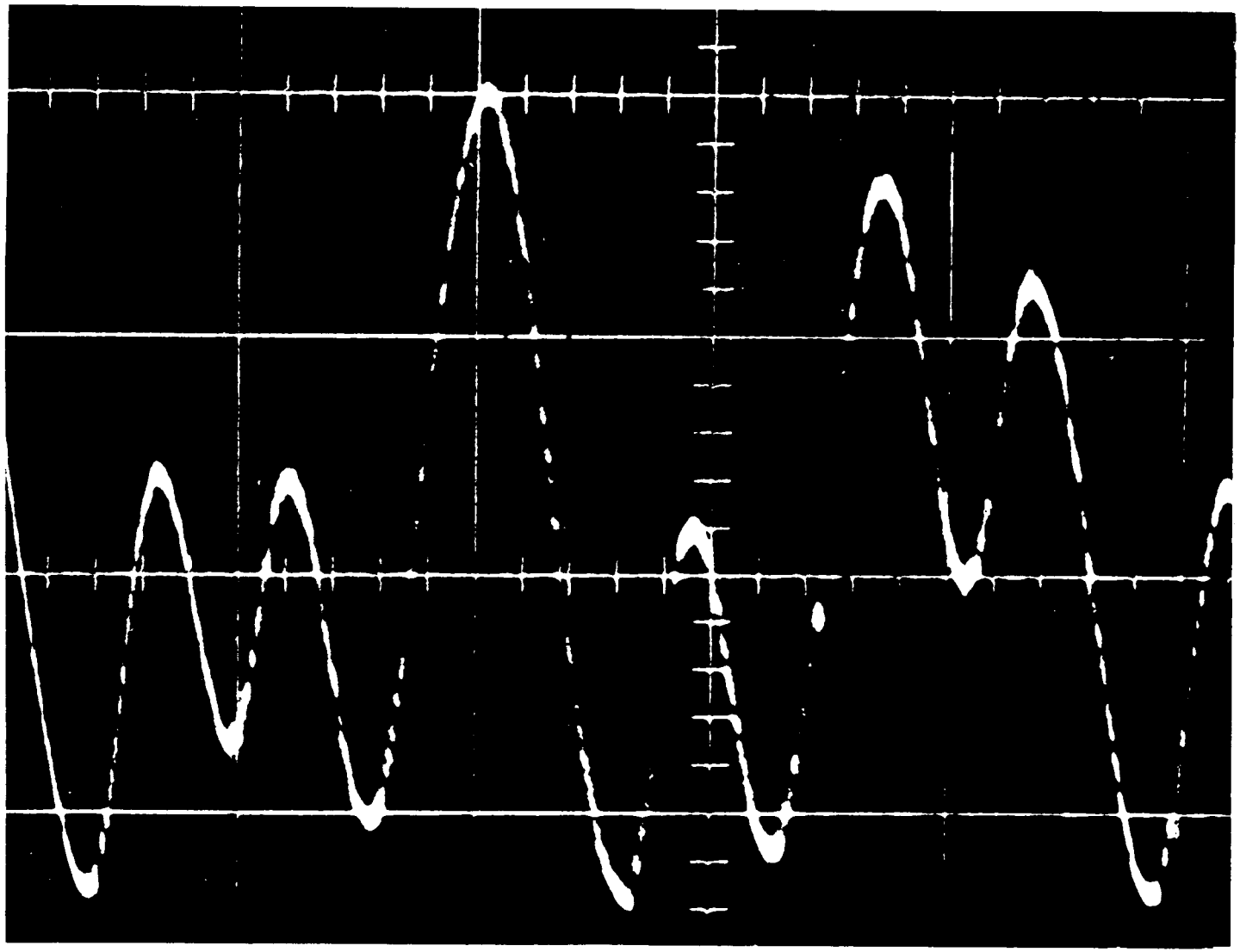

8A

Fig. 8 Coating Thickness 400 μin.
Deep Gap Field 2250 oe (1/2 x Saturation) 5000 BPI
a) Experimental Waveform
b) Computed versus Experimental
c) Computed Cross-Correlation F. O. M.

8B

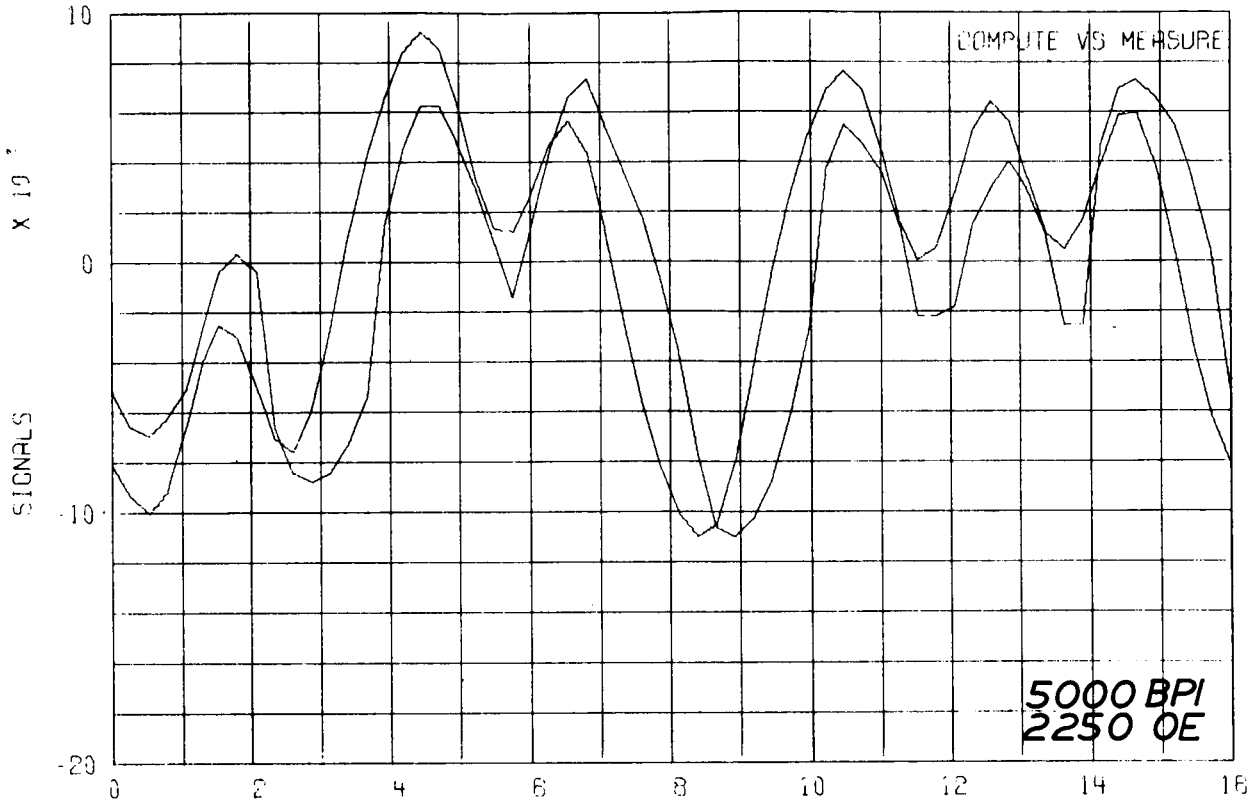
COMPUTE VS MEASURE
5000 BPI
2250 OE
SIGNALS
10
0
-10
-20
0
2
4
6
8
10
12
14
16

8C

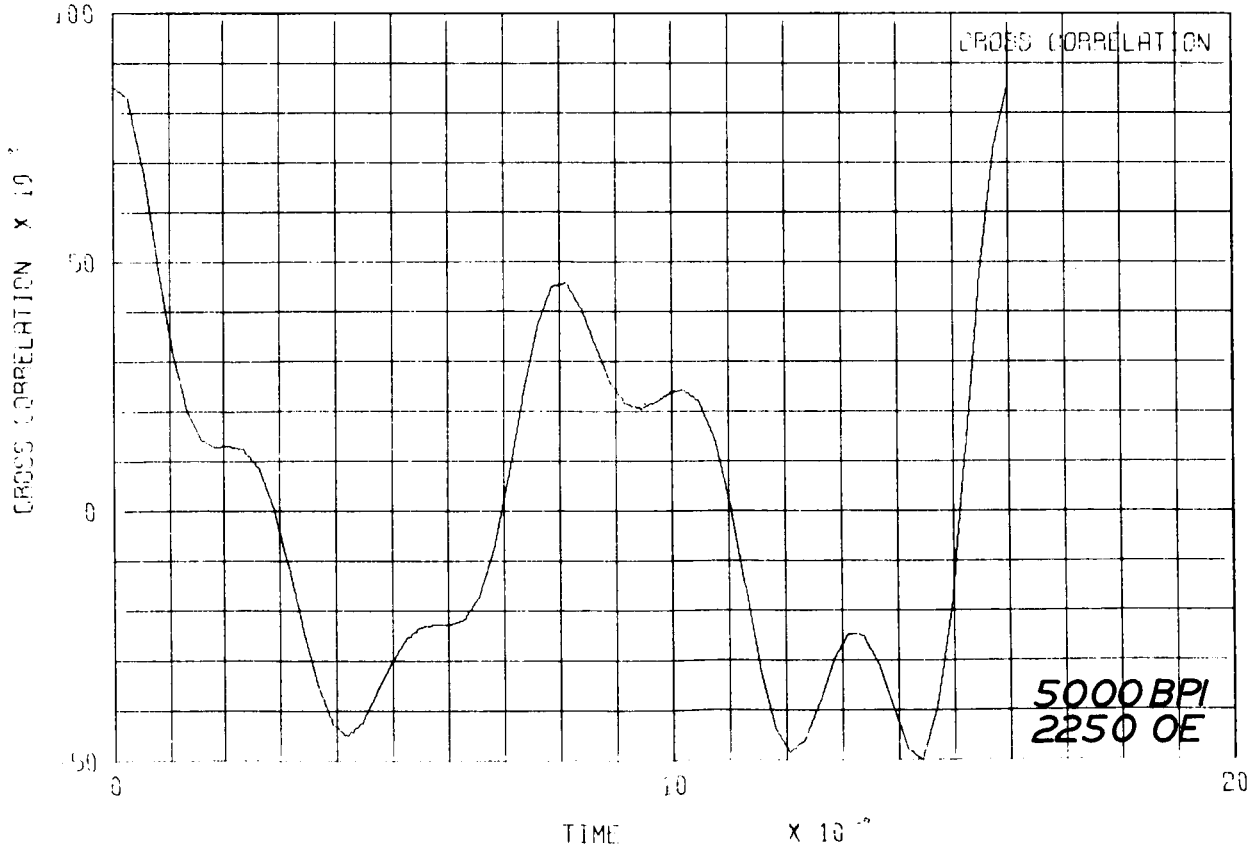
CROSS CORRELATION
5000 BPI
2250 OE
CROSS CORRELATION X 10
50
0
-50
0
10
20
TIME X 10

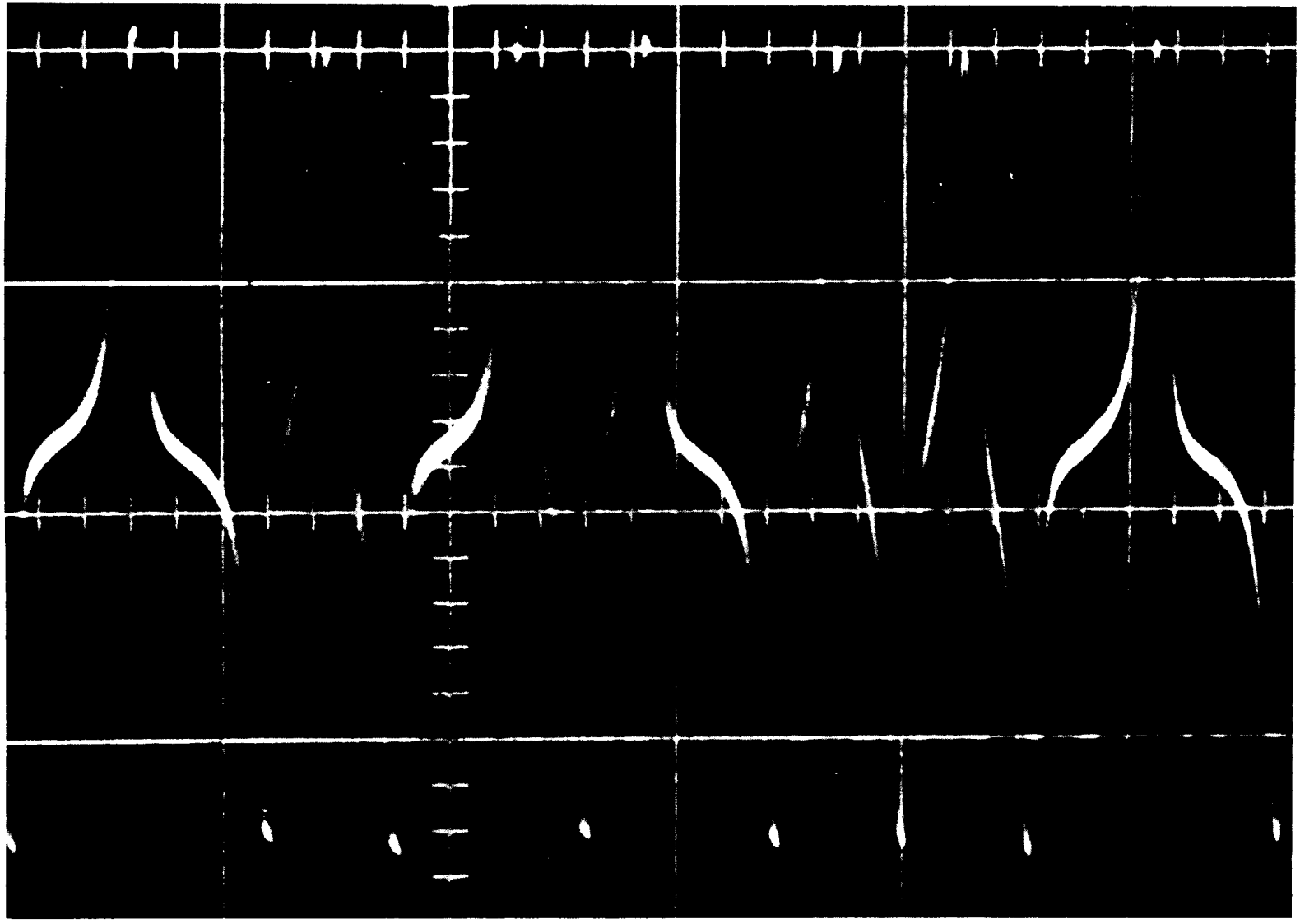

Fig. 5 Coating Thickness 400 μin. 5 A
Deep Gap Field 2250 oe (1/2 x Saturation) 625 BPI
a) Experimental Waveform
b) Computed versus Experimental
c) Computed Cross-Correlation F. O. M

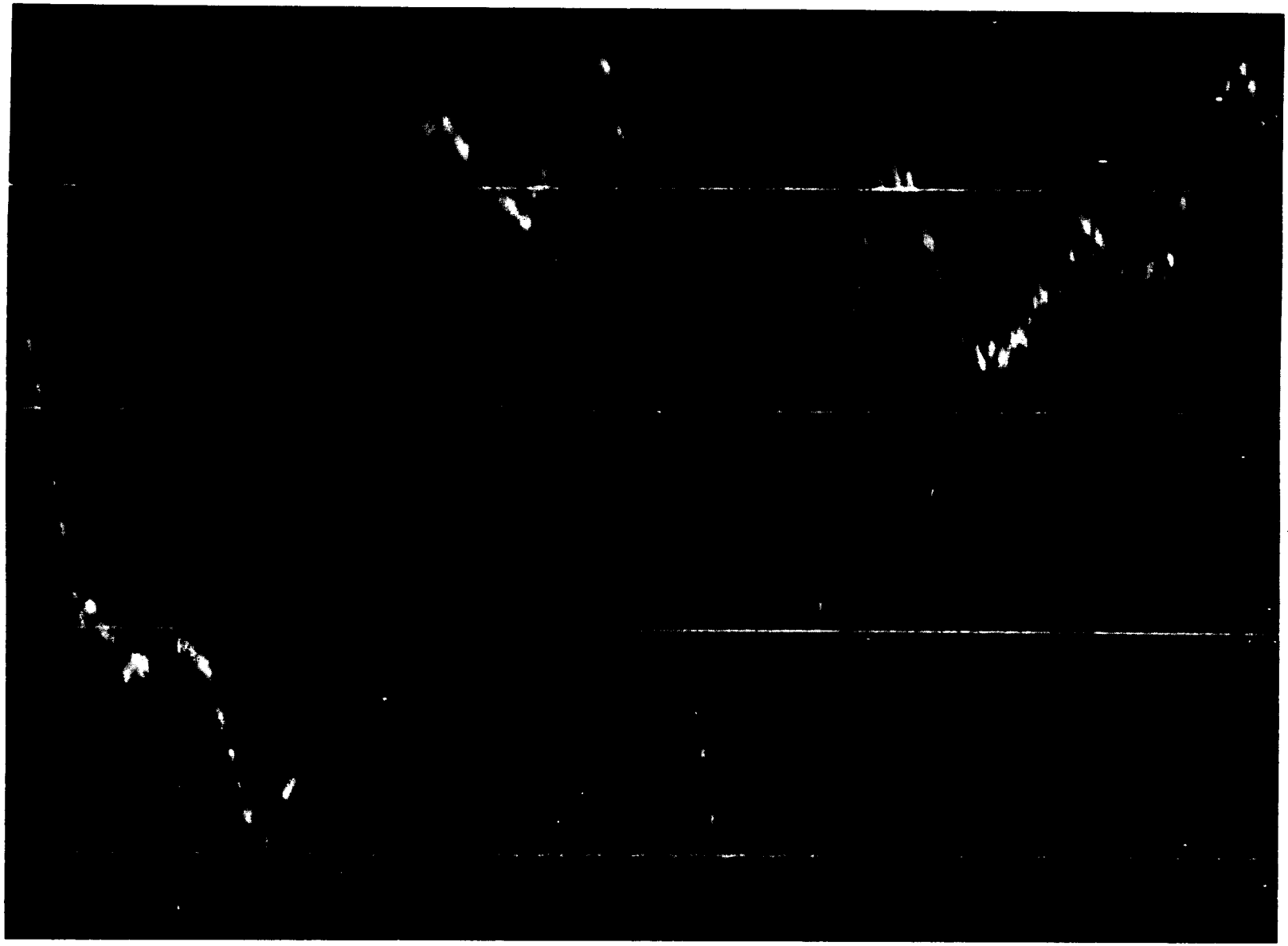

Fig. 9 Coating Thickness 400 μin. 9A
Deep Gap Field 2250 oe (1/2 x Saturation), 7500 BPI
a) Experimental Waveform
b) Computed versus Experimental
c) Computed Cross-Correlation F. O. M.

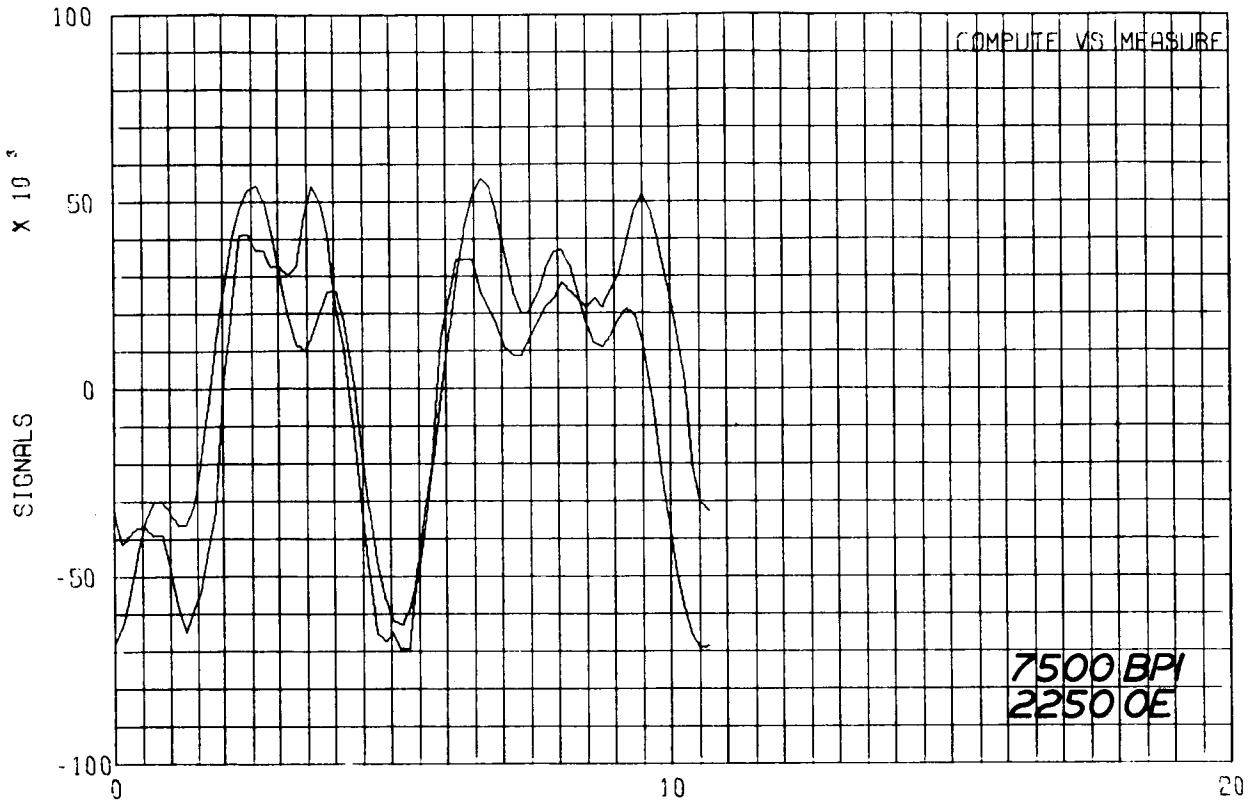
COMPUTE VS MEASURE
7500 BPI
2250 OE
SIGNALS
X 10
100
50
0
-50
-100
0
10
20

9B

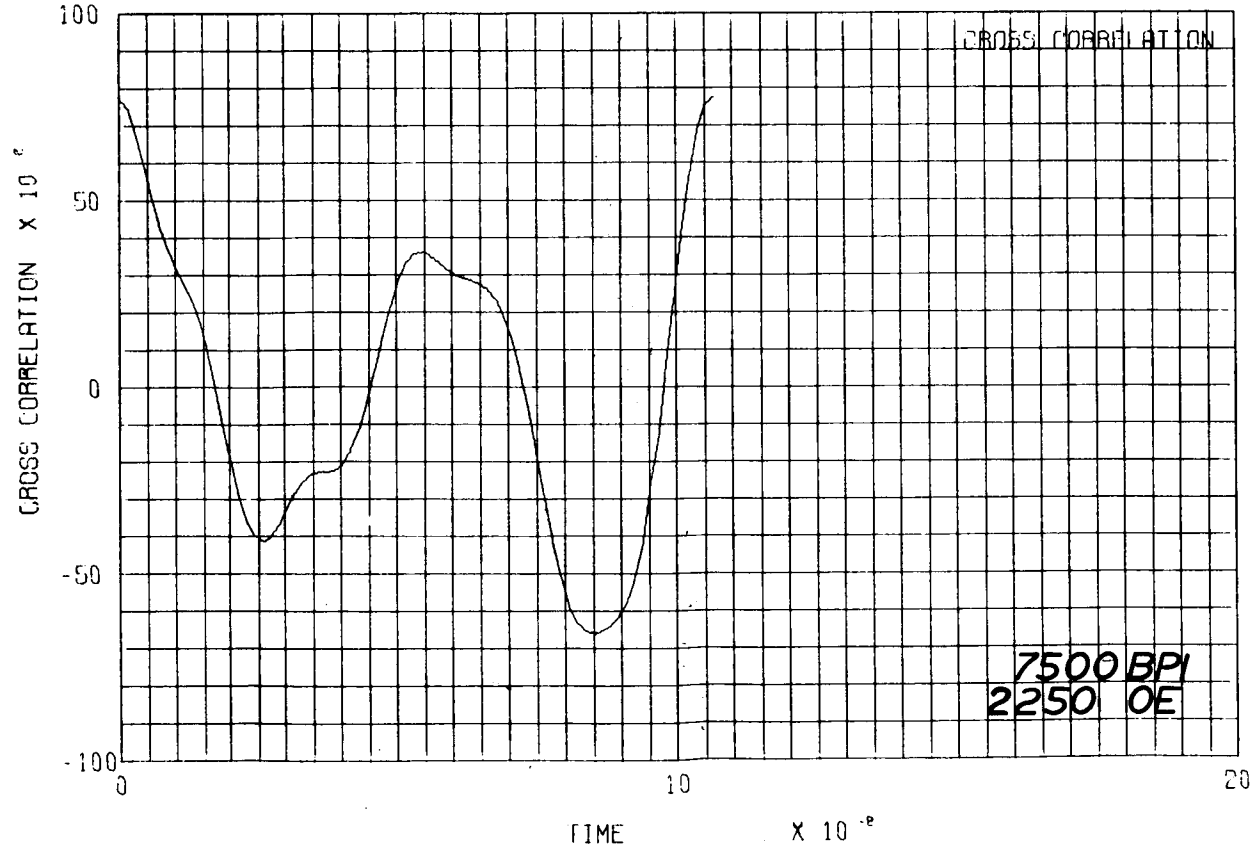
CROSS CORRELATION
7500 BPI
2250 OE
CROSS CORRELATION X 10
100
50
0
-50
-100
0
10
20
TIME X 10

9C

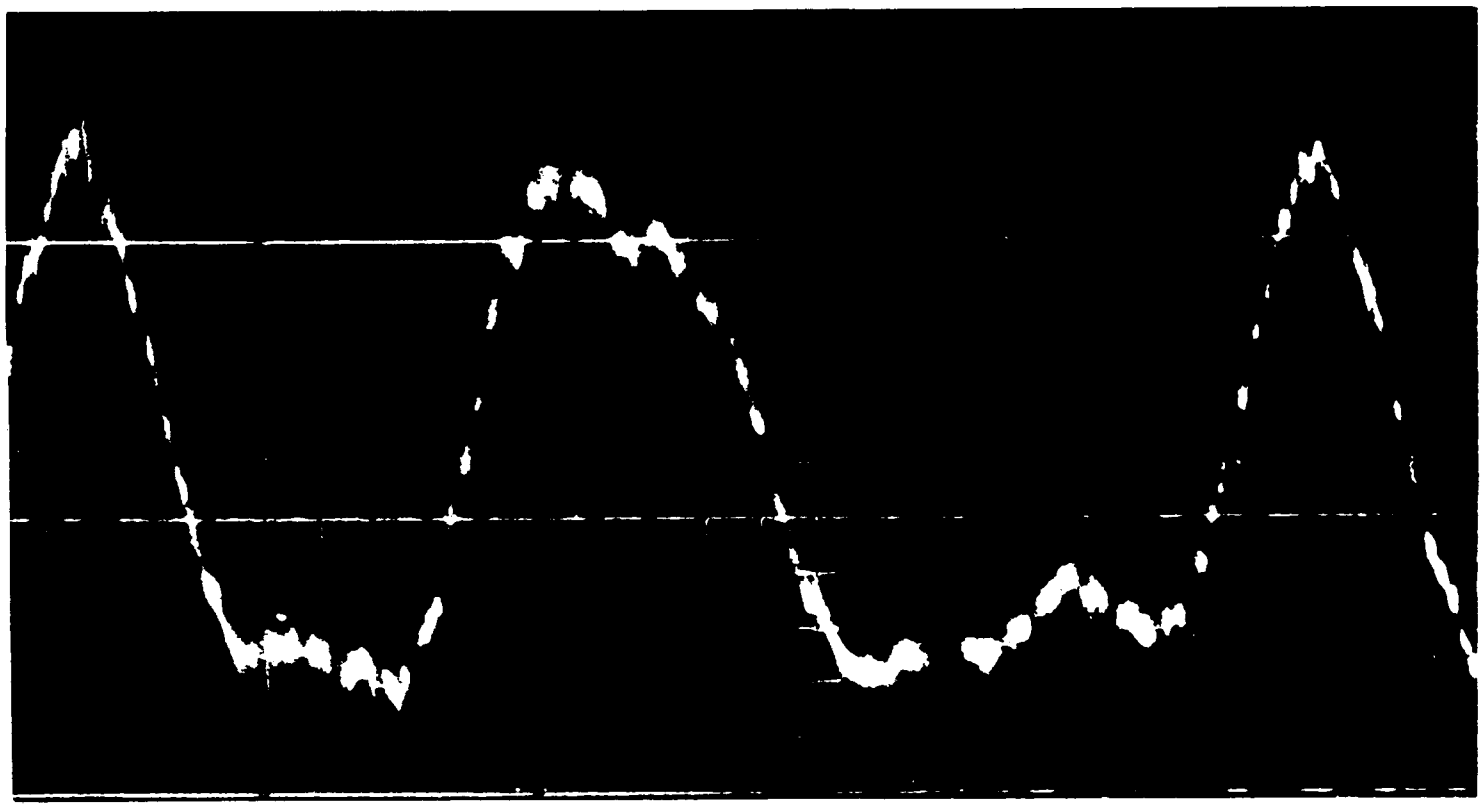

Fig. 10 Coating Thickness 400 μin. 10 A
Deep Gap Field 2250 oe (1/2 x Saturation) 10, 000 BPI
a) Experimental Waveform
b) Computed versus Experimental
c) Computed Cross-Correlation F. O. M

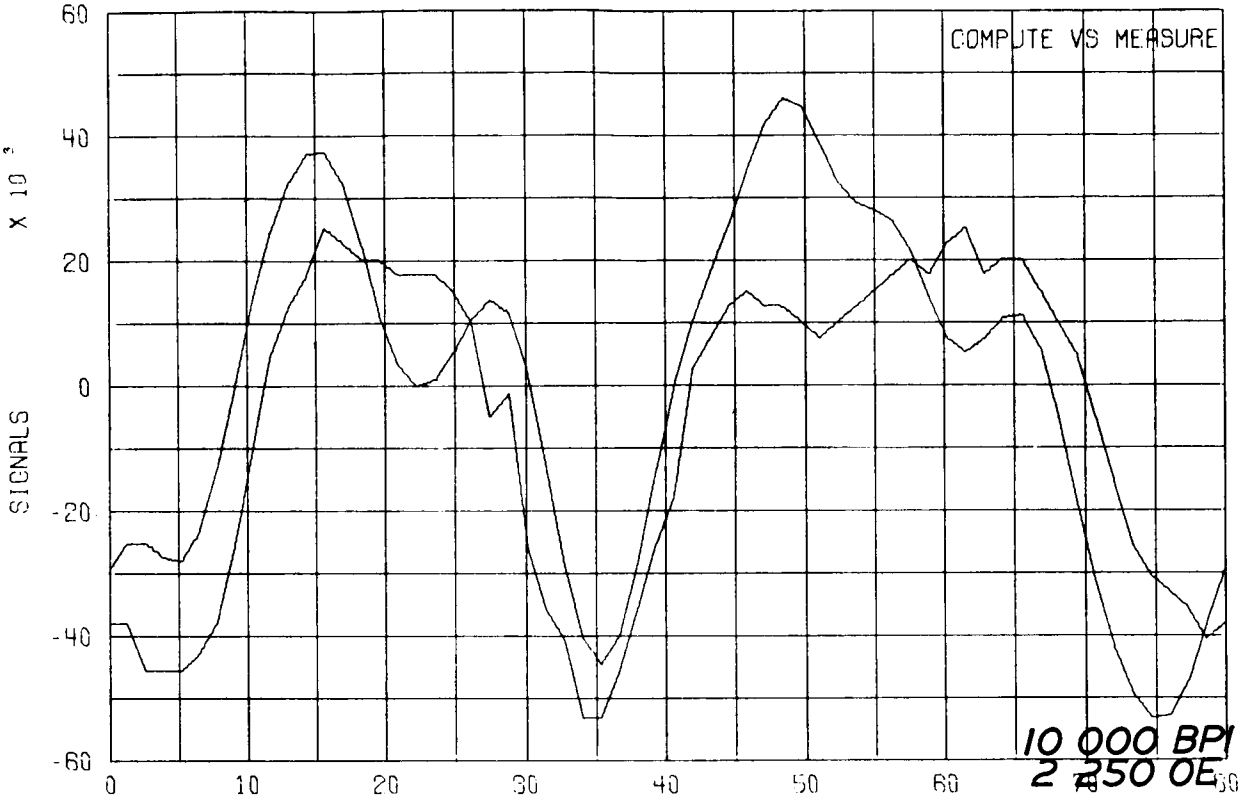
COMPUTE VS MEASURE
10B
SIGNALS
X 10 ³
60
40
20
0
-20
-40
-60
0
10
20
30
40
50
60
10 000 BPI
2 250 OE

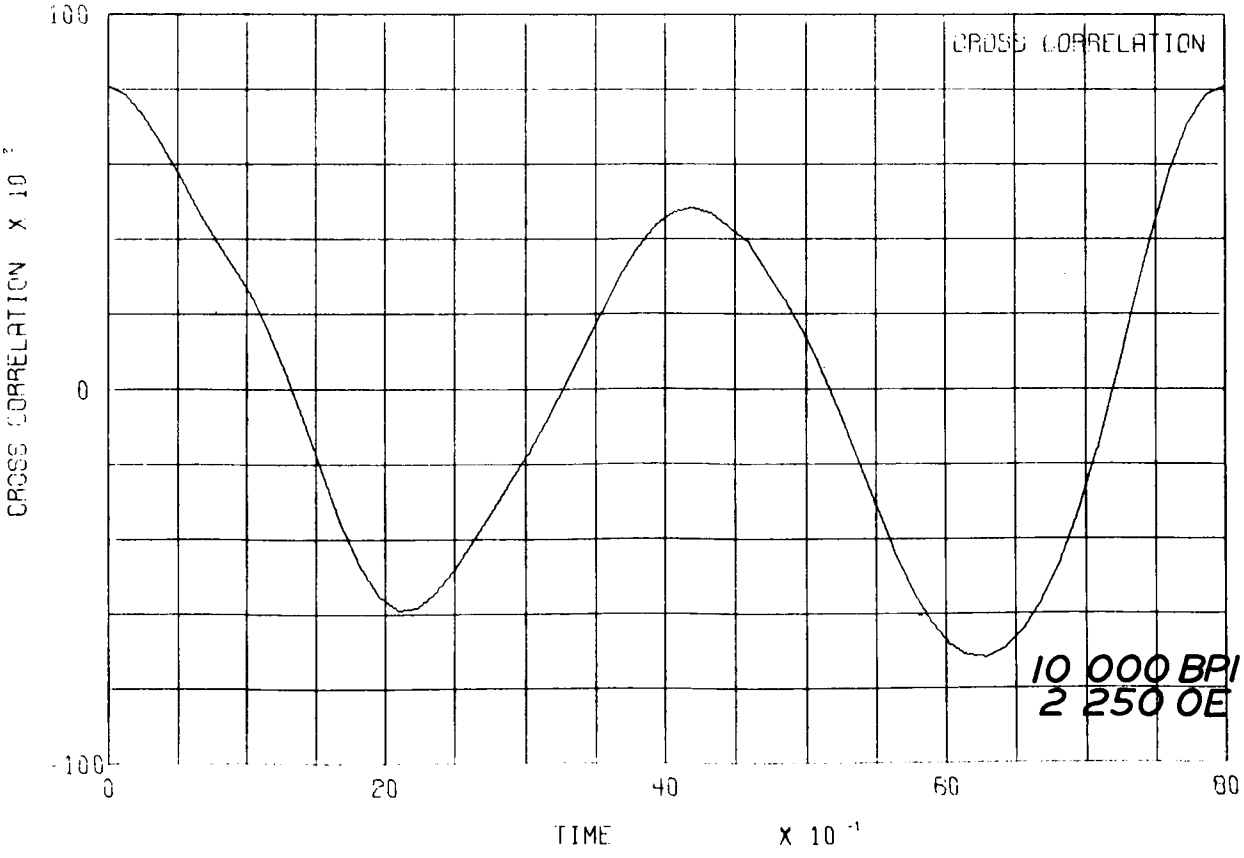
CROSS CORRELATION
10C
CROSS CORRELATION X 10 ²
100
0
-100
0
20
40
60
80
TIME X 10 ⁻¹
10 000 BPI
2 250 OE

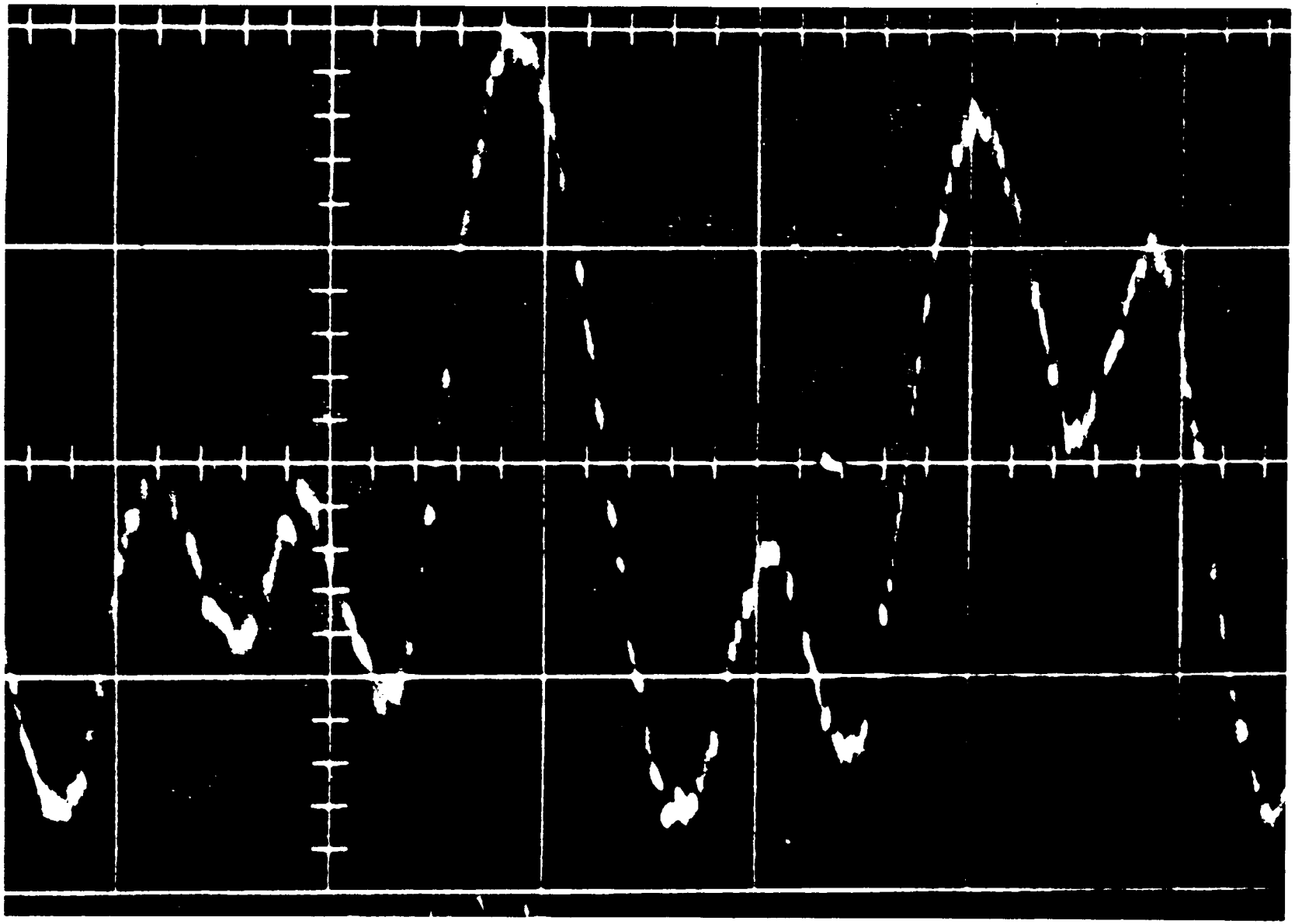

11A

Fig. 11 Coating Thickness 400 μin.
Deep Gap Field 1500 oe (1/3 x Saturation) 7500 BPI
a) Experimental Waveform
b) Computed versus Experimental
c) Computed Cross-Correlation F. O. M.

11B

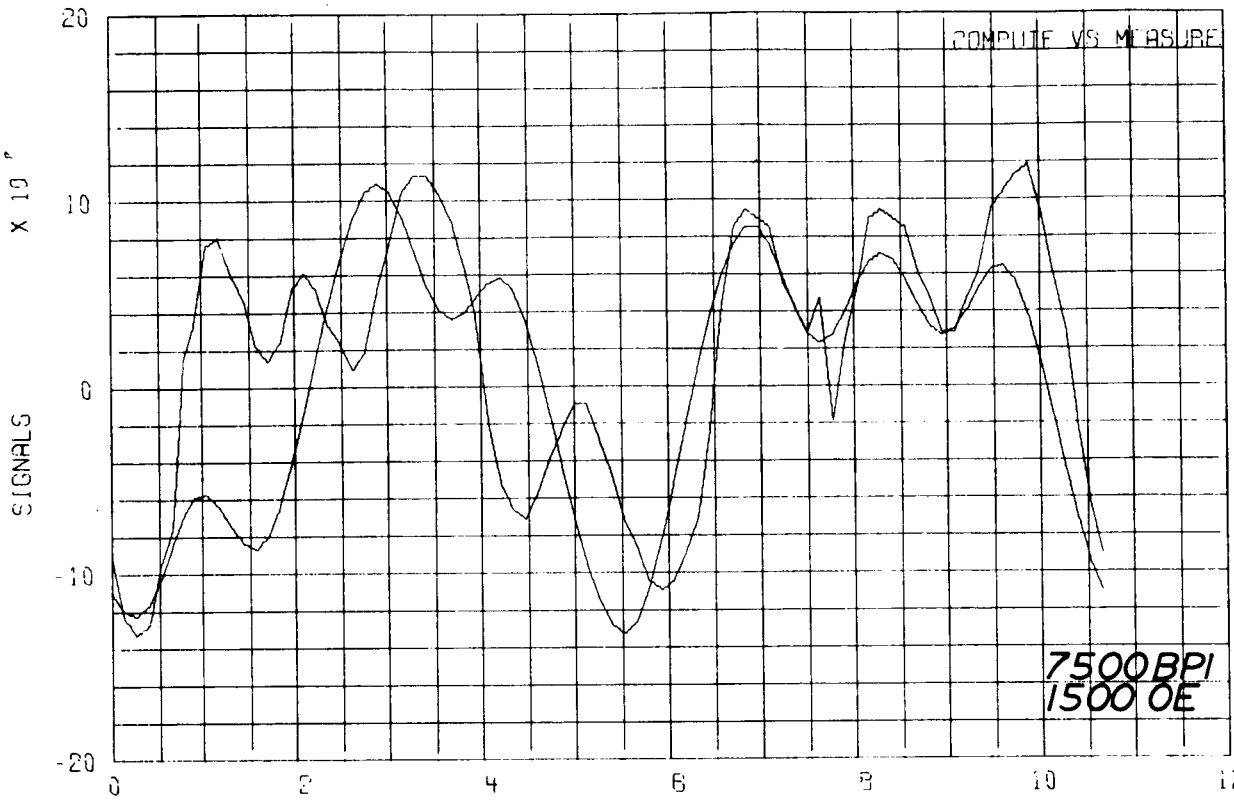
COMPUTE VS MEASURE
SIGNALS X 10
20
10
0
-10
-20
0
2
4
6
8
10
12
7500 BPI
1500 OE

11C

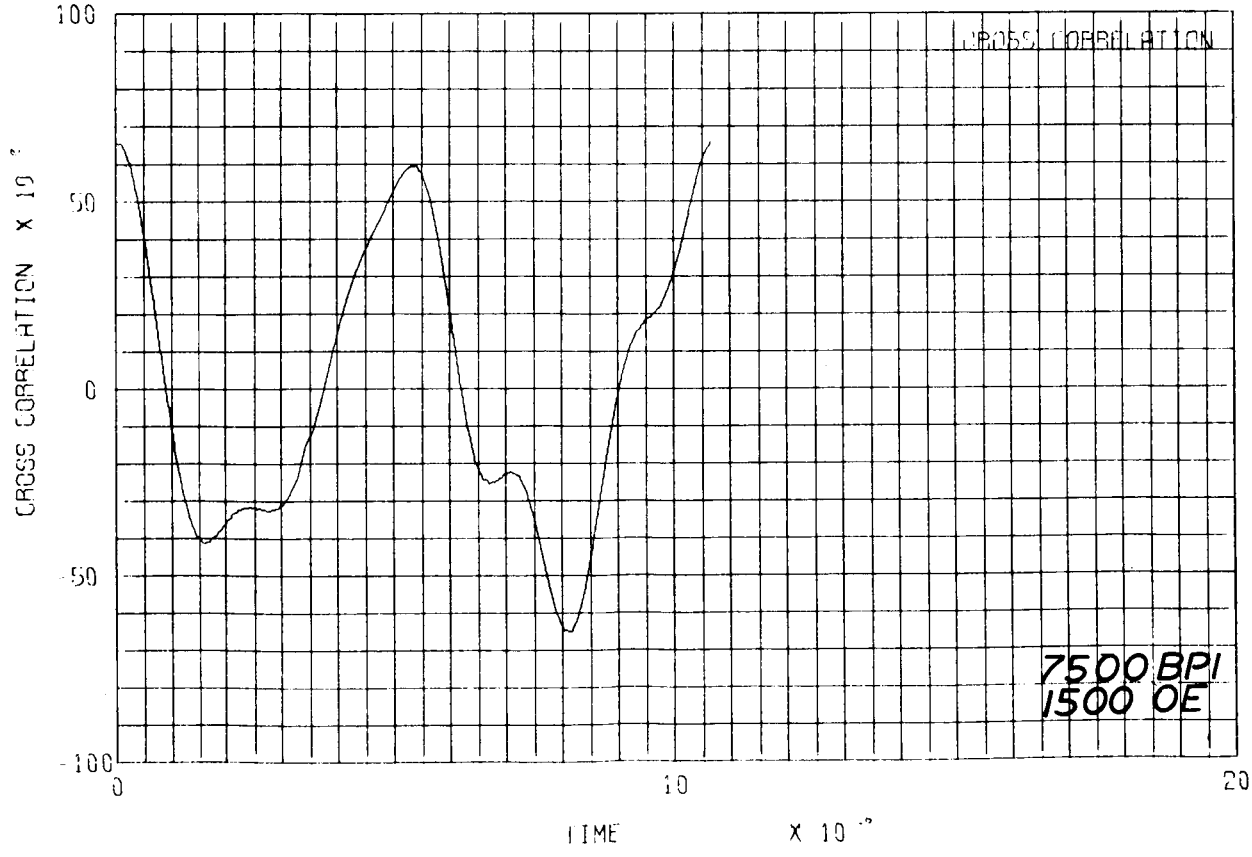
CROSS CORRELATION
CROSS CORRELATION X 10
100
50
0
-50
-100
0
10
20
TIME X 10
7500 BPI
1500 OE

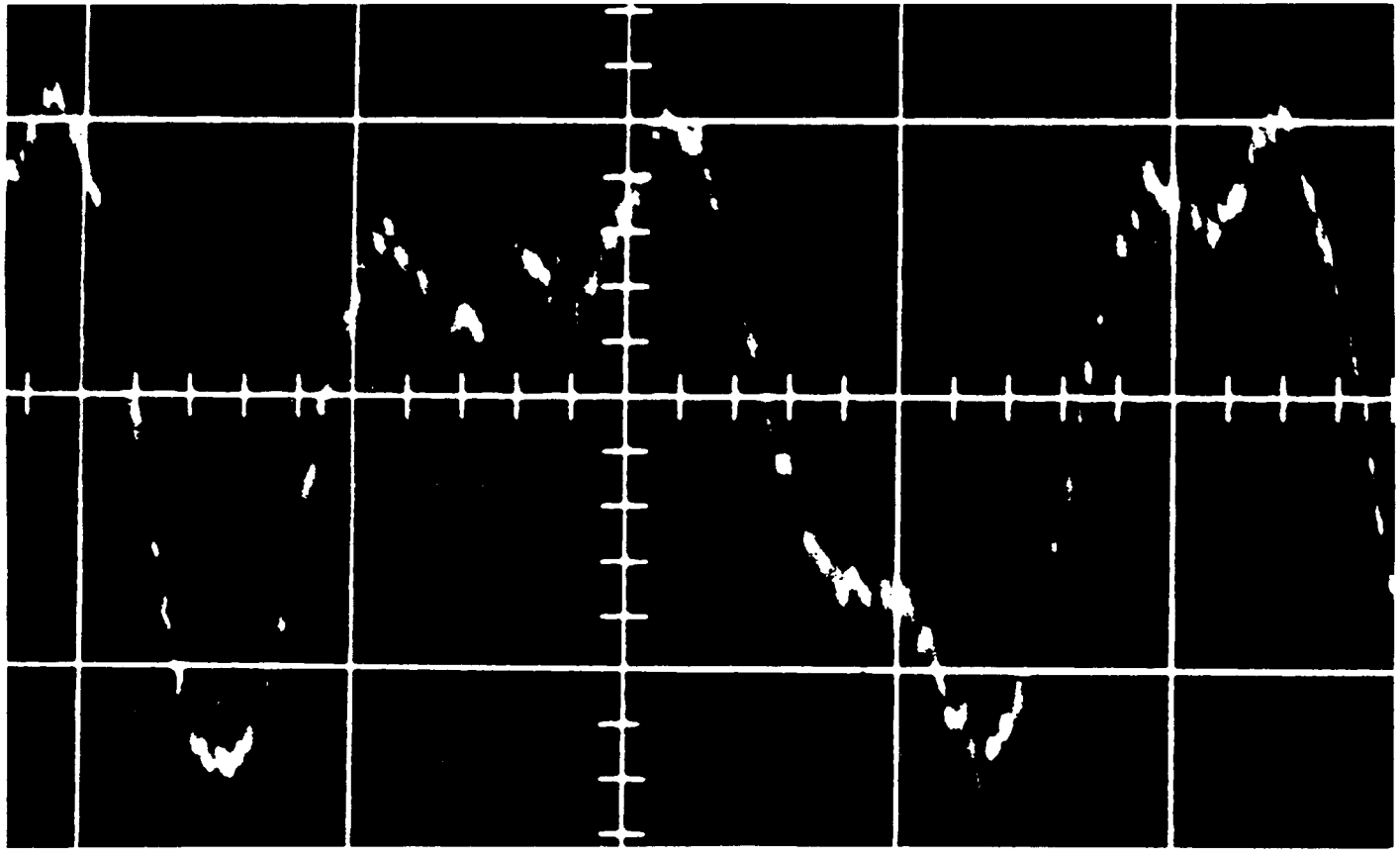

12 A

Fig. 12 Coating Thickness 400 μ in.
Deep Gap Field 1500 μin. (1/3 x Saturation) 10,000 BPI
a) Experimental Waveform
b) Computed versus Experimental
c) Computed Cross-Correlation F. O. M.

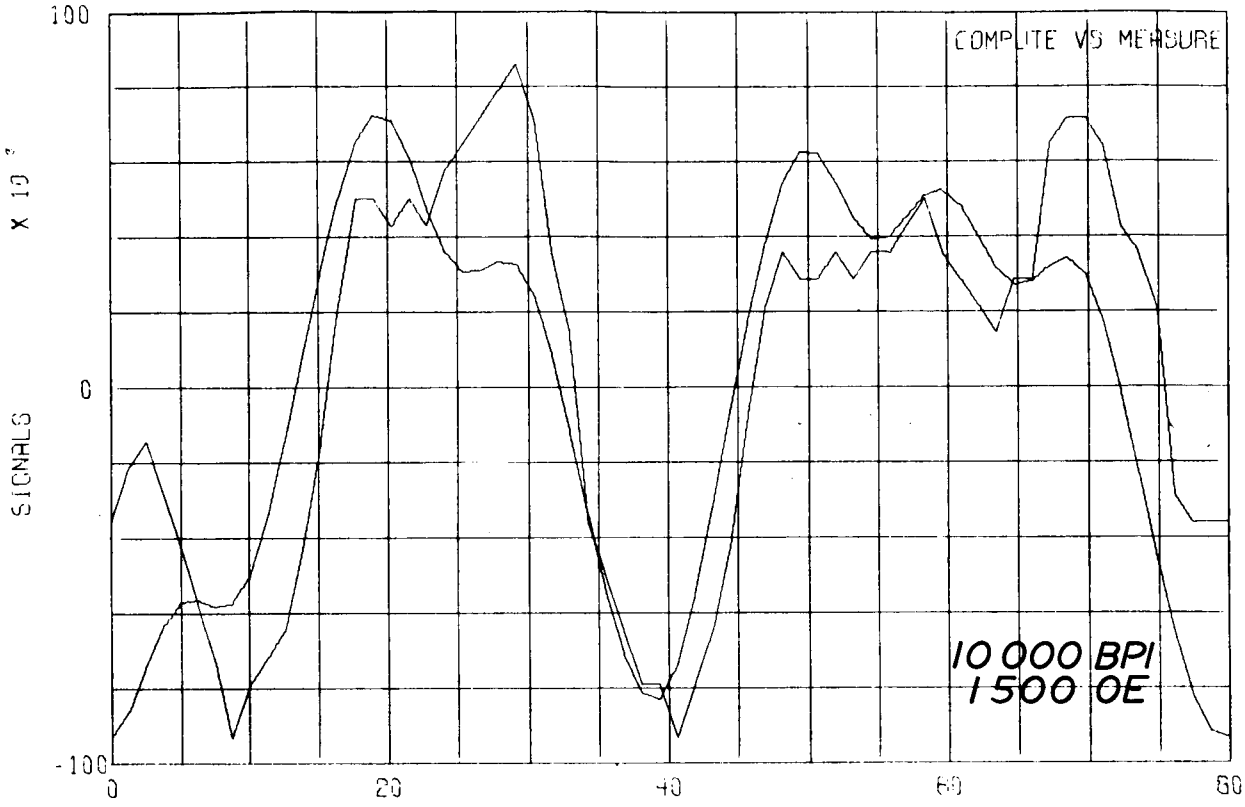
COMPUTE VS MEASURE
10 000 BPI
1 500 OE
SIGNALS
100
0
-100
0
20
40
60
80

12B

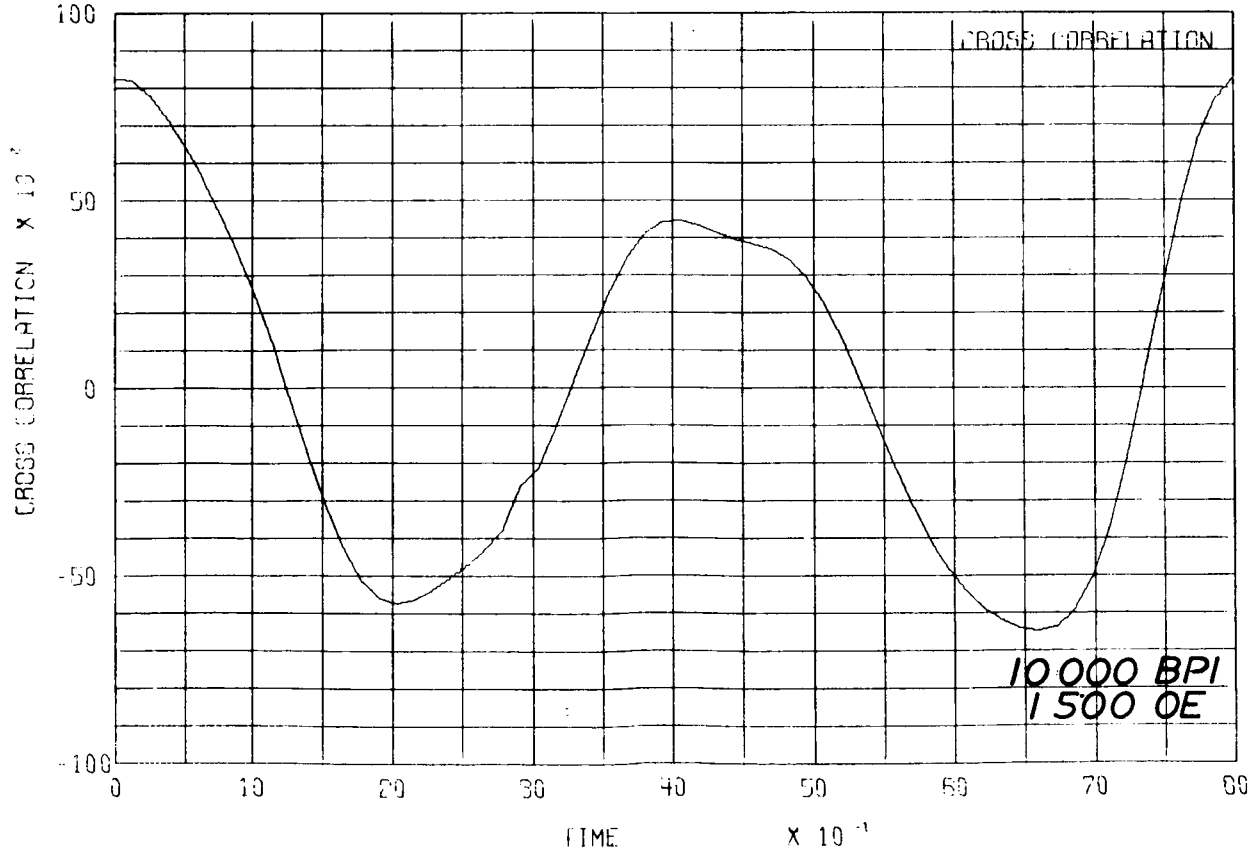
CROSS CORRELATION
10 000 BPI
1 500 OE
CROSS CORRELATION
100
50
0
-50
-100
0
10
20
30
40
50
60
70
80
TIME

12C

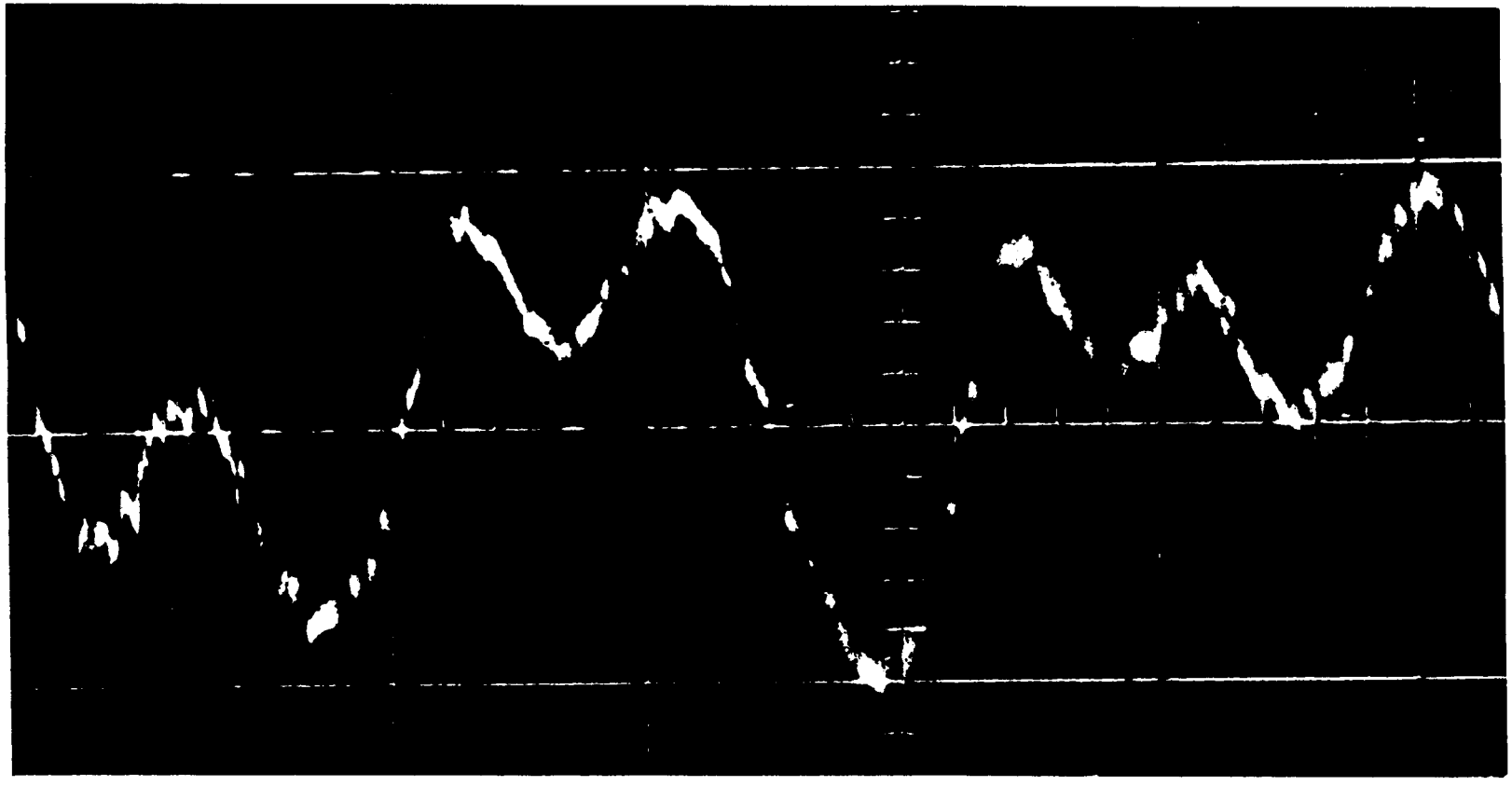

Fig. 13 Coating Thickness 400 μin. 13A
Deep Gap Field 1100 oe (1/4 x Saturation) 7500 BPI
a) Experimental Waveform
b) Computed versus Experimental
c) Computed Cross-Correlation F. O. M.

13B

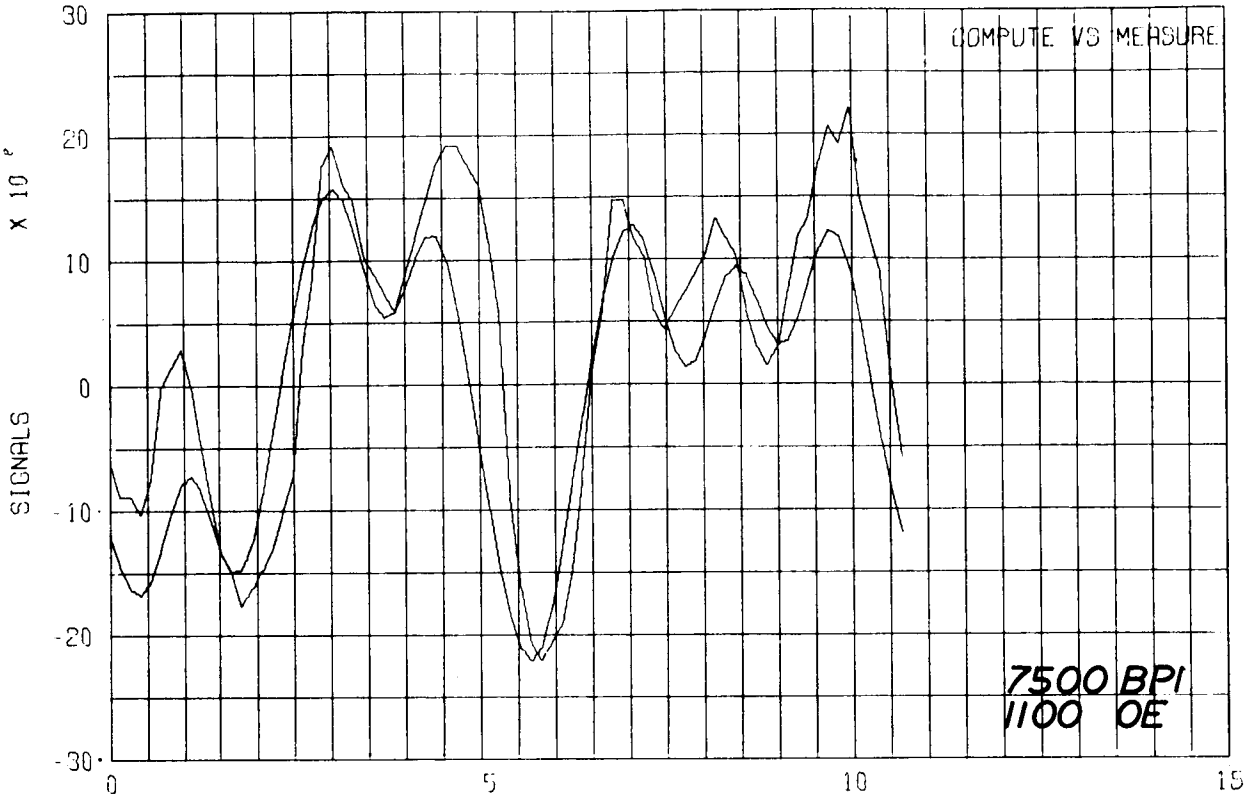
COMPUTE VS MEASURE
SIGNALS X 10
30
20
10
0
-10
-20
-30
0
5
10
15
7500 BPI
1100 OE

13C

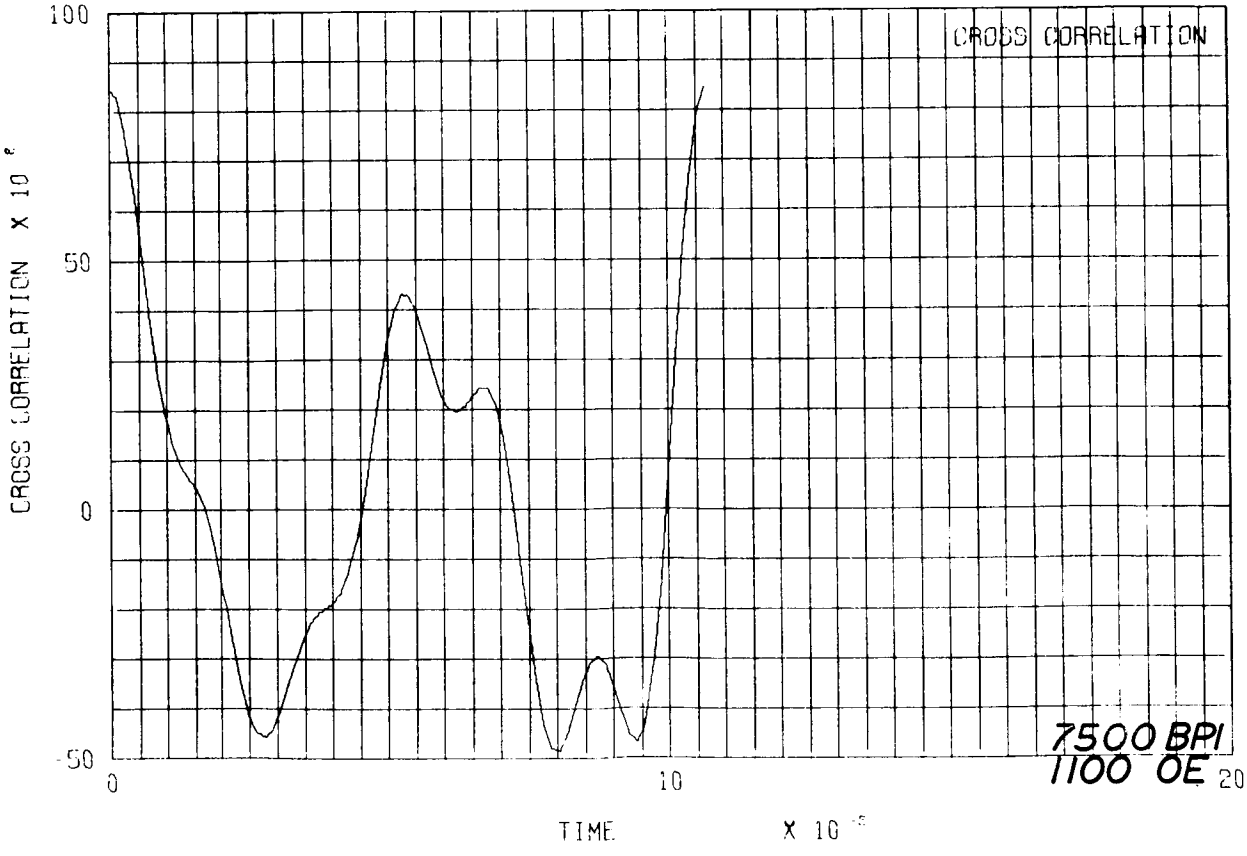
CROSS CORRELATION
CROSS CORRELATION X 10
100
50
0
-50
0
10
20
TIME X 10
7500 BPI
1100 OE

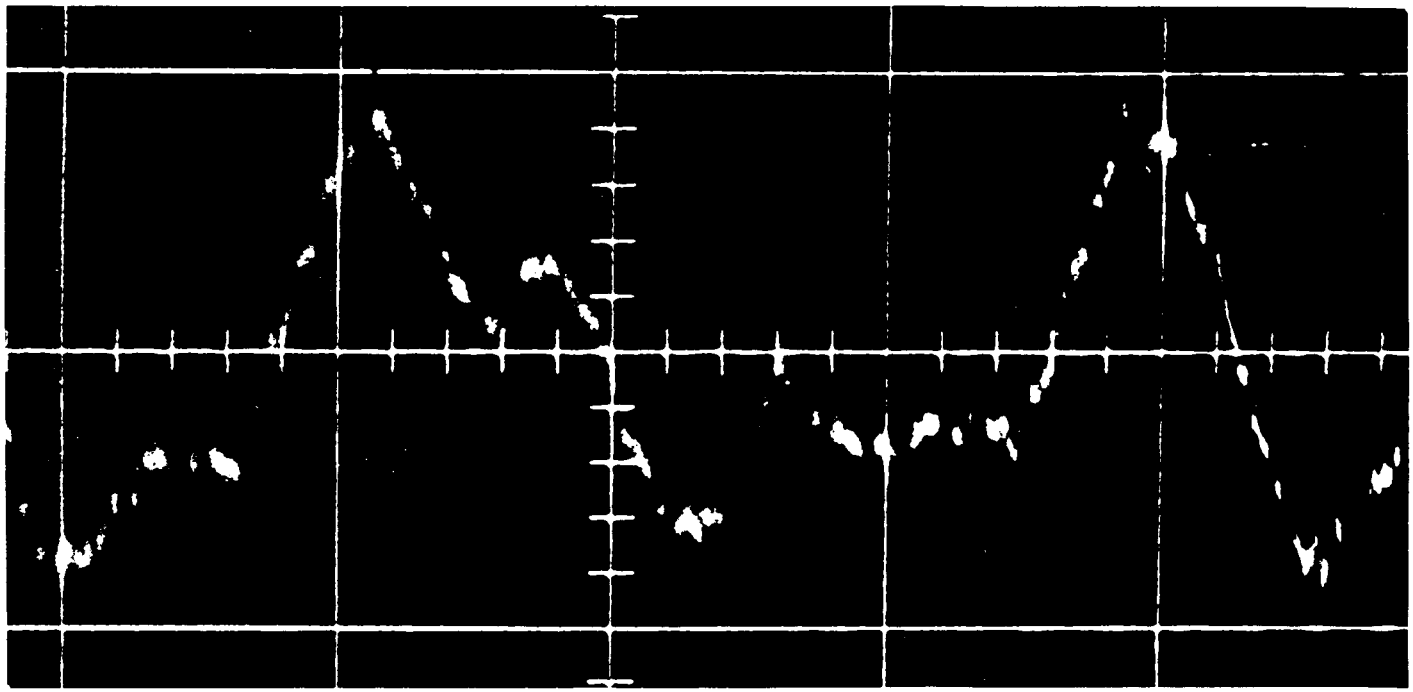

14 A

Fig. 14 Coating Thickness 400 μin.
Deep Far Field 1100 oe (1/4 x Saturation) 10,000 BPI
a) Experimental Waveform
b) Computed versus Experimental
c) Computed Cross-Correlation F. O. M.

14B

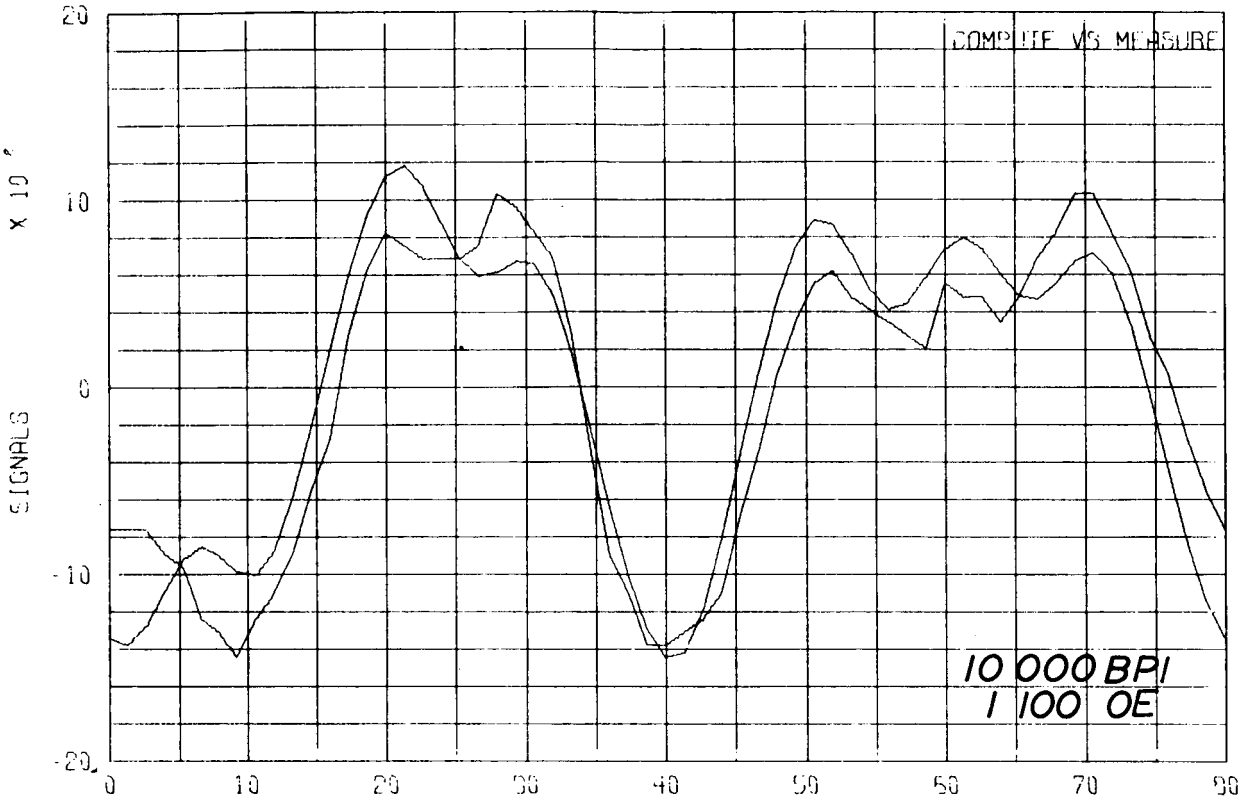
COMPUTE VS MEASURE
SIGNALS
X 10
20
10
0
-10
-20
0
10
20
30
40
50
60
70
80
10 000 BPI
1 100 OE

14C

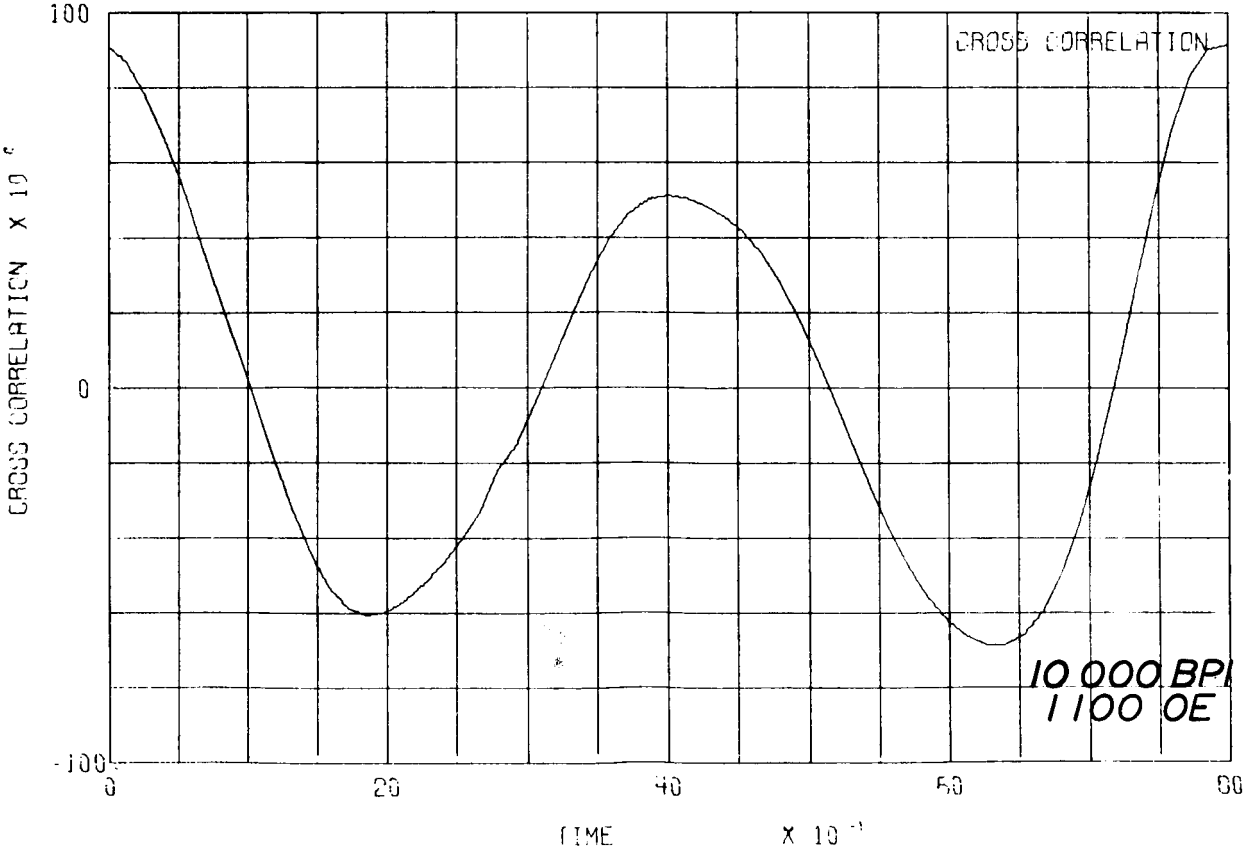
CROSS CORRELATION
CROSS CORRELATION X 10
100
0
-100
0
20
40
60
80
TIME
X 10
10 000 BPI
1100 OE

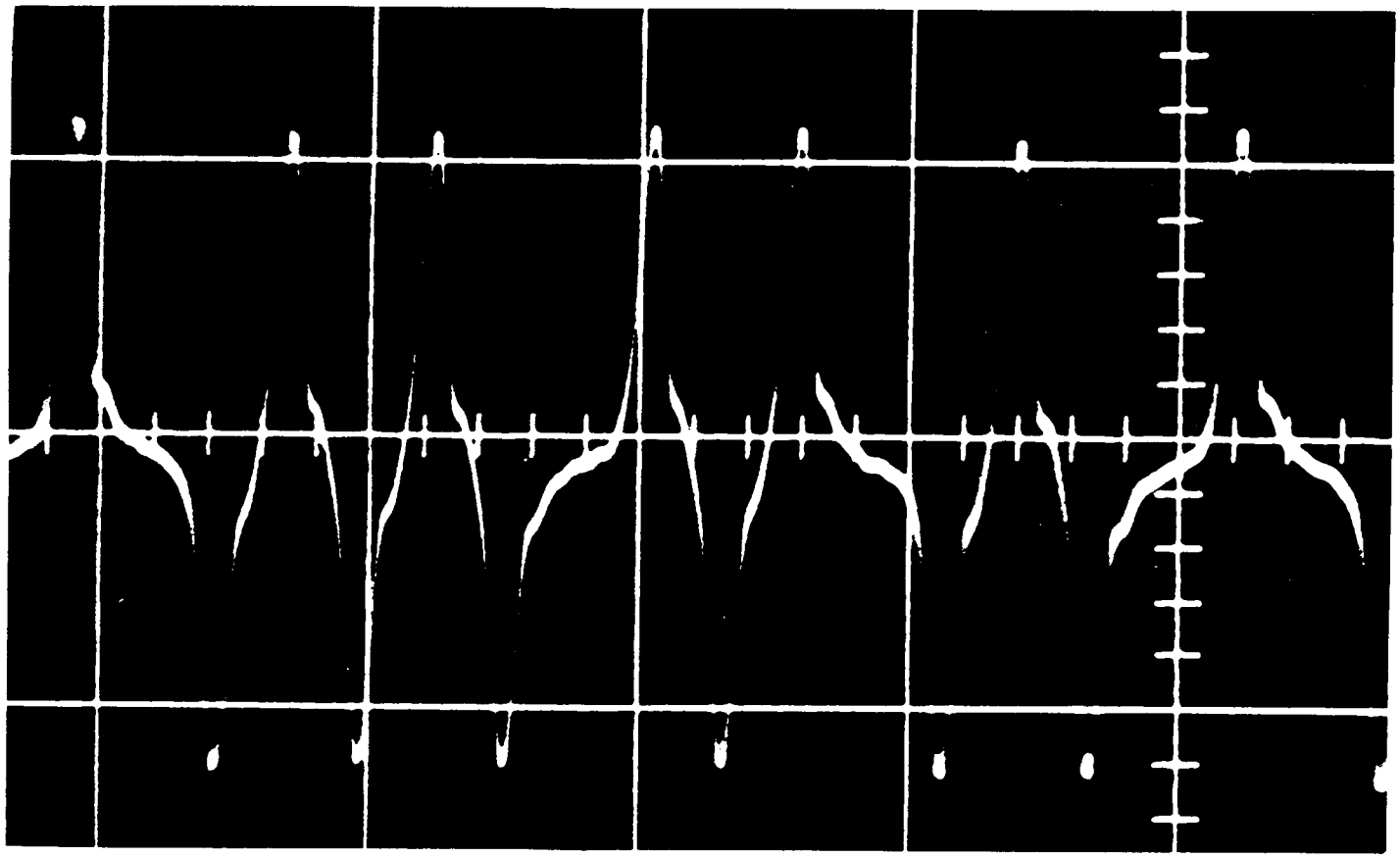

15A

Fig. 15 Coating Thickness 200 μin.
Deep Gap Field 2500 oe (1 x Saturation), 625 BPI
a) Experimental Waveform
b) Computed versus Experimental
c) Computed Cross-Correlation F. O. M.

15B

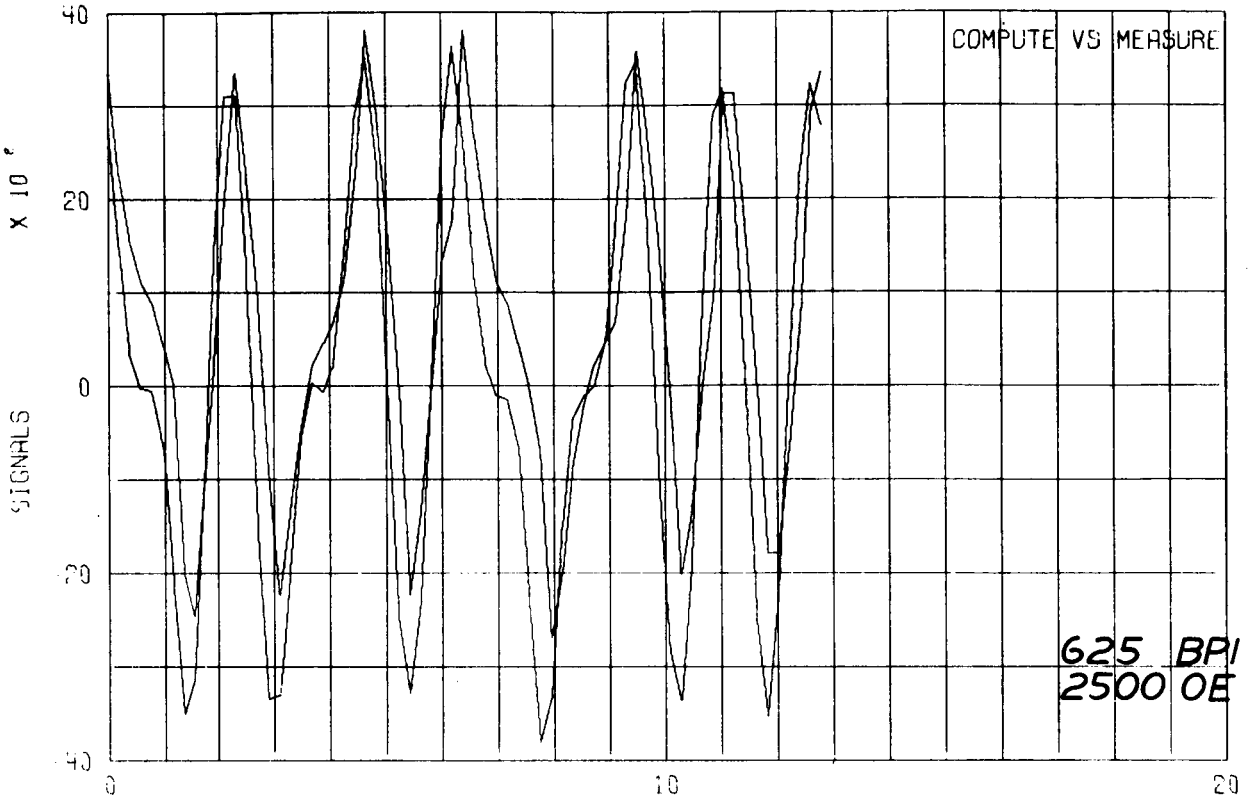
COMPUTE VS MEASURE
SIGNALS
X 10
40
20
0
-20
-40
0
10
20
625 BPI
2500 OE

15C

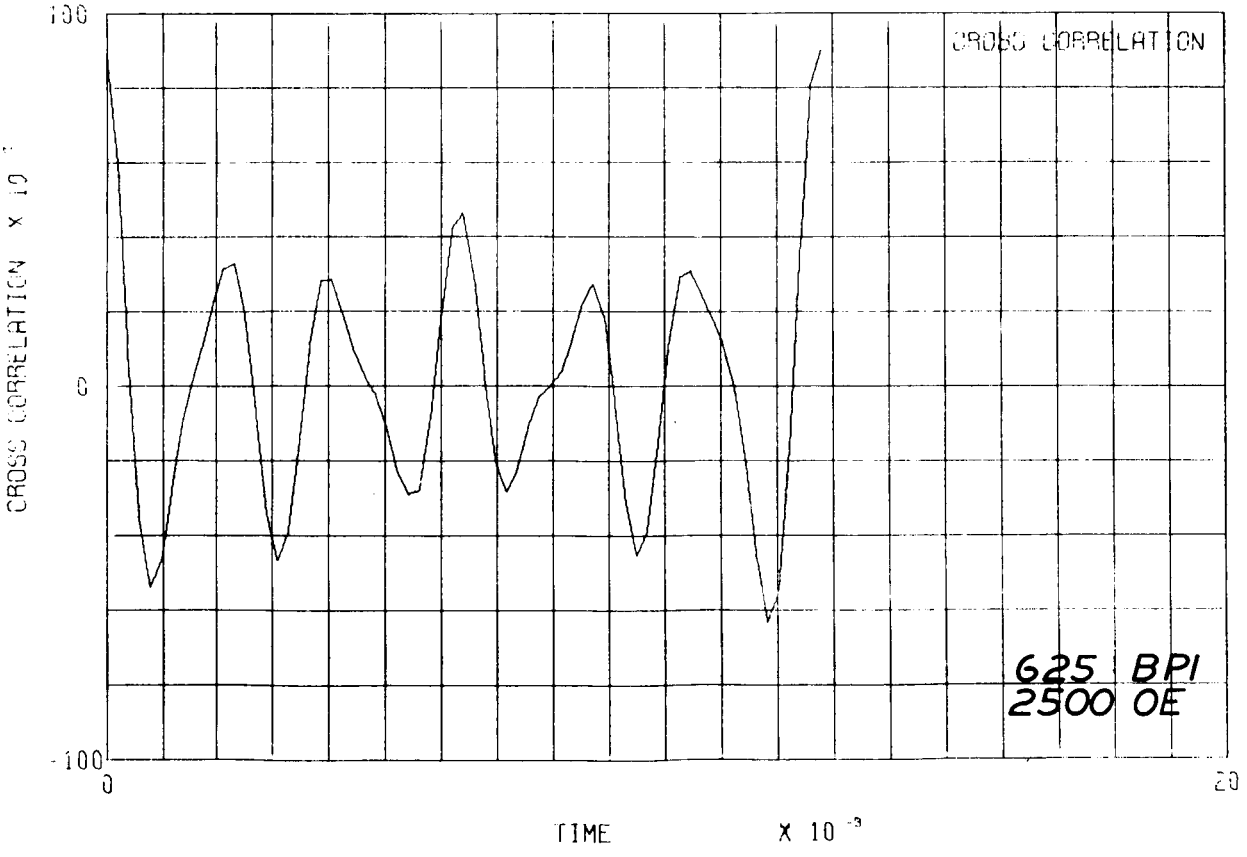
CROSS CORRELATION
CROSS CORRELATION X 10
100
0
-100
0
20
TIME X 10
625 BPI
2500 OE

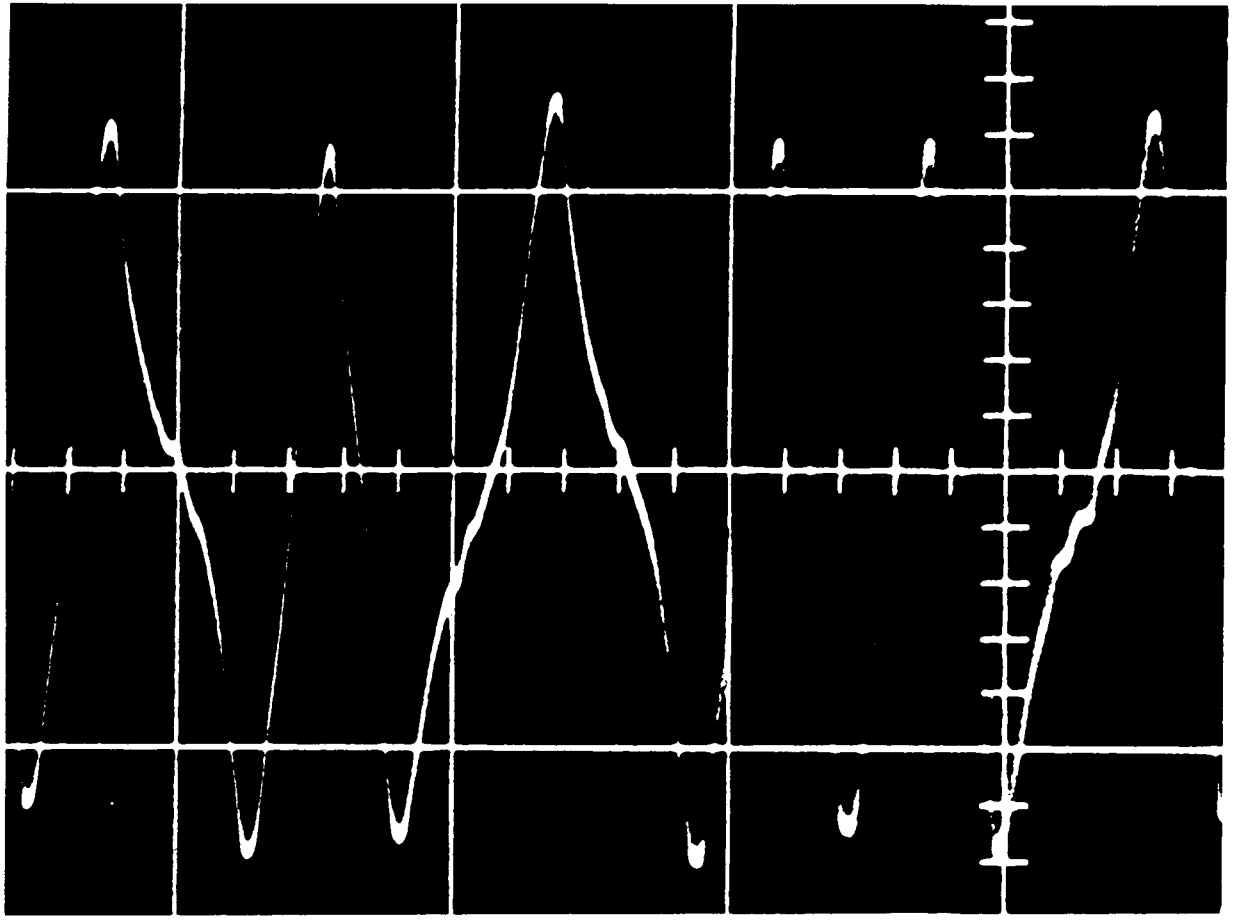

Fig. 16 Coating Thickness 200 μin. 16A
Deep Far Field 2500 oe (1 x saturation) 1250 BPI
a) Experimental Waveform
b) Computed versus Experimental
c) Computed Cross-Correlation F. O. M.

16B

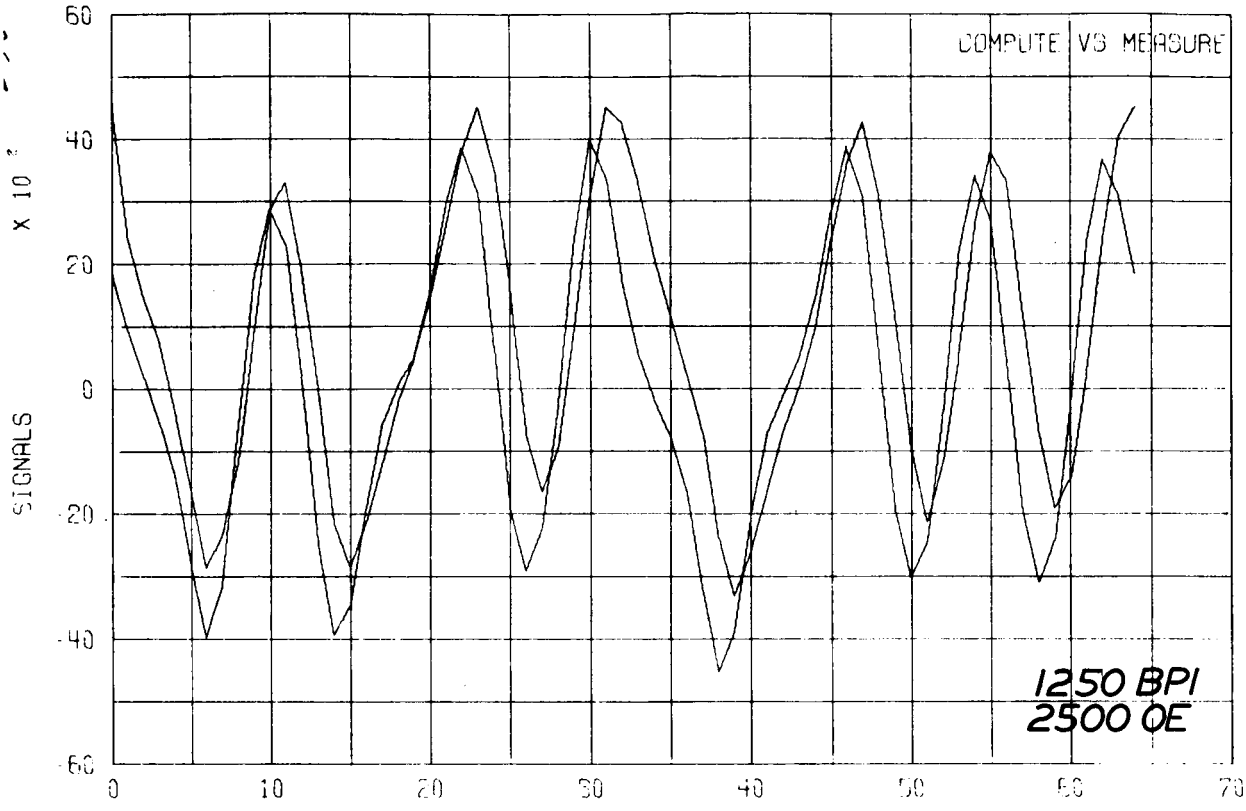
COMPUTE VS MEASURE
SIGNALS
X 10
60
40
20
0
-20
-40
-60
0
10
20
30
40
50
60
70
1250 BPI
2500 OE

16C

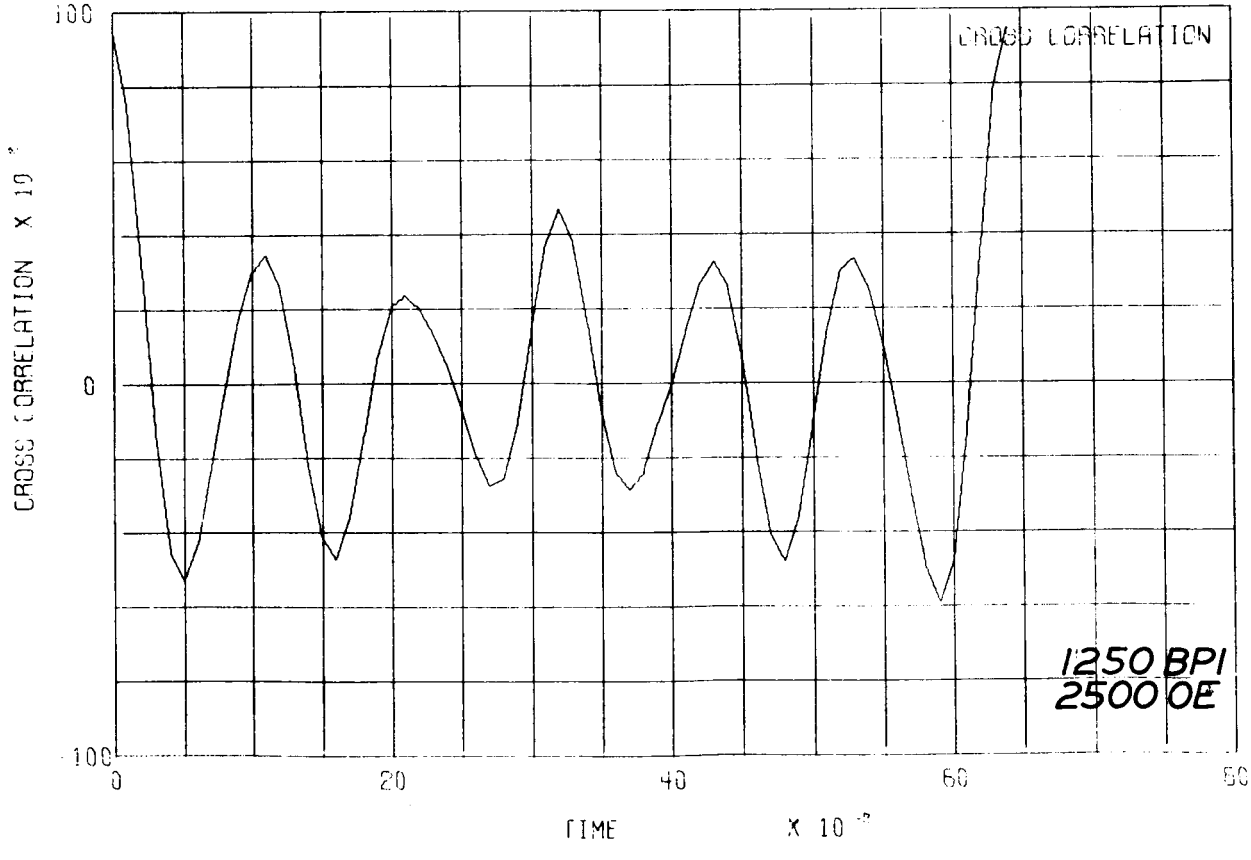
CROSS CORRELATION
CROSS CORRELATION X 10
100
0
-100
0
20
40
60
80
TIME
X 10
1250 BPI
2500 OE

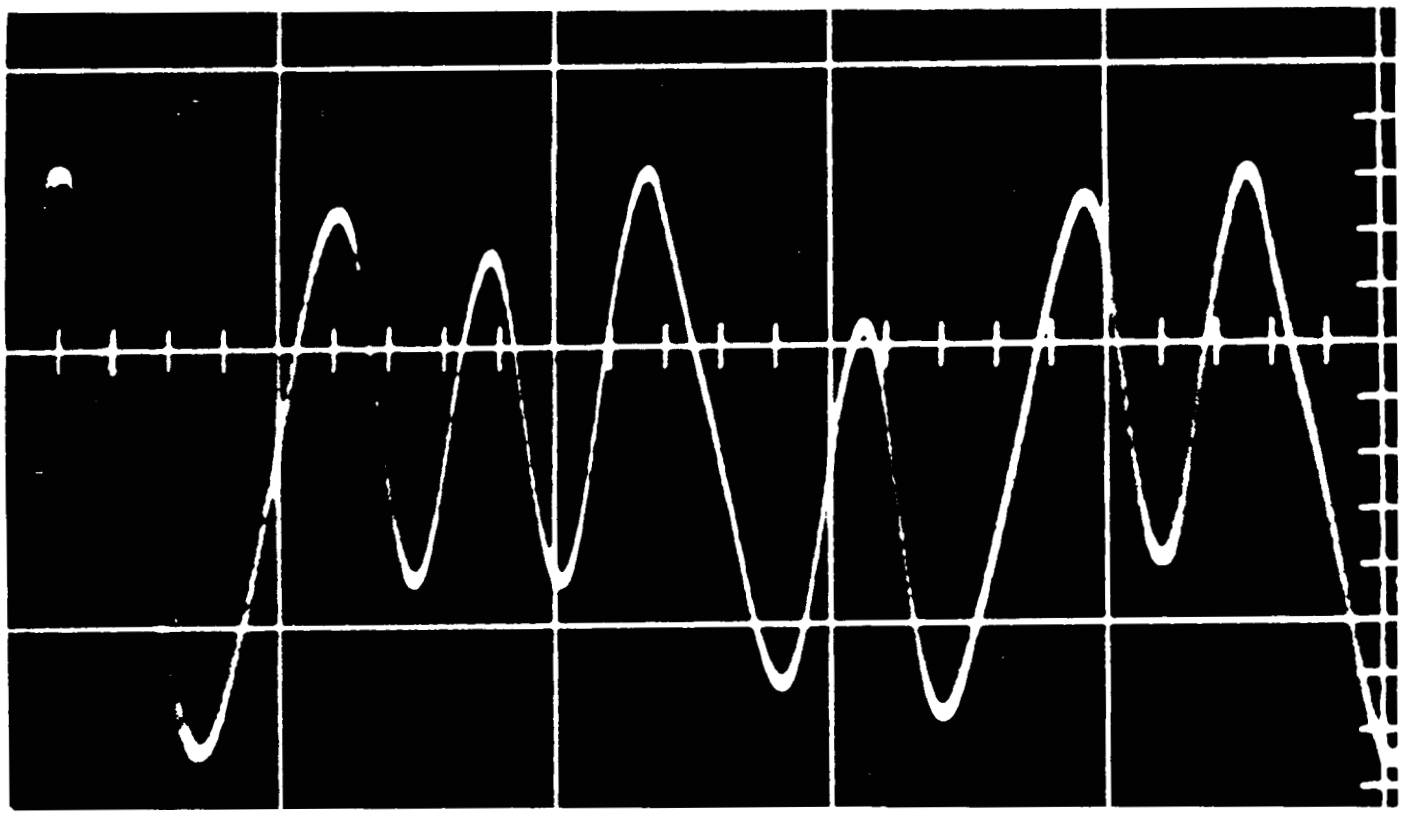

17A

Fig. 17 Coating Thickness 200 μin.
Deep Gap Field 2500 oe (1 x Saturation) 2500 BPI
a) Experimental Waveform
b) Computed versus Experimental
c) Computed Cross-Correlation F. O. M.

17B

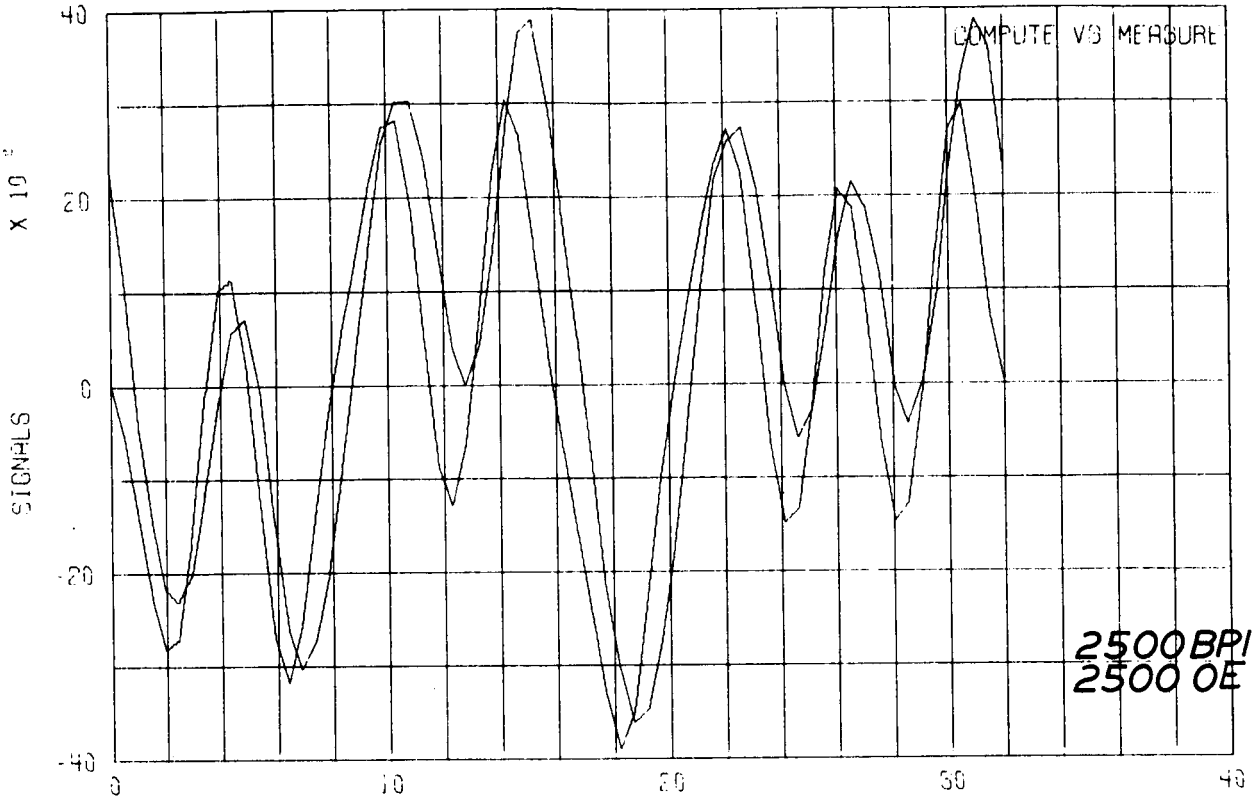
COMPUTE VS MEASURE
SIGNALS
40
20
0
-20
-40
0
10
20
30
40
2500 BPI
2500 OE

17C

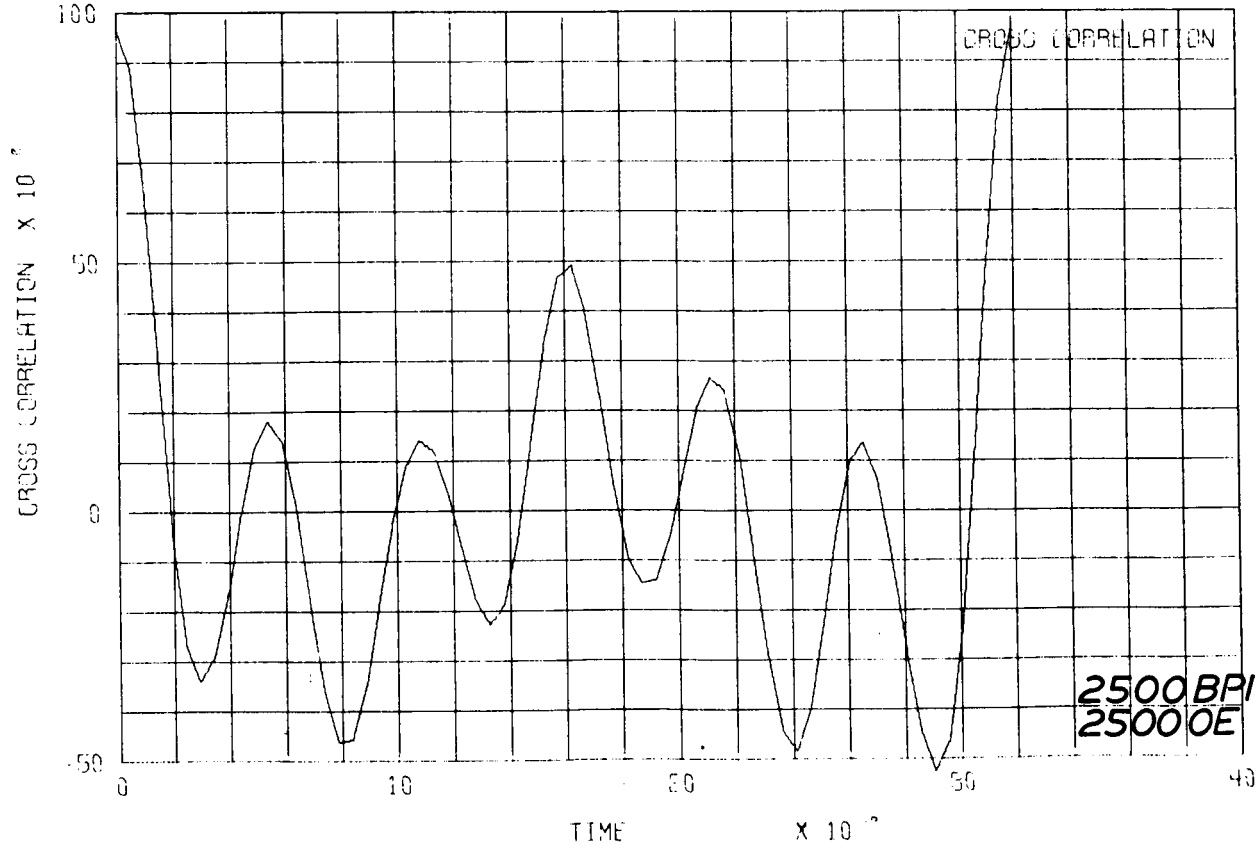
CROSS CORRELATION
CROSS CORRELATION X 10
100
50
0
-50
0
10
20
30
40
TIME X 10
2500 BPI
2500 OE

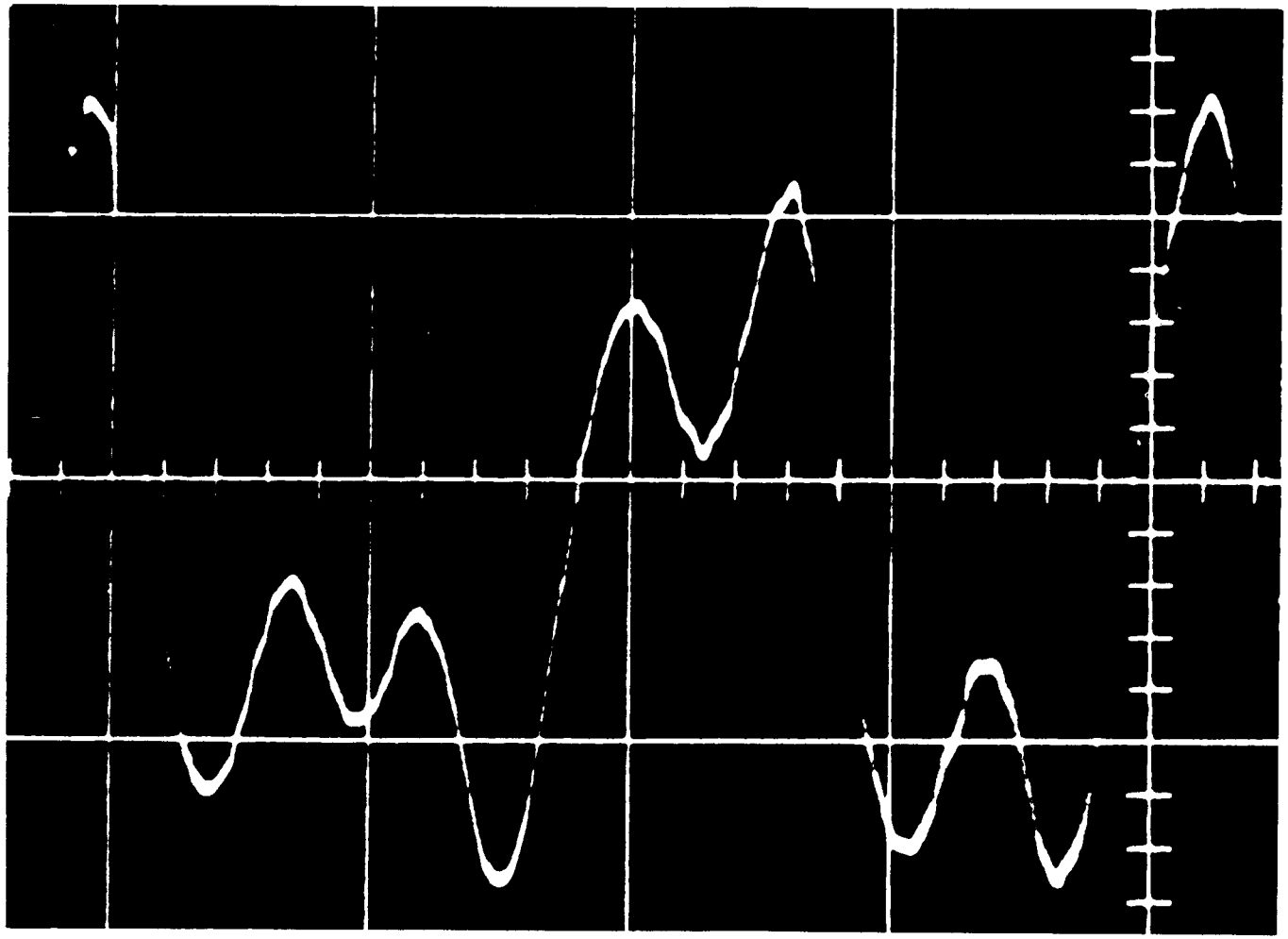

18A

Fig. 18 Coating Thickness 200 μin.
Deep Gap Field 2500 oe (1 x Saturation), 5000 BPI
a) Experimental Waveform
b) Computed versus Experimental
c) Computed Cross-Correlation F. O. M.

18B

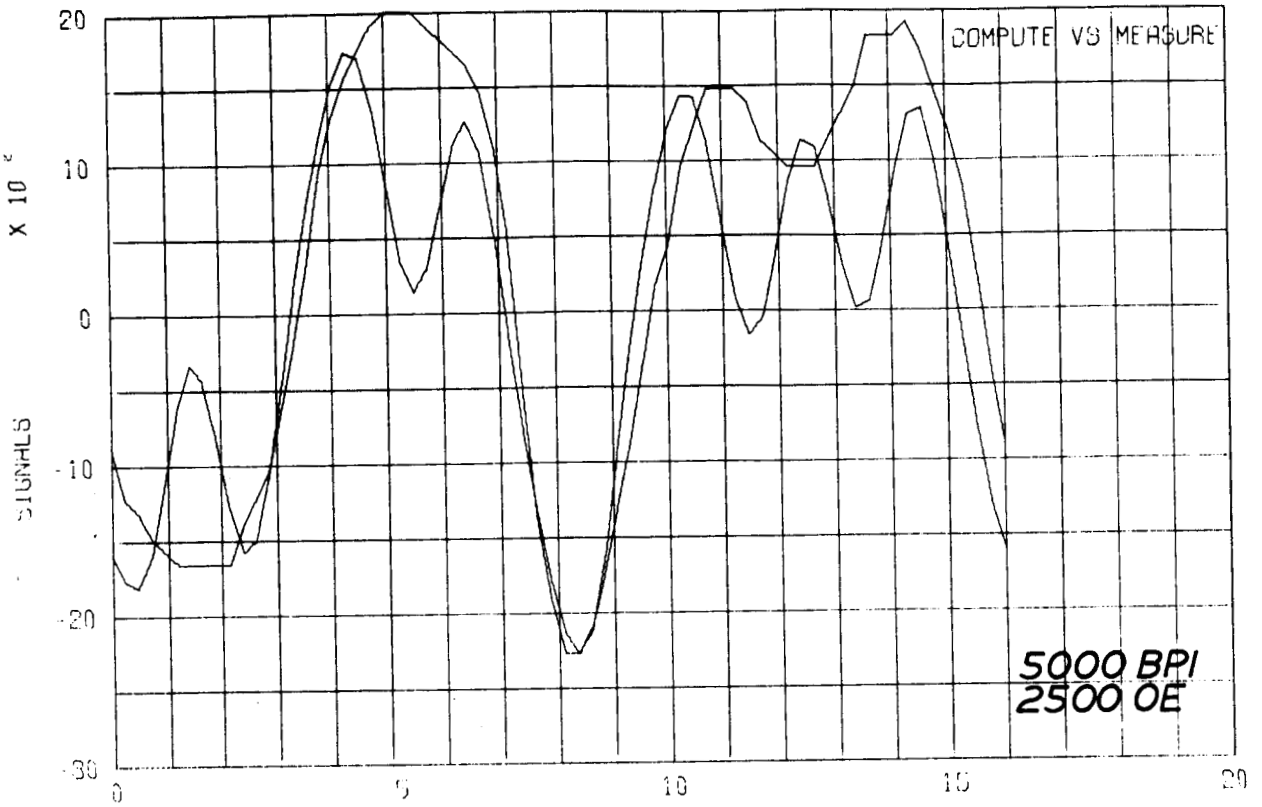
COMPUTE VS MEASURE
5000 BPI
2500 OE
X 10
20
10
0
-10
-20
-30
0
5
10
15
20

18C

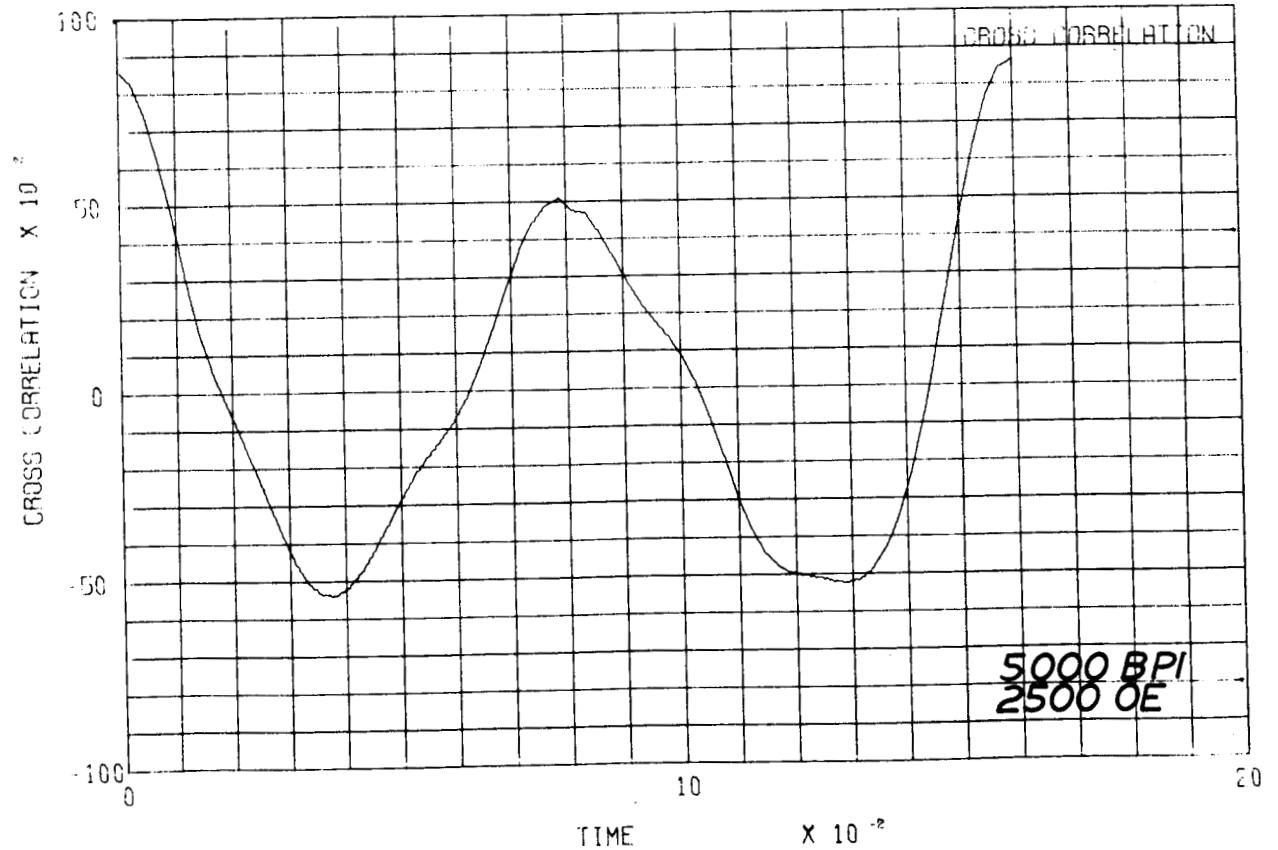
5000 BPI
2500 OE
CROSS CORRELATION X 10
100
50
0
-50
-100
0
10
20
TIME X 10